The Pennsylvania State University
APPLIED RESEARCH LABORATORY
P.O. Box 30
State College, PA 16804

A STUDY OF THE DIFFUSION OF SLOT-INJECTED DRAG-REDUCING POLYMER SOLUTION IN A TURBULENT BOUNDARY LAYER MODIFIED BY LARGE-EDDY BREAKUP DEVICES

by

Steven T. Sommer
Howard L. Petrie

Technical Report No. TR 91-015
November 1991

Supported by:
Space and Naval Warfare Systems Command

L.R. Hettche, Director
Applied Research Laboratory

Approved for public release; distribution unlimited

REPORT DOCUMENTATION PAGE

Form Approved
OMB No. 0704-0188

1. AGENCY USE ONLY (Leave blank)	2. REPORT DATE	3. REPORT TYPE AND DATES COVERED
	May 1991	

4. TITLE AND SUBTITLE

A Study of the Diffusion of Slot-Injected Drag-Reducing Polymer Solution in a turbulent Boundary Layer Modified By Large-Eddy Breakup Devices

5. FUNDING NUMBERS

6. AUTHOR(S)

S.T.Sommer, H.L.Petrie

7. PERFORMING ORGANIZATION NAME(S) AND ADDRESS(ES)

Applied Research Laboratory
The Pennsylvania State University
P.O. Box 30
State College, PA 16804

8. PERFORMING ORGANIZATION REPORT NUMBER

TR- 91-015

9. SPONSORING / MONITORING AGENCY NAME(S) AND ADDRESS(ES)

Space and Naval Warfare Systems Command
Department of the Navy
Washington, DC 20363-5100

10. SPONSORING / MONITORING AGENCY REPORT NUMBER

N000039-88-C-0051

11. SUPPLEMENTARY NOTES

12a. DISTRIBUTION / AVAILABILITY STATEMENT

Unlimited

12b. DISTRIBUTION CODE

13. ABSTRACT (Maximum 200 words)

The effects of a tandem set of large-eddy breakup (LEBU) devices on the diffusion of drag-reducing polymer solution and of water injected into a turbulent boundary layer (TBL) flow have been studied. Laser-Doppler velocimeter measurements were taken in the LEBU modified TBL with and without polymer injection. A laser-induced fluorescence technique was used to examine the development of concentration profiles of the injected fluids with increasing distance from the injection slot for a range of injected rates. The diffusion rate of water, a passive contaminant, was diminished by the LEBU devices over a distance of only 10 to 15 boundary thicknesses before returning to the case of an unmodified flow. It has been found that the initial diffusion zone of the passive contaminant has been extended in the LEBU modified TBL. The LEBU devices did have a major effect on the diffusion of polymer over the entire streamwise distance studied, compared to the case of an unmodified flow. Large reductions of turbulent normal and shear stresses were observed downstream of the devices, especially with polymer injection.

14. SUBJECT TERMS

Drag reduction, polymer, turbulent boundary layer, LEBU, large eddy breakup devices, experimental

15. NUMBER OF PAGES

140

16. PRICE CODE

17. SECURITY CLASSIFICATION OF REPORT	18. SECURITY CLASSIFICATION OF THIS PAGE	19. SECURITY CLASSIFICATION OF ABSTRACT	20. LIMITATION OF ABSTRACT
Unclassified	Unclassified	Unclassified	SAR

ABSTRACT

The effects of a tandem set of large-eddy breakup (LEBU) devices on the diffusion of drag-reducing polymer solution and of water injected into a turbulent boundary layer (TBL) flow have been studied. Laser-Doppler velocimeter measurements were taken in the LEBU modified TBL with and without polymer injection. A laser-induced fluorescence technique was used to examine the development of concentration profiles of the injected fluids with increasing distance from the injection slot for a range of injection rates. The diffusion rate of water, a passive contaminant, was diminished by the LEBU devices over a distance of only 10 to 15 boundary thicknesses before returning to the case of an unmodified flow. It has been found that the initial diffusion zone of the passive contaminant has been extended in the LEBU modified TBL. The LEBU devices did have a major effect on the diffusion of polymer over the entire streamwise distance studied, compared to the case of an unmodified flow. Large reductions of turbulent normal and shear stresses were observed downstream of the devices, especially with polymer injection.

TABLE OF CONTENTS

LIST OF FIGURES

LIST OF TABLES

LIST OF SYMBOLS

A_i	LIF calibration constant, equation (2.15)
B	law of the wall equation constant, equation (3.1)
C	local concentration (WPPM or $moles/\ell$)
C_f	skin friction coefficient in LEBU modified TBL
C_{f_0}	skin friction coefficient in standard TBL
C_{inj}	injected concentration (WPPM)
C_{max}	maximum local (wall) concentration (WPPM)
d_f	fringe spacing in LDV probe volume (m), equation (2.2)
f_{D_i}	heterodyne Doppler frequency (Hz)
f_s	Bragg cell frequency shift (Hz)
h	height of LEBU in boundary layer (mm)
H	shape factor (nondim.)
I	laser beam intensity ($watts/m^2$)
I_f	fluorescence intensity ($watts/m^2$)
K_i	equation (2.14) constant of i^{th} photo diode
KU	kurtosis or flatness of data samples (nondim.), equation (2.7)
ℓ	chord length of each LEBU element (mm)
N	number of samples taken at a location in LDV surveys
N_i	noise of LIF system at i^{th} photo diode ($counts$)
Q	quantum yield of the fluorescent dye (nondim.)
Q_s	flow rate through the viscous sublayer per unit span from the wall to $y^+ = 11.6$ (m^2/s)
s	streamwise spacing of tandem LEBU elements (mm)
SK	skewness of data samples (nondim.), equation (2.6)

t	thickness of LEBU element (mm)
$T.I.$	turbulence intensity (percent), equation (2.5)
u	deviation of the streamwise velocity component from the mean (m/s)
u'	rms fluctuation level of streamwise velocity component (m/s)
u^*	friction velocity (m/s), equation (3.1a)
u^+	nondimensional streamwise velocity, equation (3.1b)
u_i	instantaneous streamwise velocity of i^{th} LDV sample (m/s), equation (2.1)
U	local mean streamwise velocity (m/s), equation (2.3)
U_e	freestream or edge velocity (m/s)
v	deviation of the vertical velocity component from the mean (m/s)
v'	rms fluctuation level of vertical velocity component (m/s)
v_i	instantaneous vertical velocity of i^{th} LDV sample (m/s)
V_i	output voltage of i^{th} photo diode ($counts$)
w_i	one- or two-dimensional velocity inverse weighting function, equation (2.8) and (2.9)
WPPM	weight parts per million
x	streamwise distance measured from polymer injection slot (mm)
x_u	streamwise distance measured from the leading edge of the upstream LEBU (mm)
x_0	streamwise distance measured from virtual origin of boundary layer (mm)
y	distance normal to the plate (mm)
y^+	nondimensional distance normal to the plate, equation (3.1c)
δ	99% boundary layer thickness (mm)

δ^*	displacement thickness (mm)
δ_u	boundary layer thickness at leading edge of upstream LEBU (mm)
ε	extinction coefficient $(\ell/cm \times moles)$
θ	momentum thickness (mm)
κ	law of the wall equation constant, equation (3.1)
λ	value of y where $C/C_{max} = 0.5$ (mm)
λ_{beam}	wavelength of laser beam in LDV system (m)
ν	kinematic viscosity of water (m^2/s)
ξ	streamwise distance measured from the leading edge of the upstream LEBU device normalized with δ_u
ρ	density of water (kg/m^3)
σ	standard deviation of data samples, equation (2.4)
τ_w	wall shear stress (N/m^2)
ϕ	half angle of focusing lens in LDV system $(degrees)$
$\bar{}$	mean quantity

Chapter 1
INTRODUCTION

1.1 Background and Previous Work

Research in the area of fluid dynamic drag reduction has received increased emphasis in recent years. Various drag reducing techniques have been developed which can be categorized into two primary areas: (1) maintaining laminar flow over a body through various methods of boundary layer control, and (2) modifying the boundary layer turbulence to reduce the wall shear stress. Hefner (1988) points out that maintaining laminar flow offers a greater potential payoff, but modifying the turbulence offers a more cost effective way of reducing skin friction drag. Wilkinson *et al.* (1988), Bushnell (1985), Bandyopadhyay (1986), and Hefner (1988) present a good review of the many different methods of turbulence modification techniques currently being researched, and Bushnell (1985) points out that very little research has been done with combinations of these techniques. This paper will deal with the combination of large-eddy breakup devices and slot-injected polymer solutions in a flat plate turbulent boundary layer (TBL) flow.

1.1.1 Large-Eddy Breakup Devices

There are several names associated with large-eddy breakup (LEBU) devices, including outer-layer devices (OLD) and boundary layer alteration devices (BLADE). The remainder of this paper will refer to these devices as LEBUs. A LEBU is a ribbon, an airfoil, or a wire suspended above a wall

in the TBL to break up, redistribute, and modify the large scales of turbulence in order to achieve skin friction reduction at the wall. It is interesting to note that LEBUs were initially screens or honeycomb devices placed in the flow [see Yajnik and Ancharya (1977)] but due to their large wetted area and high device drag, more efficient LEBUs were derived.

The key effect in the reduction of skin friction seems to be the suppression of the large scales of turbulence, which was shown with flow visualization by Corke *et al.* (1979) and Savill and Mumford (1988). These authors also observed a lower intermittency in the LEBU modified TBL due to the smoothing of the turbulent–nonturbulent interface at the edge of the boundary layer. A number of the mechanisms in which LEBUs alter a TBL to achieve skin friction reduction have been proposed by Anders and Watson (1985), Corke *et al.* (1979), Coughran and Bogard (1986), Dowling (1985), Hefner *et al.* (1979), and Savill and Mumford (1988). They include:

- restriction of vertical components of velocity responsible for transporting turbulent energy
- interuption of the turbulence production process through the momentum deficit in the wake of the LEBU
- reduction in the number of bursts at the wall which transports low momentum fluid into high momentum fluid
- reduction of the fluctuating velocity by introducing shed vortices from the LEBU

The effects of the LEBUs on the TBL can persist up to 150 boundary layer thicknesses downstream of the LEBU.

Guezennec and Nagib (1985) define three regions associated with the LEBU wake. These are:

1) Immediate effects region – A momentum deficit is introduced just behind the LEBU.
2) Persistent effects region – The majority of the skin friction reduction occurs within the first 30 to 50 boundary layer thicknesses downstream of the LEBU.
3) Relaxation region – The characteristics of the manipulated boundary layer relax and approach that of an unmanipulated boundary layer 150 to 200 boundary layer thicknesses downstream of the LEBU.

Most researchers, for example, Plesniak and Nagib (1985), Anders and Watson (1985), Lemay *et al.* (1985), and Savill and Mumford (1988), agree that there is an optimal geometry for the LEBU configuration, which consists of two devices in tandem with the following parameters:

$$\ell/\delta_u \cong 1.0$$

$$h/\delta_u \cong 0.8$$

$$s/\delta_u \cong 5 \text{ to } 15$$

$$t/\delta_u \cong 0.005$$

where ℓ = chord length of each LEBU element

h = height from the wall to the LEBU element

s = streamwise spacing of tandem LEBU elements

t = thickness of LEBU element

δ_u = boundary layer thickness at leading edge of upstream LEBU

LEBU performance is very sensitive to the height above the wall, h, in the boundary layer. As the LEBU devices are dropped below the optimum value, the magnitude of the maximum local skin friction reduction is increased, but the length of the persistent effects region is reduced. The result is a lower integrated skin friction reduction. Conversely, raising the LEBU devices above the optimum value decreases the maximum local skin friction reduction to such an extent that the integrated skin friction reduction is lower even though the persistent effects region is lengthened. The chord length and thickness are important in efficiently introducing a momentum deficit into the boundary layer. There seems to be a performance peak when the chord is the same length as, or slightly larger than, δ_u. A larger thickness, t, introduces a larger momentum deficit, but the device drag also increases. LEBU devices with zero thickness would still work because of the no-slip condition on both surfaces. The thickness adds a pressure load to the LEBU corresponding to the deficit addition to the wake. LEBU performance is very insensitive to the streamwise spacing, s, in the range indicated. The major point is that the tandem arrangement is optimum because the second LEBU operates in the wake of the first one, thus paying less of a drag penalty while reaping similar benefits [Plesniak and Nagib (1985)].

Using the above mentioned geometry, Plesniak and Nagib (1985) achieved local skin friction reductions up to 35 percent with a net drag reduction of 20 percent, which includes device drag. Anders and Watson (1985) report similar skin friction reductions but with a 7 percent reduction in net drag.

Most researchers use a thin flat ribbon for the LEBU elements while some [e.g. Anders and Watson (1985)] use tiny fabricated airfoils. Unfortunately, stability problems often arise when using both types, especially when tested in water. Reidy and Mautner (1986) tested flat ribbons in a water tunnel and experienced lifting, bowing, and vibration due to flow-induced instabilities. Reidy and Mautner (1986) point out that this is the main reason their results did not compare favorably with other researchers. Plesniak and Nagib (1985) and Lynn (1987) found that they could greatly reduce this problem by spanwise tensioning the ribbons. Tension was varied across the chord of the LEBUs.

Lynn (1987) also tested a tandem pair of wires as well as ribbons. The diameter of the wires were chosen such that the momentum deficit matched that of the ribbons. Lynn (1987) found that the effect of the two types of LEBUs were very similar; the integrated skin friction reduction of the wires was slightly less because downstream effects of the wires relaxed sooner than the effects of the ribbons. This was attributed to the fact that the ribbon LEBUs effectively broke up the large scale structures, which were similar in size to the ribbons, whereas the wires introduced more energetic small scales which have been shown to hinder skin friction reduction.

Although large local skin friction reductions have been achieved by Plesniak and Nagib (1985) and Anders and Watson (1985), there is usually no significant net drag reduction because of the high drag associated with the devices and the supports that are present to suspend them above the wall. Many researchers that report a net reduction use indirect methods of computing drag (e.g. momentum balance, addition of device drag to computed skin friction reduction) and do not account for the drag associated with the supports. Sahlin *et al.* (1986, 1988) made direct drag measurements in a towing tank and achieved no net drag

reduction in all but one case, and in that case the reduction was very slight, only 2 percent.

1.1.2 Polymer Injection

The interest in using polymers to achieve skin friction reduction was initially generated when Toms (1948) observed that the pressure drop in a turbulent pipe flow was reduced with the addition of polymers to a solvent over that of the solvent flow alone. This has become known as the Toms Phenomenon. The pressure drop in the pipe demonstrated that the wall shear stress at a given mass flow rate was reduced. Since then, Wells and Spangler (1967) have verified that the addition of polymer into a turbulent pipe flow reduces local shear stress on the wall. Turbulent pipe flow with either homogeneous or heterogeneous polymer solutions have been studied extensively. Lumley (1969) and Berman (1978) provide review article discussions.

Polymer skin friction reduction in external flows is also of interest and attempts have been made to optimize the use of slot injected polymer solutions for skin friction reduction. Wu and Tulin (1972) conclude that the slot injection angle should be small with respect to the flow direction and the slot opening should be comparable with the thickness of the viscous sublayer to achieve the most effective polymer skin friction reduction in external TBL flows. However, Tiederman *et al.* (1985) have demonstrated that there is a minimal slot width effect. By injecting polymer solutions into a flat plate TBL, Wu and Tulin (1972) report a maximum integrated drag reduction over a large drag balance on the order of 50 percent. Fruman and Marshall (1976) and Latto and El Riedy (1976) also report similar results. These results support the theory that polymers are

the most effective drag reduction method in turbulent flows.

Although there is no precise understanding on the acting mechanisms involved, it is generally accepted that the injected polymer must be in the near wall region for maximum benefit, and that drag reduction is achieved through the suppression of high frequency turbulence associated with the buffer region of the TBL.

1.2 Objectives

Upon injecting polymer into a flat plate TBL, a diffusion process is initiated which dilutes the concentration of the polymer solution in the near wall region of the TBL. If the diffusion rate of injected polymer could be suppressed, higher concentrations of polymer could be maintained near the wall over a greater streamwise distance resulting in more skin friction reduction with the same amount of injected polymer. Park (1988) was successful in showing qualitatively with flow visualization that LEBU devices appear to diminish the polymer diffusion rate away from the wall after slot injection into a TBL.

It is the objective of this research to use LEBU devices and polymer injection in combination and quantify, from velocity profiles and polymer concentration measurements, these effects far downstream of the injection slot. Also, the diffusion of a passive contaminant, water, in a LEBU modified TBL was investigated.

This investigation was primarily a proof of concept. Only one LEBU configuration close to that deemed optimum from previous work was examined and no optimization process was pursued.

Chapter 2

EXPERIMENTAL APPARATUS AND PROCEDURE

2.1 Experimental Facility

Experiments were performed in the axisymmetric test section of the Penn State Applied Research Laboratory 0.3048 m diameter water tunnel. This facility is a closed circuit tunnel with a 15,400 ℓ water capacity. The 9:1 inlet contraction ratio and various honeycomb turbulence control sections produced a measured freestream turbulence intensity of less than 0.3%. Acrylic windows permitted optical access to the bottom and both sides of the water tunnel test section and were mounted such that a smoothly blended fitting was made with the interior of the test section. A tent constructed of black plastic was erected around the entire test section area to prevent ambient light from entering. This was crucial for the LIF measurements, as will be discussed later.

All tests were conducted at a freestream velocity of 4.6 m/s and a tunnel pressure of 172.4 kPa. The pressure was chosen to prevent cavitation on the flat plate leading edge.

2.2 Flat Plate and LEBU Assembly

A brass flat plate mounted in the horizontal centerplane of the water tunnel test section was used for all experiments, and a scale drawing is shown in figure 2.1. The plate has a length of 1.2 m, a span of 0.3048 m, and a thickness of 19.05 mm. A two-dimensional Shiebe form nose was constructed to reduce leading edge cavitation. An asymmetric tail was used to induce a negative angle of attack at the leading edge to avoid unsteady separation on the

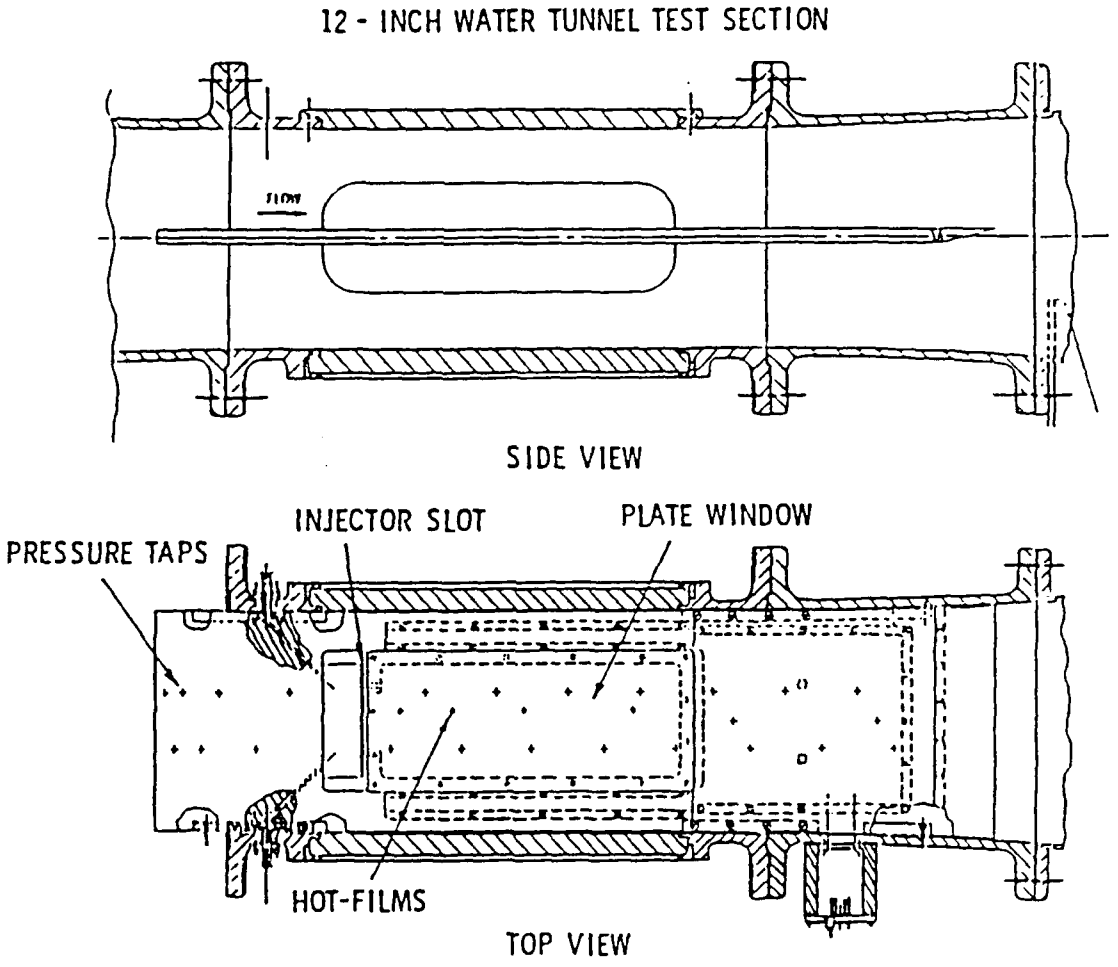

Figure 2.1. Scale drawing of flat plate mounted in axisymmetric test section

working surface side of the nose of the plate. A 0.455 m long by 0.190 m wide rectangular portion of the plate beginning 5 mm downstream of the injection slot was acrylic to provide laser beam access through the plate. Static pressure surveys indicate no significant axial pressure gradient exists in the test section at the surface of the plate and laser-Doppler velocimeter profiles from Fontaine *et al.* (1990) show that the TBL develops in good agreement with established empirical relationships for zero pressure gradient two-dimensional TBLs.

The polymer injection slot spans 0.152 m of the plate center and is located 0.292 m downstream of the plate leading edge and 0.355 m downstream of the boundary layer virtual origin. The slot has a 1 mm wide exit and the convergent walls comprising the slot are shown in figure 2.2. A small plenum is located in the plate beneath the injection slot and is packed with a coarse nonmetallic fiber to ensure a uniform exit flow. The plenum is supplied by two 12.7 mm diameter tubes, one on each side, which connects to a pressure tank fed from a 100 ℓ storage vat by means of a peristaltic pump. An air bubble in the pressure tank removes pump pulsations from the injection flow. The pump was calibrated at the test pressure and velocity to give a desired flow rate by setting the motor rpm. The pump calibration was verified to within 6% several times throughout the investigation.

Although not shown in figure 2.1, a tandem pair of ribbon LEBU devices with cylindrical leading and trailing edges were mounted upstream of the polymer injection slot. The LEBU dimensions normalized with the unmodified boundary layer thickness at the leading edge of the upstream LEBU, δ_u, are shown in table 2.1. Figure 2.2 shows the general layout of the LEBUs and the location relative to the injection slot position. The LEBU elements did not appear to flutter or bow at the test velocity when examined visually through a

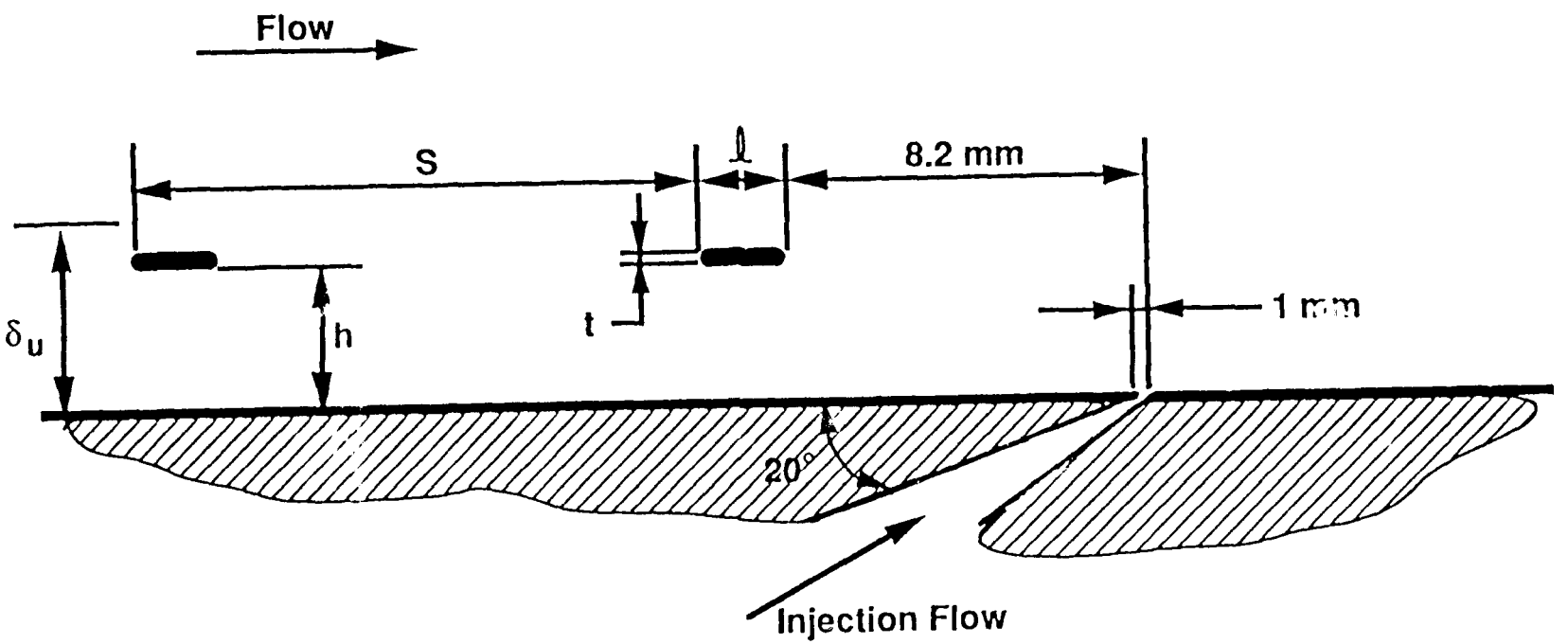

Figure 2.2. Drawing of LEBU devices and their position on the flat plate relative to the injection slot (not to scale)

Table 2.1 Optimal and present LEBU configuration

LEBU parameter*	optimal value**	present value
ℓ/δ_u	1.0	0.5
h/δ_u	0.8	0.8
s/δ_u	5 to 15	6.2
t/δ_u	0.005	0.08

* δ_u is the boundary layer thickness at the leading edge of the upstream LEBU

** As given by Plesniak and Nagib (1985)

long range microscope under stroboscopic light illumination. Several factors required the use of thicker than optimum LEBU elements. These include the high dynamic head of water compared to air, the constraints of the test section, and the small boundary layer thickness due to the size of the test section and flat plate. Since the devices are thicker, a smaller than optimum chord length was used to produce a momentum deficit similar to the optimum devices. The device drag is in all likelihood larger than it would be if the optimum geometry were used, but it is more important in this investigation to introduce a momentum deficit from stable LEBUs to determine the effects on polymer diffusion than to use thinner, unstable devices.

The LEBU devices were constructed by tensioning four strands of 0.38 *mm* diameter stainless steel wire across the plate with a center-to-center wire spacing of 0.64 *mm*. The wires were wrapped around the plate and were held on threaded rods mounted on blocks. These blocks were fitted into a cut-out section of each side of the plate. Tensioning the wires was done manually. Two cylindrical aerodynamic struts with a diameter slightly greater than the height of the wires were then positioned between the plate surface and wires approximately 63.5 *mm* from the tunnel side walls. This was done to provide extra stability by cutting down on the large unsupported distance the wires must span. These struts were well outside the measurement locations to avoid interference with the flow in that area. The gaps between the wires were filled with a metal bonding and filling material. Imperfections in the filler surface were sanded smooth with emery paper.

2.3 Polymer Preparation

The polymer solution used in this investigation was polyethelene oxide (polyox) at a 500 weight part per million (WPPM) concentration. The mean molecular weight, according to the manufacturer, was 5×10^6.

The 500 WPPM polyox solutions were made as follows. Tap water was stored in 100 ℓ storage vats for a period of at least 24 hours to dechlorinate, because the chlorine in tap water is known to degrade polyox. After this period of time, 49.9 grams of polyox were slowly stirred into the water and allowed 15 to 24 hours to completely hydrate. During this time, the solution was periodically agitated to further stimulate hydration.

2.4 LDV Technique

One- and two-component forward scatter laser-Doppler velocimeter (LDV) systems were used to map the LEBU wake and resulting TBL modifications. The one-component system was used in the initial experiments to determine the gross features of the modified TBL, whereas a two-color two-component LDV system was used in subsequent tests to obtain more detailed information.

2.4.1 LDV Instrumentation and Procedures

A 15 mW Helium-Neon laser provided a red 632.8 nm wavelength beam for the one-component forward scatter system. The transmitting optics produced a nominal probe volume diameter to the e^{-2} intensity level of 61 microns and included a 2.27× beam expander and a 242.6 mm focal length lens.

A 5 W Argon-Ion laser was used in the two-component forward scatter system. Here, the transmitting optics produced a nominal probe volume diam-

eter to the e^{-2} intensity level of 84 microns and included two Bragg cells, a 3.75× beam expander, and a 480 *mm* focal length lens. This system required two probe volumes, from four laser beams, to be focused at the same point in space to achieve coincident data. Two blue 488 *nm* wavelength beams formed the probe volume to measure the streamwise velocity component, and two green 514.5 *nm* wavelength beams formed the second probe volume to measure the vertical velocity component. One of the green beams was positioned on the optical centerline to allow easier optical access to the wall.

The transmitting optics for both systems were mounted on a breadboard which was secured to a traversing table. Vertical increments of 0.025 *mm* (0.001 inch) could be accurately measured by means of a dial gage attached to the table. The laser beams were directed at a slight angle, approximately 1.5 degrees, through the test section to get the probe volumes closer to the surface for near wall measurements.

Collection optics were mounted on the opposite side of the water tunnel test section on an x-y translation stage which was mounted on a precision jack for three degrees of freedom. For the two-component system, color separation was achieved with a dichroic mirror and narrow bandpass color filters.

Coincident two-component data were obtained at all but the most upstream locations. Here, window warpage due to stress from a retaining ring deflected the laser beams slightly such that coincidence was not achieved. Consequently, two-component noncoincident data were obtained at these locations.

LDV data were obtained both with and without polymer injection. Water injection is known to have little effect on the velocity profiles except for small effects on the turbulence levels very near the slot, as reported by Fontaine *et al.* (1990). Therefore, no LDV data were taken with water injection. Polymer was injected at a rate of $5Q_s$ for the LDV surveys, where $1Q_s$ is the flow rate per

unit span through the viscous sublayer from the wall to $y^+ = 11.6$, as defined by Wu and Tulin (1972). For the present setup, $1Q_s$ is 0.62 $\ell/min.$, approximately.

Different amounts of LDV data were taken at various locations in each survey for consistent statistical accuracy. Outside the boundary layer, the velocity fluctuations are very small and thus only 1000 samples were needed. Once inside the wake region, the velocity fluctuations are larger and the number of samples increased to 2000 to get the same accuracy. Finally, inside the logarithmic region where the velocity fluctuations are quite large, the number of samples increased to 4000. Also, close to the LEBUs, 4000 samples were taken within the LEBU wake. Using this procedure, a maximum of 0.9% uncertainty in the mean velocity was realized.

The tunnel was seeded with approximately 3.5 g of silicon carbide particles, with a mean diameter of 1.5 μm. A proportional amount of seed was added to the 100 ℓ storage vats of polymer to reduce the possibility of statistical biasing of the velocity measurements due to particle number density differences. This particular type of biasing arises often in mixing flows.

Boundary layer and LEBU wake profiles were acquired at various streamwise locations. At each location, for a given vertical position in the TBL, data were first taken with no injection and then with polymer injection. This ensures that comparisons can be made between the two cases based on the exact same vertical position in the boundary layer. After each survey, the tunnel was drained, refilled, and seeded before moving to the next measurement location. The polymer concentration buildup in the tunnel never exceeded 1.5 WPPM. Since a typical boundary layer LDV survey took 2 hours to complete, it is expected that the low background concentration polymer solution in the freestream is degraded appreciably during the period of the survey.

2.4.2 LDV Data Reduction Procedures

Partial on-line data reduction was employed while performing the LDV surveys to help insure the acquisition of good data. At each location in the boundary layer, the mean, standard deviation, local turbulence intensity, skewness, and kurtosis of the velocity samples were calculated and displayed on the personal computer. Also, a graphical display of the data in one-dimensional histograms and two-dimensional scatter plots was possible.

The local flow velocity is determined solely from the heterodyne frequency of light scattered by particles traversing the probe volume formed at the intersection of two focussed laser beams. The photodetector converts the light signal to an electrical signal and TSI model 1980B counter signal processors determine this heterodyne frequency. The velocity of the particles normal to the fringes is:

$$u_i = (f_{D_i} - f_s) d_f \tag{2.1}$$

where u_i = velocity of i^{th} particle
f_{D_i} = frequency of i^{th} particle detected by photodetector
f_s = Bragg cell shift frequency
d_f = fringe spacing

The fringe spacing is determined from the laser beam wavelength, λ_{beam}, and the focussing lens half angle, ϕ, through the relation:

$$d_f = \frac{\lambda_{beam}}{2 \sin \phi} \tag{2.2}$$

At each vertical location in an LDV boundary layer survey, N velocity samples, u_i, were obtained and the local mean velocity, U, was determined by:

$$U = \frac{\sum_{i=1}^{N} u_i}{N} \tag{2.3}$$

The standard deviation, σ, of the samples is given by:

$$\sigma^2 = \frac{\sum_{i=1}^{N} (u_i - U)^2}{N-1} \tag{2.4}$$

and the local turbulence intensity, $T.I.$, is given by:

$$T.I. = \frac{\sqrt{\overline{u^2}}}{U} \times 100 \tag{2.5}$$

Here, u is the deviation of the streamwise velocity component from the mean and its rms value, u', is approximately equal to the standard deviation for large N. Finally, the higher order statistics are given as:

$$SK = \frac{\sum_{i=1}^{N} (u_i - U)^3}{N\sigma^3} \tag{2.6}$$

$$KU = \frac{\sum_{i=1}^{N} (u_i - U)^4}{N\sigma^4} \tag{2.7}$$

where SK and KU are the skewness and kurtosis of the data sampled, respectively. Note that kurtosis is often referred to as the flatness factor.

Skewness is a nondimensional measure of a function's symmetry about a given origin. A Gaussian function is symmetric about the origin and $SK = 0$. Positive skewness indicates that a function has more large positive values than large negative values and a characteristic positive tail is observed in the function. The opposite is true for negative skewness.

Kurtosis is a nondimensional measure of the function's flatness and a Gaussian function has a value of $KU = 3$. A large kurtosis indicates that a function

has large deviations far away from the mean, whereas a small kurtosis indicates that data are distributed consistently closer to the mean.

Determination of the vertical velocity component, v_i, and statistics is exactly analogous to the procedure given above. Thus, documentation will not be presented here.

The statistical biasing of the measured velocities was investigated. A velocity bias arises in turbulent flows when the instantaneous velocity is of different magnitude than the mean. More fluid passes through the probe volume when the instantaneous velocity is higher than the mean and less fluid passes through the LDV prove volume when the instantaneous velocity is lower than the mean. Thus, McLaughlin and Tiederman (1973) argue that the probability for measuring a velocity larger than the mean is greater than the probability of measuring velocity slower than the mean and the histogram of the individual velocity realizations is biased toward the faster end of the velocity range.

To correct this bias, an inverse weighting function may be used. McLaughlin and Tiederman (1973) proposed a one-dimensional velocity inverse weighting function (w_i) as:

$$w_i = |u_i|^{-1} \tag{2.8}$$

This has been extended to a two-dimensional velocity inverse weighting function as:

$$w_i = \frac{1}{(u_i^2 + v_i^2)^{\frac{1}{2}}} \tag{2.9}$$

A detailed examination of the two-dimensional weighting function is presented by Petrie *et al.* (1988). Comparison of biased and corrected velocity profiles in a LEBU modified TBL, figure 2.3, shows that there is a negligible velocity bias in the present investigation. This is due to the fact that the turbulence intensities,

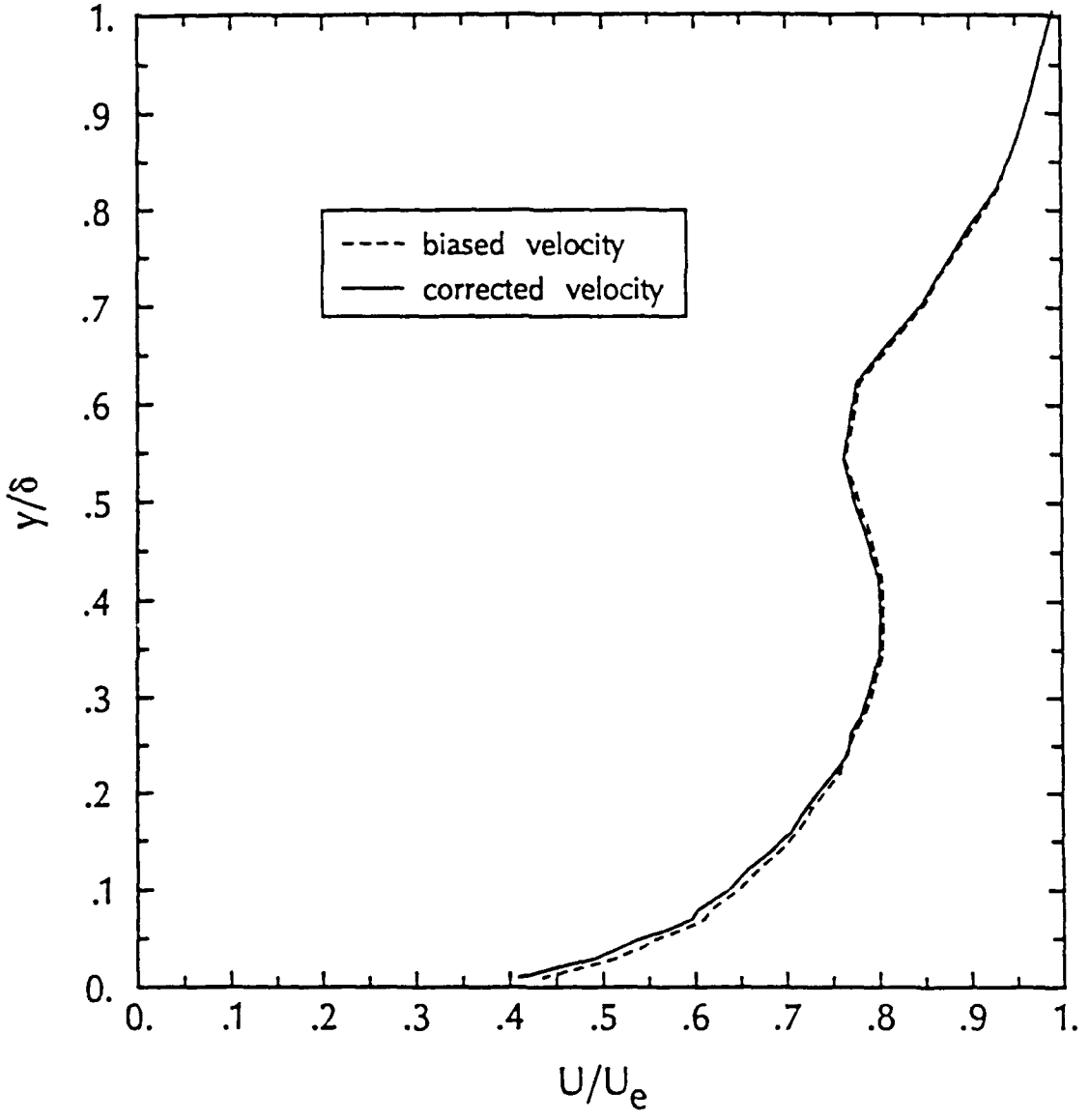

Figure 2.3. Comparison of velocity biased and corrected velocity profiles in a LEBU modified TBL

or velocity fluctuations, are not too large throughout the entire TBL. Thus, no velocity bias correction was used on any of the LDV profiles.

2.5 LIF Technique

A laser-induced fluorescence (LIF) technique to measure near instantaneous concentration profiles of a fluid injected into a TBL developed by Brungart *et al.* (1990) was used. Walker and Tiederman (1989) have examined polymer diffusion in a low speed channel by a similar approach. This technique was based on that originally developed by Koochesfahani and Dimotakis (1985). Excitation optics and system components are shown in figures 2.4 and 2.5, respectively, and were taken from Brungart *et al.* (1990).

The injectant fluid was seeded with a fluorescent dye prior to injection. The dye, fluorescein disodium salt, fluoresces with an intensity proportional to it's local concentration as it passes through an excitation laser beam. Since the Schmidt number for the diffusion of polymer and dye in water is $\gg 1$, molecular diffusion in water flow is negligible. Tennekes and Lumley (1972) also argue that diffusion by turbulent fluctuations is very rapid compared to molecular diffusion. Thus, since molecular diffusion is very small, both the polymer and dye concentrations remain proportional as they mix with the surrounding water.

2.5.1 LIF Theory

The present section outlines the theory and relationships behind the LIF procedure. For a more detailed account, please refer to Koochesfahani and Dimotakis (1985), Brungart *et al.* (1990), and Brungart (1990).

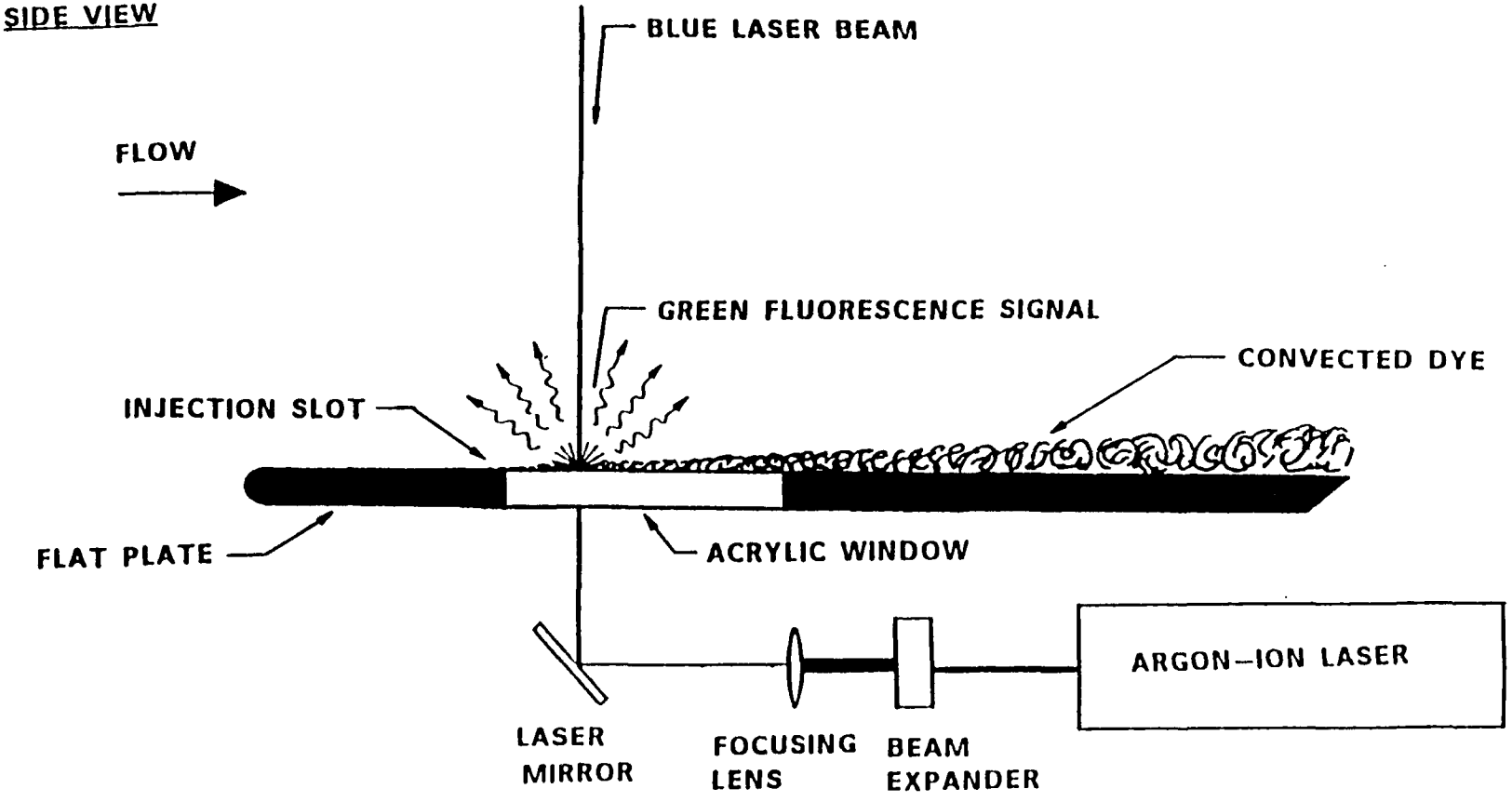

Figure 2.4. LIF excitation optics [taken from Brungart *et al.* (1990)]

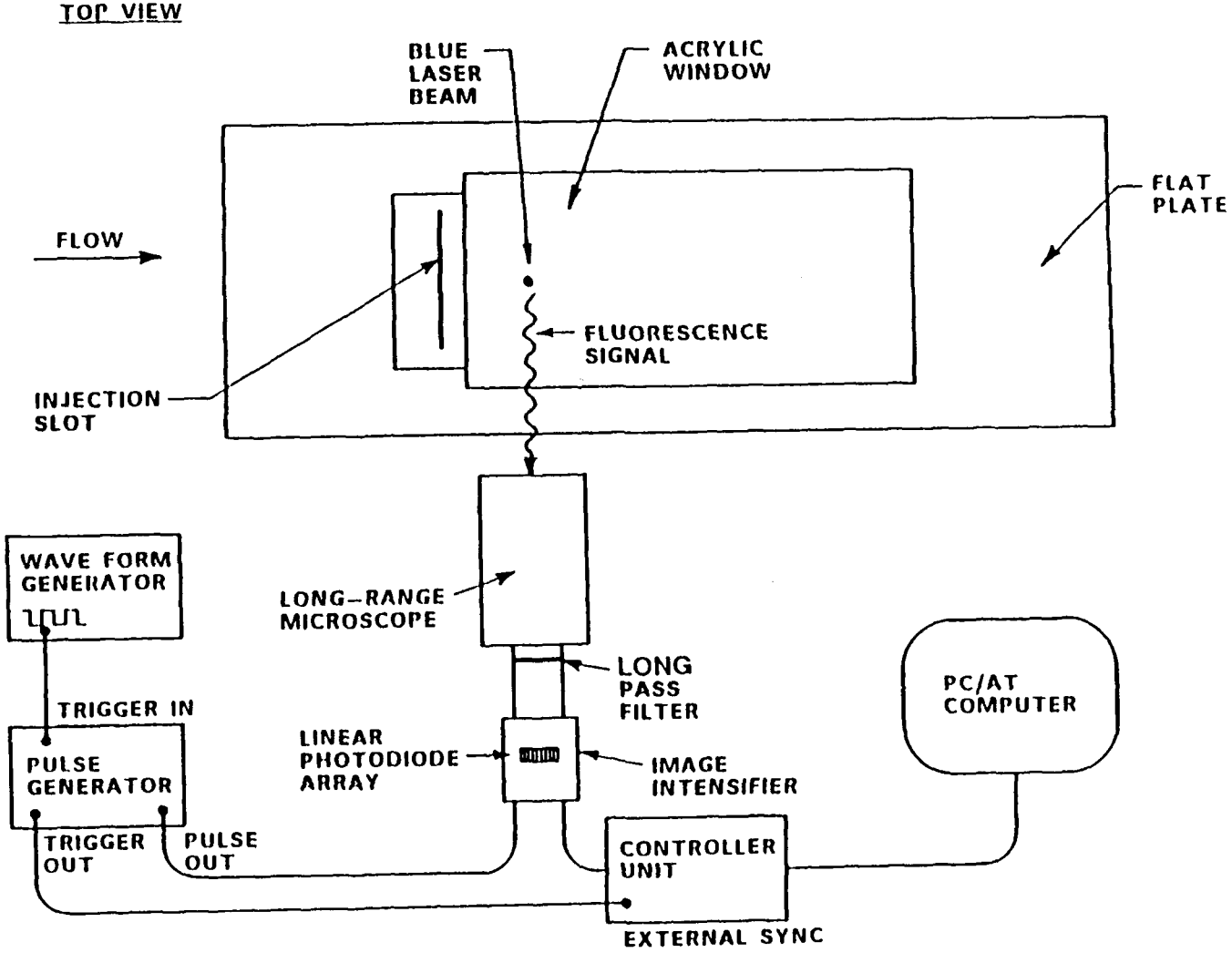

Figure 2.5. LIF imaging optics, electro-optics, and electronics [taken from Brungart *et al.* (1990)]

The integrated form of the Lambert-Beer law for the attenuation of a laser beam passing through a fluorescent dye solution is given as:

$$I(y) = I(y_0)\mathrm{e}^{-\varepsilon \int_{y_0}^{y} C(y)dy} \tag{2.10}$$

where I = laser beam intensity $(watts/m^2)$

y = distance from reference position on laser beam axis (cm)

y_0 = reference position (cm)

ε = *extinction coefficient* of the dye in the solvent$(\ell/cm \times moles)$

C = dye concentration $(moles/\ell)$

Walker (1987) gives a value of $87200/(cm \times moles/\ell)$ for the extinction coefficient of fluorescein disodium salt excited at the present 488 nm wavelength laser beam.

The fluorescence intensity emitted for an assumed average dye concentration, C, over a small Δy slice of the excitation laser beam at a point y is given as:

$$I_f(y) = QI(y)(1 - \mathrm{e}^{-\varepsilon C \Delta y}) \tag{2.11}$$

where I_f = fluorescence intensity

Q = quantum yield of the dye

Using a series expansion for the exponential term for $\varepsilon C \Delta y \ll 1$ (the largest value of $\varepsilon C \Delta y$ in this investigation was approximately 8.7×10^{-4}), equation (2.11) yields:

$$I_f(y) = QI(y)\varepsilon C \Delta y \tag{2.12}$$

Substituting (2.10) into (2.12) yields, for $\varepsilon C \Delta y \ll 1$:

$$I_f(y) = Q\varepsilon C \Delta y I(y_0)\mathrm{e}^{-\varepsilon \int_{y_0}^{y} C(y)dy} \tag{2.13}$$

Equation (2.13) gives a relation for the fluorescence intensity emitted from a small slice of the laser beam and accounts for beam attenuation between y_0 and y.

A general expression for the output signal strength of the i^{th} photo diode is:

$$V_i = K_i I_{f_i} + N_i \tag{2.14}$$

where V_i = output signal of i^{th} photo diode in counts

K_i = equation constant of i^{th} photo diode

I_{f_i} = fluorescence intensity emitted by the slice of the laser beam imaged onto the i^{th} photo diode

N_i = noise and background signal at i^{th} photo diode

The equation constant, K_i, takes into account factors inherent to the system, such as light collection solid angle, window and lens reflections and imperfections, pixel sensitivity, image intensifier gain, gate period, etc. Discretizing equation (2.13) and substituting into (2.14) yields:

$$V_i = A_i C_i \prod_{j=1}^{i-1} e^{-\varepsilon C_j \Delta y} + N_i \tag{2.15}$$

where A_i is a combination of constants. Equation (2.15) relates the local dye concentration directly to the output signal from the i^{th} photodiode of the intensified line camera and takes into account the laser beam attenuation over its path to the i^{th} pixel.

2.5.2 LIF Instrumentation

A 488 nm wavelength excitation laser beam was provided by a 5 W Argon-Ion laser, which was mounted beneath the water tunnel test section, figure 2.4.

The laser was operated at an output power at this wavelength of 400 mW in the constant power mode to limit output fluctuations to 0.5%. The laser beam passed through a 5× beam expander and a 580 mm focal length lens before being directed normal to the plate by a dielectric laser mirror. The focused beam waist was slightly above the test plate surface and had a theoretical diameter to the e^{-2} intensity level of less than 50 microns.

The fluorescent radiation was collected by a Questar model QM1 long range microscope (figure 2.5) and focused onto the input window of an electronically gated Princeton Instruments model IRY-512 single stage image intensifier. The intensifier was fiber optically coupled to a 512 pixel element linear photo diode array. The center-to-center pixel spacing on the array was 25 microns. Microscope magnifications were typically 2.5×. Scattered 488 nm excitation radiation was eliminated from the signal by placing a long pass optical filter between the long range microscope and the input window. This filter had a 50% cut-off at 515 nm. The image intensifier provides a high luminus gain and was gated open to pass photons for a shutter period of approximately 7 microseconds to obtain ensembles of near instantaneous concentration profiles. The controller, shown in figure 2.5, scanned and reset the array after each gate period of the image intensifier. A square wave generator provided the trigger signal that initiated gating of the image intensifier at a 55 Hz trigger frequency. The digitized data were stored on a personal computer. A more complete description of the development and capabilities of this system can be found in Brungart (1990) and Brungart *et al.* (1990).

2.5.3 LIF Procedures

LIF data were obtained with both water and polymer injection at injection rates of 2, 3, 4, 5, and 10 Q_s. Water injection was performed to determine the effects of LEBUs on the diffusion of a passive contaminant in a LEBU modified TBL.

Fluorescein disodium salt was premixed with the injectant solutions prior to injection. Once mixed, the dyed solutions were allowed to sit for at least 15 hours before using because the fluorescence intensity is known to decay exponentially with time. This effect is more pronounced in the water than in the polymer solutions. Thus, the fluorescence of the dyed solutions was allowed to stabilize before calibrating and running the experiment. During this waiting period, the storage vats were covered with black plastic to minimize photobleaching effects. Dye was added to the polymer solutions to a concentration of 1×10^{-6} $moles/\ell$. Water was allowed to sit for a period of at least 24 hours to dechlorinate before the dye was added to a concentration of 4×10^{-6} $moles/\ell$. Higher dye concentrations were used for water because of the very large diffusion rate. This high concentration is still well below values at which Koochesfahani (1984) reports the linear relationship between fluorescent intensity and concentration breaks down.

The pH of the injected solutions and tunnel water was also of some concern. Walker (1987) shows that the fluorescence of fluorescein disodium salt is very dependent on the pH, through the effects on the extinction coefficient, in the range of pH from 4 to 7.5. Above this pH, there is only a slight dependence. In the present experiment, the pH of the tunnel water and injectant water solutions was 7.57 and the pH of the polymer solutions was 7.58. Thus, there was negligible effect due to pH in the present experiments.

To obtain concentration profiles, several steps must be performed. These steps are:

A. Calibration
   1. Focus image of the laser beam on image intensifier input window
   2. Determine microscope magnification
   3. Obtain *tunnel as a flow cell* data to compare with all future calibrations
   4. Obtain flow cell calibration data

B. Obtain concentration profile data

The term A_i in equation (2.15) is determined during calibration and involves relating the output signal to a known dye concentration. During calibration, the dye concentration in the flow cell is constant; thus, dropping the indices on C and solving (2.15) for A_i yields:

$$A_i = \frac{V_i - N_i}{C \prod_{j=1}^{i-1} e^{-\epsilon C \Delta y}} \tag{2.16}$$

The term N_i, is determined at each pixel location before injecting a particular dyed solution into the TBL to account for and subtract off the noise present in the signal with no input. For accurate results, calibration must be performed at each measurement location with the same dyed water and polymer solutions to be injected into the TBL. With the laser beam waist positioned just above the working surface of the acrylic window in the flat plate, a scribed ruler was placed in the vertical laser beam. Focusing the system was accomplished by adjusting the microscope to produce a sharp image of the scribes on the ruler on the near-real time display of the personal computer. Once focused, the microscope magnification was determined by counting the number of pixels between a given

number of ruler scribes. This procedure was done with water in the test section at a level a few inches above the plate to match the index of refraction and solid angle effects to the actual experiment.

Calibrations were performed by placing a small flow cell in the test section on the flat plate. This cell had no bottom surface and sealed against the plate acrylic window when weights were placed on top if it. Diluted concentrations of injectant solution were circulated through the flow cell as shown in figure 2.6. Three different concentrations of dye, ranging from the injection concentration to 1/4 of the injection concentration, were used for calibration to verify the linearity of fluorescence of fluorescein. Tunnel water was used for diluting the calibration solutions to simulate the actual diffusion and mixing. The calibration fluid reservoir was positioned well above the cell to allow gravity to drive the flow. This eliminated problems caused by air bubbles entering the cell as was encountered by Brungart (1990) when using a high speed pump to drive the flow. Air bubbles can significantly decrease the measured signal.

An alternative to this flow cell calibration procedure that is possible because the water tunnel volume is known accurately is to use the tunnel itself as a flow cell. However, this is only practical at dye concentrations two orders of magnitude lower than the injection dye concentrations due to excitation laser beam extinction and is not generally useful. Using the tunnel as a flow cell does serve a needed purpose by determining the form of the calibration curve free of any complications from the small flow cell. Only the magnitude of this calibration curve should differ from the higher concentration flow cell calibrations. The tunnel as a flow cell data were sampled after adding dye to the water tunnel to bring the entire tunnel to a concentration of approximately 2×10^{-8} $moles/\ell$. The freestream velocity used was the same as during the injection experiments.

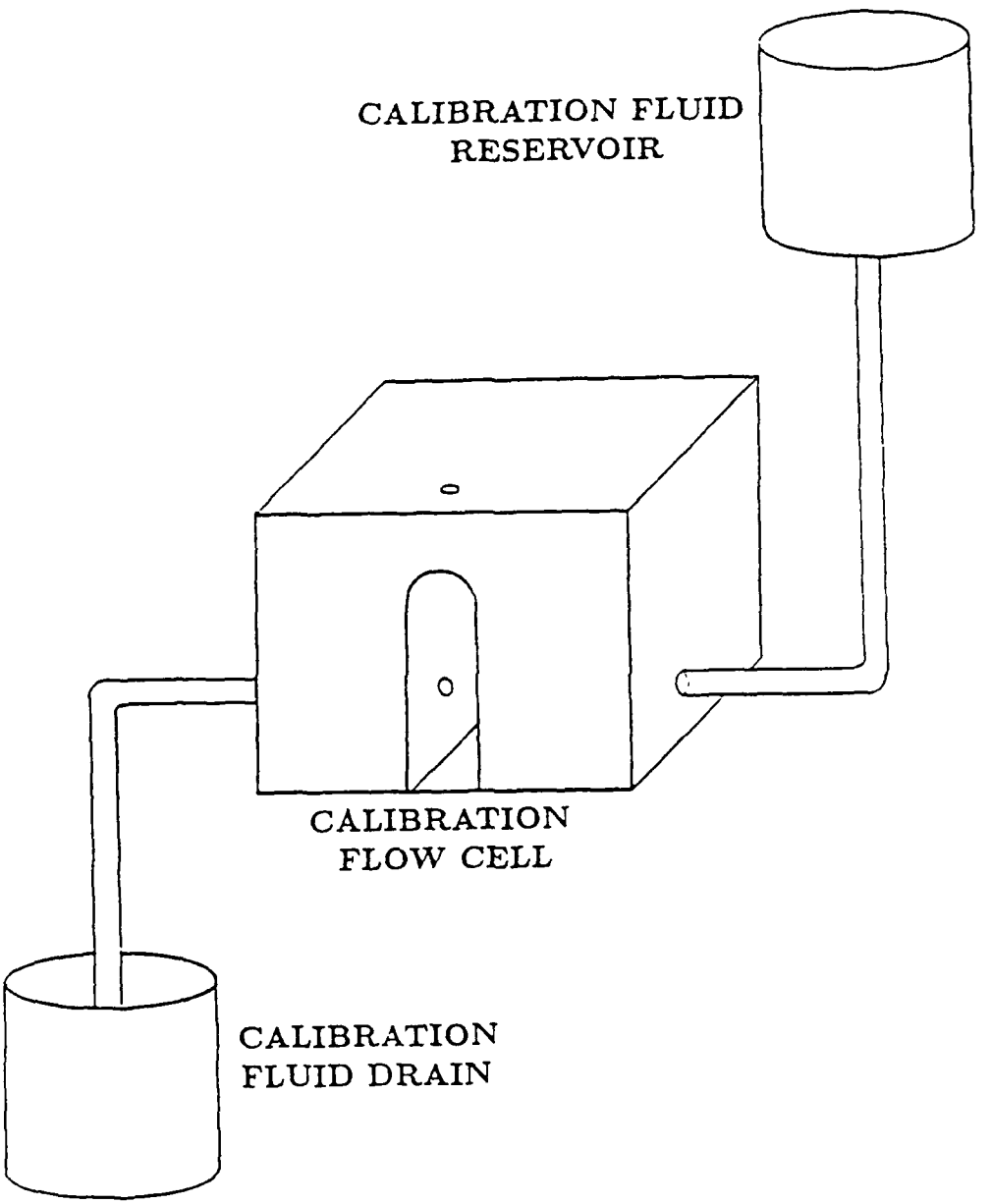

Figure 2.6. Diagram of the calibration flow cell system

The form of the water calibrations obtained with the flow cell were in excellent agreement with the tunnel as a flow cell, consistent with Brungart (1990). The form of the polymer calibrations were also in excellent agreement with the tunnel as a flow cell except near the wall. Both calibrations should have the same form because there is a uniform concentration of dye in the cell. Figure 2.7 is a plot of the normalized counts versus pixel number for a polymer calibration. The data were taken with the wall set at pixel 50, but the data in figure 2.7 have been shifted so that the wall is at pixel 0 and data below the wall is not shown. The tunnel as a flow cell data has been scaled for this comparison so the curves have the same value away from the wall. Normalizing in such a manner makes it possible to compare the output signal of different dye concentration profiles. Figure 2.7 shows a dropoff in output signal of the flow cell compared to the tunnel as a flow cell calibrations in the near wall region. This discrepancy was typical of all the polymer calibrations and may be attributed to photobleaching effects. Fluorescent dyes photobleach when continuously exposed to excitation radiation. See Brungart (1990) for a discussion of the effects of photobleaching on fluorescein.

The 50 pixel region in figure 2.7, where photobleaching is a problem, is a layer on the wall only 500 microns thick. Several factors could contribute to this photobleaching of the dye near the wall. The higher viscosity of the polymer slowed the mean flow down through the flow cell system by approximately 30% compared to water. The absolute viscosity for polymer was estimated with a viscometer at varying shear rates. For 500 WPPM polyox, the absolute viscosity was approximately 7 *cps* at very low shear rates and dropped off to a fairly constant value of approximately 3 *cps* above a shear rate of $100/s$. The average Reynolds number of the water calibrations, based on the diameter of the connecting hose, was approximately $11,600$. But the average Reynolds number

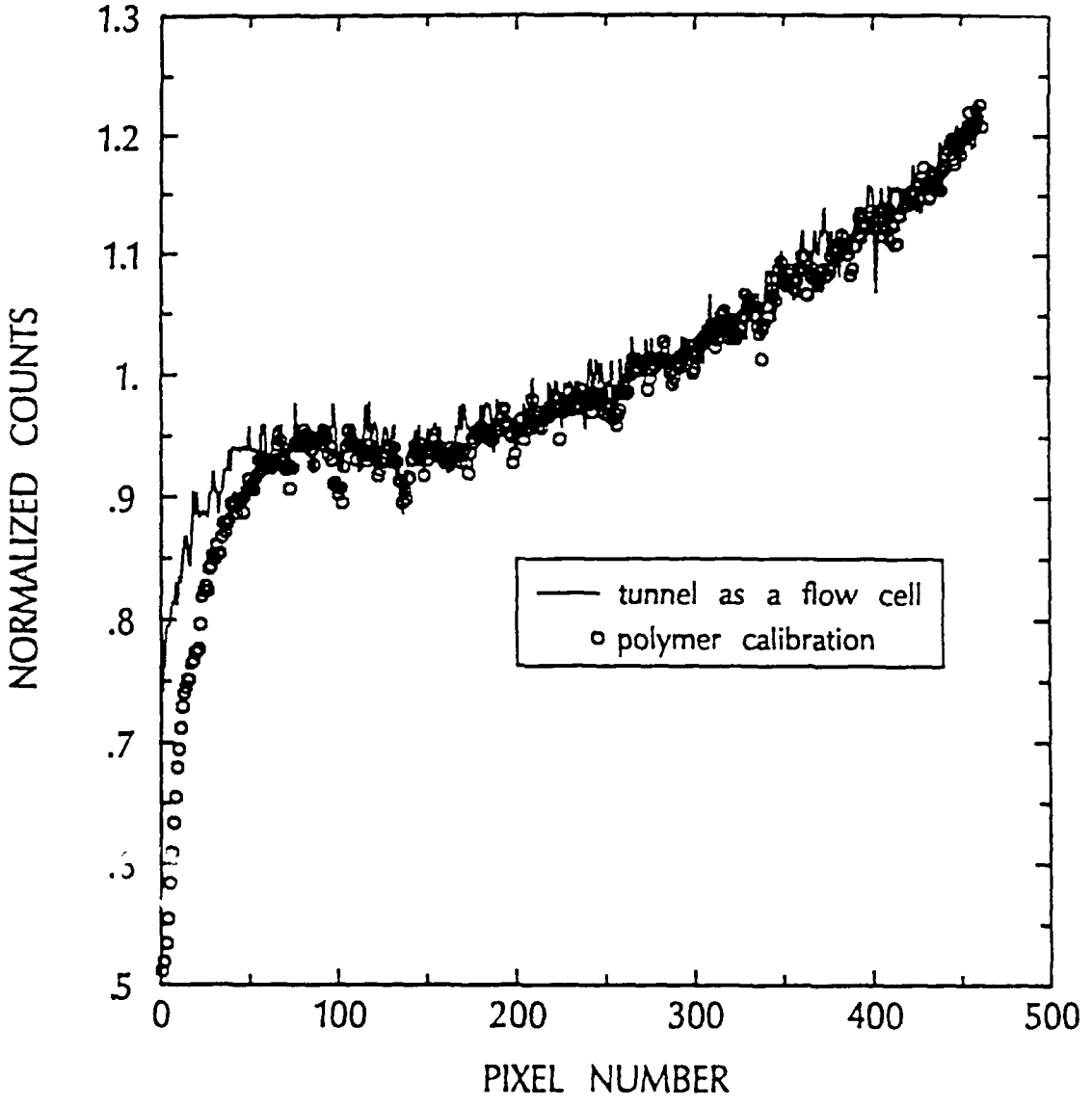

Figure 2.7. Comparison of normalized polymer calibration profile to the tunnel as a flow cell profile

of the polymer calibrations, based on the diameter of the connecting hose and using an absolute viscosity value of 3 *cps*, was approximately 2700. Because the Reynolds number of the flow in the polymer calibration is considerably lower, the flow could be transitional or even laminar. This would decrease the velocity gradient close to the wall, and the slower moving polymer solution could photobleach more readily near the wall. Also, there is the possibility of unsteady or recirculating flow near the wall in the flow cell which is more pronounced with the polymer solutions. The small excitation laser beam waist, required for resolution, and the laser power result in high photon fluxes making photobleaching a possibility if the flow does not continuously move through the laser beam.

The flow cell polymer calibrations were tested on data that was taken just downstream of the injection slot where the near wall region should be saturated with polymer at high polymer solution injection rates. The reduced results showed that there was approximately 130% of the injected concentration of polymer on the wall using the flow cell calibrations with the polymer solution. Since this is not possible, one can conclude that the dropoff in the flow cell calibration signal at the wall is inherent to the calibration flow cell system and not to the water tunnel itself. To correct for these flow cell calibration errors, scaled tunnel as a flow cell calibrations were used for the affected pixels near the wall. As shown in figure 2.7, the tunnel as a flow cell calibration can be scaled by a constant multiplicative factor to agree with the flow cell calibration away from the wall. The scaled tunnel as a flow cell curve is then used as the corrected calibration curve near the wall. The corrected calibrations were used on the same set of data as above and the results showed that there was approximately 100% of the injected concentration of polymer still on the wall, as expected close to the injection slot. Thus, all subsequent polymer calibrations were corrected in such a manner.

After calibration was completed, the flow cell was removed and the tunnel was filled. Data were obtained for water and polymer injection as detailed earlier. The tunnel was drained and refilled before moving to another measurement location. As with LDV surveys, the polymer concentration in the tunnel never exceeded 1.5 WPPM. Also, the background dye concentration never exceeded 8×10^{-9} $moles/\ell$ which resulted in slightly less than a 1% attenuation of the excitation laser beam from the bottom tunnel access window to the flat plate test surface.

The dye concentration at a given pixel can be determined by solving (2.15) for C_i (neglecting laser beam attenuation) as:

$$C_i = \frac{V_i - N_i}{A_i} \tag{2.17}$$

The calibration constants, A_i, have been determined from equation (2.16). Since the dye and injectant concentration remain proportional in the TBL, the local injectant concentration, WPPM_i, can be determined from the simple relation:

$$\frac{\mathrm{WPPM}_i}{\mathrm{WPPM}_{inj}} = \frac{C_i}{C_{inj}} \tag{2.18}$$

Here, C_i was determined from equation (2.17) and C_{inj} and WPPM_{inj} are the known injected dye and solution concentrations, respectively.

The mean higher order statistics of the concentration data samples were determined using C_i in place of u_i in equations 2.3, 2.4, 2.6, and 2.7 for the mean, standard deviation, skewness, and kurtosis.

Chapter 3
RESULTS

3.1 Velocity Profile Data

Velocity profile data were taken with the LDV systems described earlier at 6 stations downstream of the LEBU devices and the injection slot. Table 3.1 lists the streamwise distance from the slot to these measurement stations, x, and the nondimensionalized distance from the leading edge of the upstream LEBU, $\xi = x_u/\delta_u$. Various Reynolds numbers and boundary layer integral thicknesses and parameters for the LEBU modified boundary layer are also listed in table 3.1. Fontaine *et al.* (1990) have determined the standard boundary layer parameters for the same facility, flat plate, and flow conditions and these are listed in table 3.2.

Many comparisons in this chapter are made to a standard boundary layer. This simply refers to the flat plate boundary layer that has not been modified by LEBU devices.

3.1.1 Mean Profile Data

The downstream development of the streamwise component mean velocity profiles in the LEBU modified flow without (open symbols) and with (solid symbols) polymer injection are shown in outer variables in figure 3.1. The distance above the wall has been normalized with the local displacement thickness because it is better defined than the 99% boundary layer thickness in a TBL. A significant momentum deficit has been introduced by the LEBUs, as observed

Table 3.1 Measured LEBU modified boundary layer parameters

station	x (mm)	ξ	Ue (m/s)	$\mathrm{Re}^{a}_{x_0}$ 10^{-6}	Q_s	δ (mm)	δ^* (mm)	θ (mm)	H	Re_{δ^*}	Re_θ
1	25.4	14.0	4.58	1.72	0	6.84	1.04	0.72	1.44	4744	3284
2	38.1	16.8	4.59	1.79	0	7.23	1.09	0.75	1.45	4754	3429
3	50.8	19.5	4.59	1.84	0	7.39	1.16	0.79	1.47	5303	3612
					5	7.39	1.34	0.84	1.59	6126	3840
4	128.6	36.4	4.60	2.21	0	8.92	1.31	0.88	1.49	6002	4032
					5	8.92	1.44	0.95	1.52	6598	4352
5	231.8	58.9	4.60	2.68	0	10.46	1.46	1.04	1.41	6689	4765
					5	10.46	1.51	1.03	1.47	6918	4719
6	384.2	92.0	4.59	3.37	0	10.86	1.58	1.16	1.36	7223	5303
					5	10.86	1.59	1.09	1.46	7269	4983

a: x_0 measured from virtual origin of boundary layer

LEADING EDGE TO SLOT: 292.1 mm

VIRTUAL ORIGIN TO SLOT: 352.9 mm

Table 3.2 Measured standard boundary layer parameters [taken from Fontaine *et al.* (1990)]

x (mm)	U_e (m/s)	$Re^a_{x_0}$ 10^{-6}	Q_s	δ (mm)	δ^* (mm)	θ (mm)	H	Re_{δ^*}	Re_θ
50.8	4.48	1.81	0	5.74	0.99	0.69	1.43	4408	3088
			5	5.74	1.23	0.77	1.60	5482	3437
128.6	4.45	2.14	0	7.29	1.20	0.84	1.43	5340	3738
			5	7.29	1.30	0.86	1.51	5785	3835
231.8	4.44	2.60	0	8.23	1.43	1.03	1.38	6355	4595
			5	8.23	1.33	0.98	1.36	5910	4355
384.2	4.50	3.32	0	10.79	1.60	1.20	1.33	7191	5391
			5	10.79	1.62	1.12	1.45	7290	5040

a: x_0 measured from virtual origin of boundary layer

LEADING EDGE TO SLOT: 292.1 *mm*

VIRTUAL ORIGIN TO SLOT: 352.9 *mm*

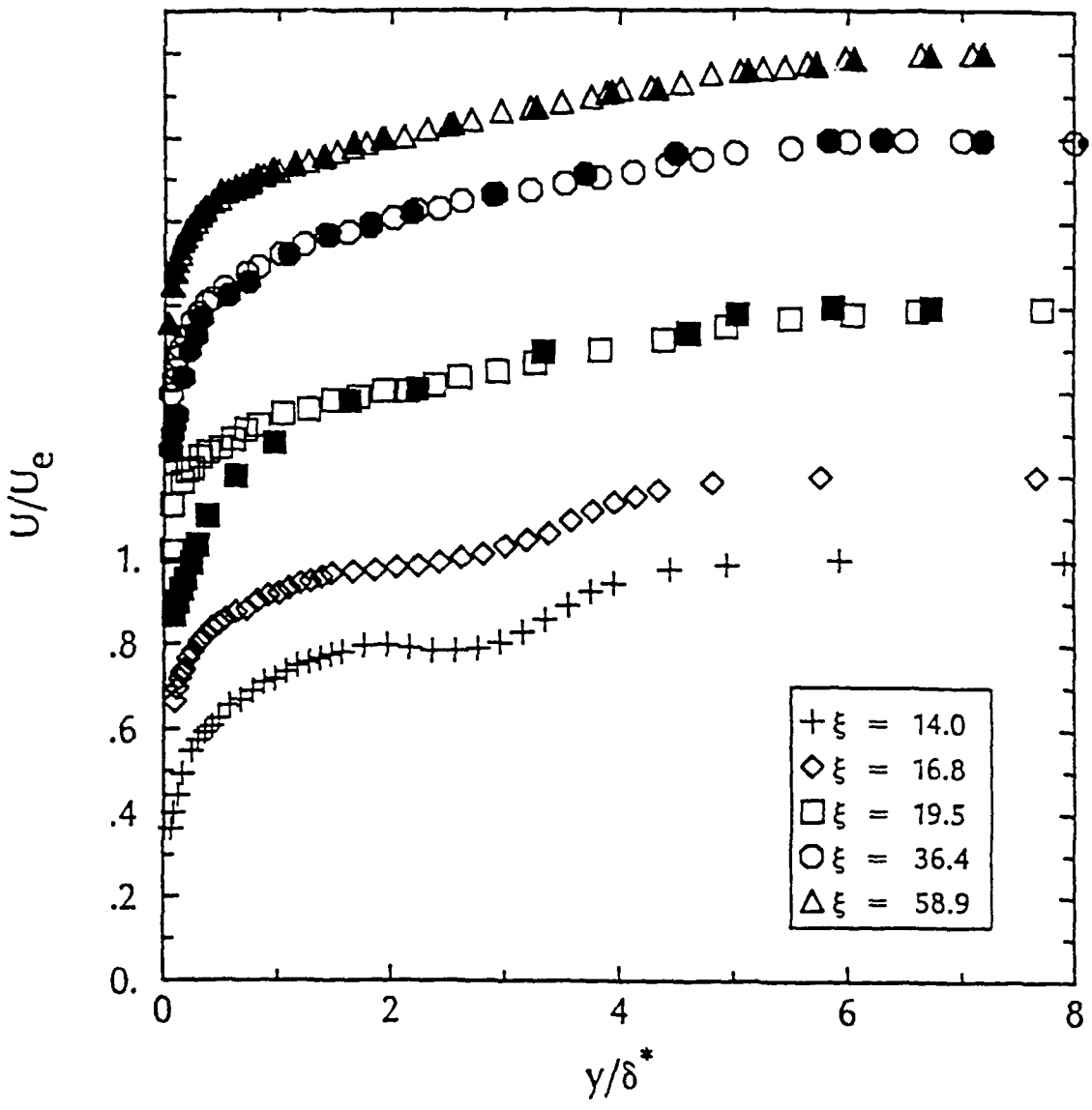

Figure 3.1. Downstream development of the mean streamwise velocity profiles in a LEBU modified TBL. Closed symbols for $5Q_s$ polymer injection

in figure 3.1 at $\xi = 14.0$. Slight LEBU effects on the mean velocity remain at $\xi = 36.4$, but by $\xi = 58.9$ the velocity profile has returned to a nearly standard shape. Westphal (1986) and Trigui and Guezennec (1990) observed that the effects of the LEBUs on the mean velocity profiles have relaxed by $\xi = 33$, and $\xi = 34$, respectively, while Chang and Blackwelder (1990) notice a slight effect on the mean velocity as far downstream as $\xi = 71$. Profiles with polymer injection show a deceleration of the mean flow near the wall that relaxes with increasing streamwise distance, consistent with the standard boundary layer data of Fontaine *et al.* (1990).

A good estimate of the friction velocity, u^*, is required for nondimensionalization purposes and skin friction estimates. This was done in the LEBU modified TBL with no polymer injection by using a method proposed by Chang and Blackwelder (1990) which uses a least-squares fit of the wall data to Spalding's (1961) law of the wall equation:

$$y^+ = u^+ + e^{-\kappa B}\left\{e^{\kappa u^+} - 1 - \kappa u^+ - \frac{1}{2}(\kappa u^+)^2 - \frac{1}{6}(\kappa u^+)^3\right\} \tag{3.1}$$

$$\text{where } u^* = \sqrt{\frac{\tau_w}{\rho}} \tag{3.1a}$$

$$u^+ = \frac{U}{u^*} \tag{3.1b}$$

$$y^+ = \frac{yu^*}{\nu} \tag{3.1c}$$

ν = kinametic viscosity of water

κ, B = equation constants

Since κ, B, and ν are known constants and y and U are the experimental data, the only unknown variable in equation (3.1) is u^*. Chang and Blackwelder (1990) only used data below $y^+ = 200$ to determine u^* from equation (3.1), thus avoiding the nonequilibrium portion of the LEBU modified boundary layer profile.

The same technique and cutoff on y^+ was used in the present investigation. This method was compared to results in which u^* was found by a least-squares error fit of the data to Coles (1956) law of the wall plus wake function, initially developed by Deutsch and Zierke (1986), used by Fontaine *et al.* (1990) in a standard TBL. A maximum of 1.7% difference in u^* was found using the two methods in a standard TBL.

Figure 3.2 shows the mean streamwise component velocity profile with no polymer injection at $\xi = 14.0$ in inner variables. Nondimensionalization was done using the estimated value of the friction velocity in the LEBU modified TBL described above. The solid line is Spalding's (1961) law of the wall equation, equation (3.1). The data below $y^+ = 200$ are in good agreement to Spalding's equation, but the momentum deficit introduced by the LEBUs altered the rest of the log region such that the data lie slightly below the curve out to approximately $y^+ = 400$. Between $y^+ = 400$ and 800, the LEBU wake is evident through the large decrease in the mean velocity. By $\xi = 58.9$, the data takes the form of Spalding's equation except between approximately $y^+ = 200$ and 600 where the data are slightly below the curve, as shown in figure 3.3. The constants in the universal law of the wall equation were found to be the same as for a standard boundary layer for every measurement location in the present investigation. This is in good agreement with Lemay *et al.* (1985), who found that the universal law of the wall was verified in a LEBU modified TBL at all locations except less than 10 boundary layer thicknesses (δ_u) downstream of the trailing edge of the downstream most device.

The friction velocities estimated for the streamwise component mean velocity profiles from above were used to determine the skin friction coefficient, C_f, through the relation:

$$C_f = 2(u^*/U_e)^2 \tag{3.2}$$

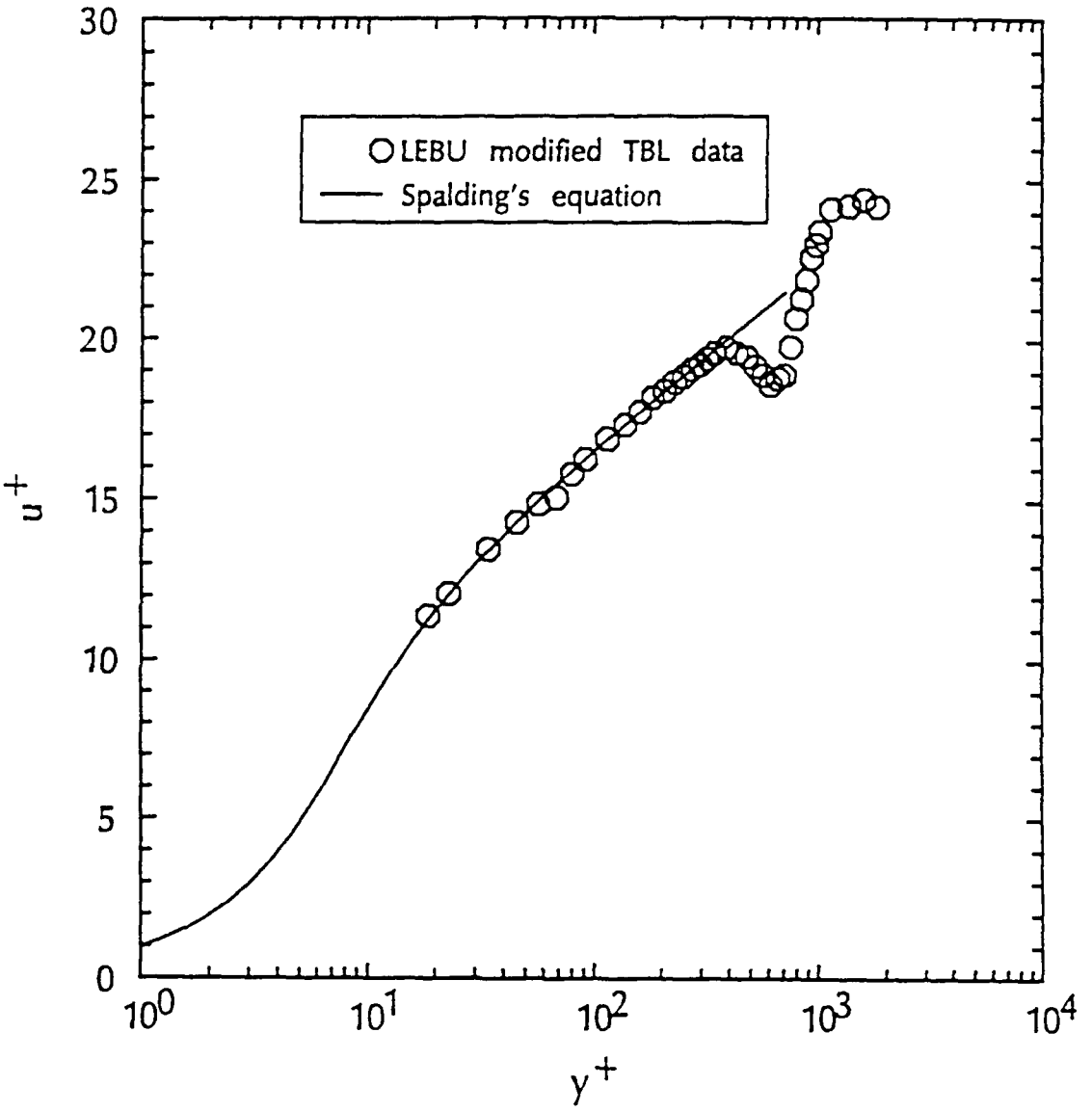

Figure 3.2. Inner variable plot of the mean streamwise velocity profile in a LEBU modified TBL at $\xi = 14.0$, no injection

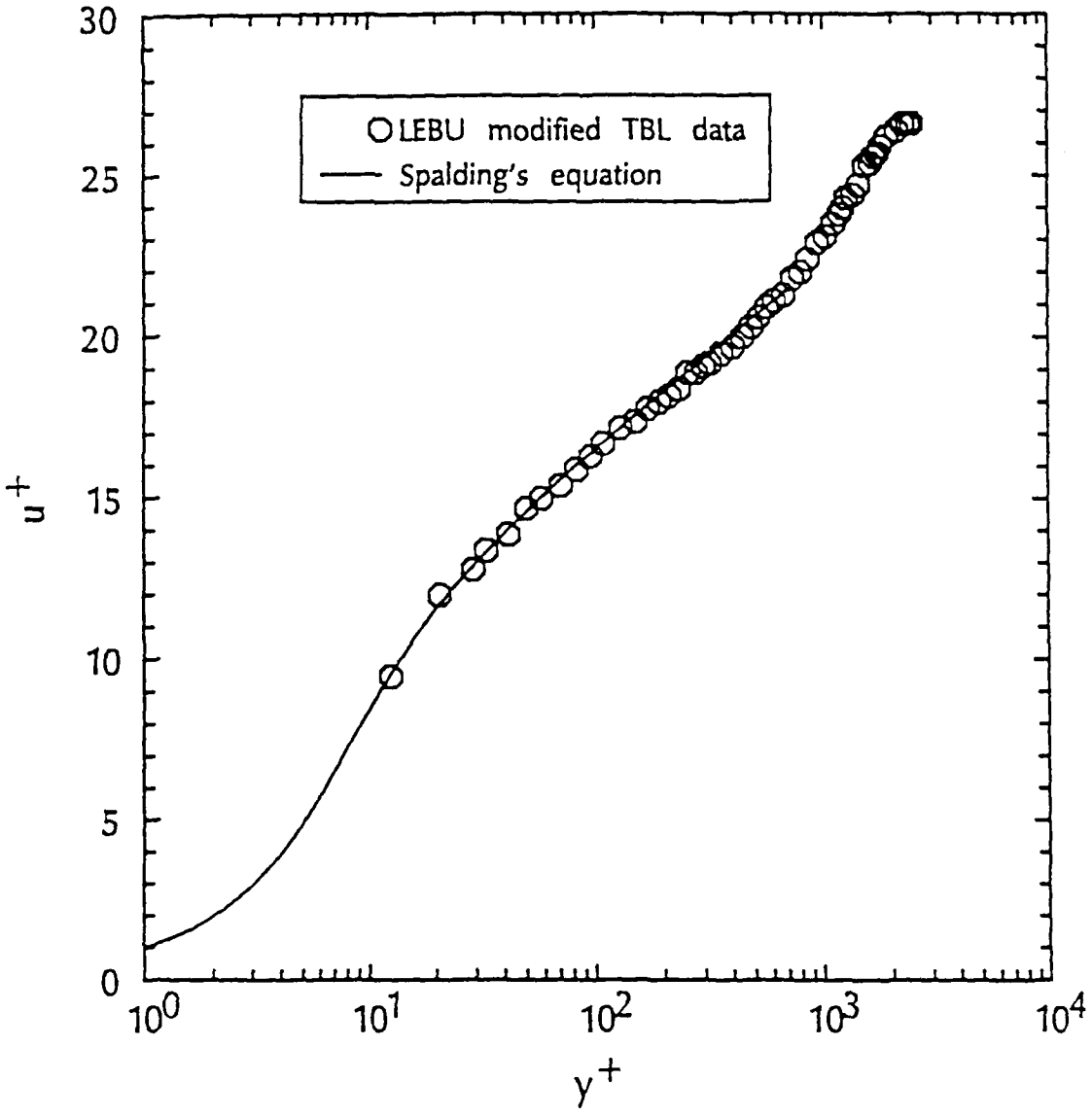

Figure 3.3. Inner variable plot of the mean streamwise velocity profile in a LEBU modified TBL at $\xi = 58.9$, no injection

Figure 3.4 shows a plot of the ratio of the LEBU modified to standard TBL skin friction coefficients, C_f/C_{f_o}, versus ξ with no polymer injection. The solid line is a parametric spline fit of the data. A maximum local skin friction reduction of approximately 30% was found at $\xi = 36$. The trends and magnitude in local skin friction reductions are consistent with Westphal (1986), Lemay *et al.* (1985), Savill and Mumford (1988), Plesniak and Nagib (1985), and Anders and Watson (1985). Savill and Mumford (1988) observed that the location of the maximum skin friction reduction corresponds to where the LEBU wake spreads to the wall.

The procedure to determine u^* described above does not work when polymer is injected into the TBL. The polymer modifies the near wall region increasing the scales in the buffer region and viscous sublayer. Hoyt (1985), Willmarth *et al.* (1987), and Reischman and Tiederman (1975) show that a positive ΔB shift of the wall intercept in the log region is typical of polymer flow in pipes and channels, but the slope remains the same. The outer flow is still modified by the LEBUs. As a result, near the injection slot there is not a region of near equilibruim flow from which to determine u^*. Also, the viscosity, ν, is no longer constant but is a function of both y and x as the injected polymer diffuses. Finally, Fontaine *et al.* (1990) did not even observe an identifiable log region at locations close to the injection slot indicating that the approach discussed above is of limited applicability.

Figure 3.5 shows the mean streamwise component velocity profile at $\xi = 19.5$ in inner variables with polymer injection. LEBU modified pure water boundary layer values of the friction velocity and kinematic viscosity were used to nondimensionalize the open symbol results. Note the large deviation of the data from Spalding's equation that extends out to near the wake region.

Although an accurate value of u^* cannot be determined from the profile in figure 3.5 due to the limitations described above, a more accurate estimate of

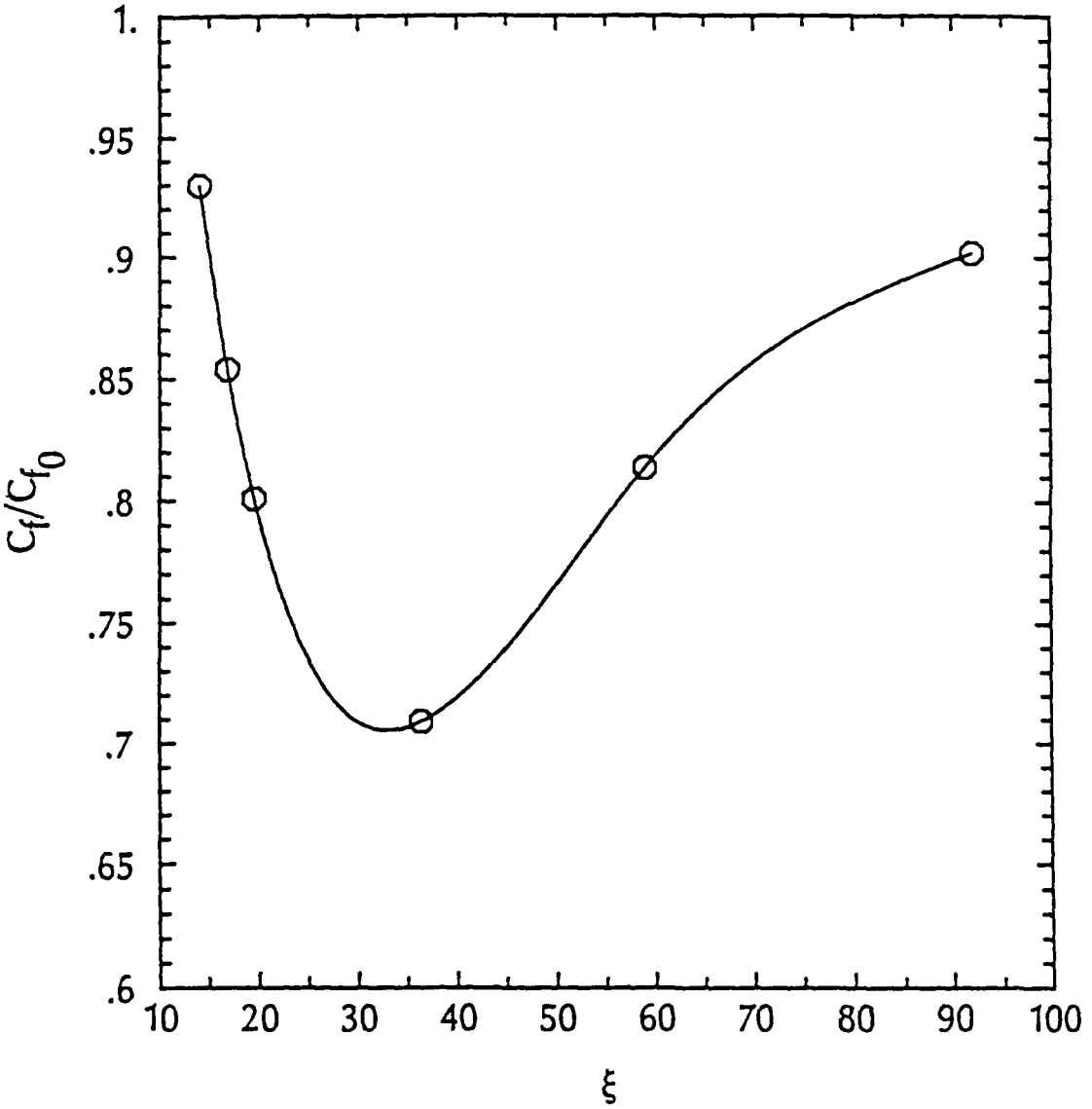

Figure 3.4. Ratio of LEBU modified to standard TBL skin friction coefficients as a function of the nondimensionalized downstream distance from leading edge of upstream LEBU, no injection

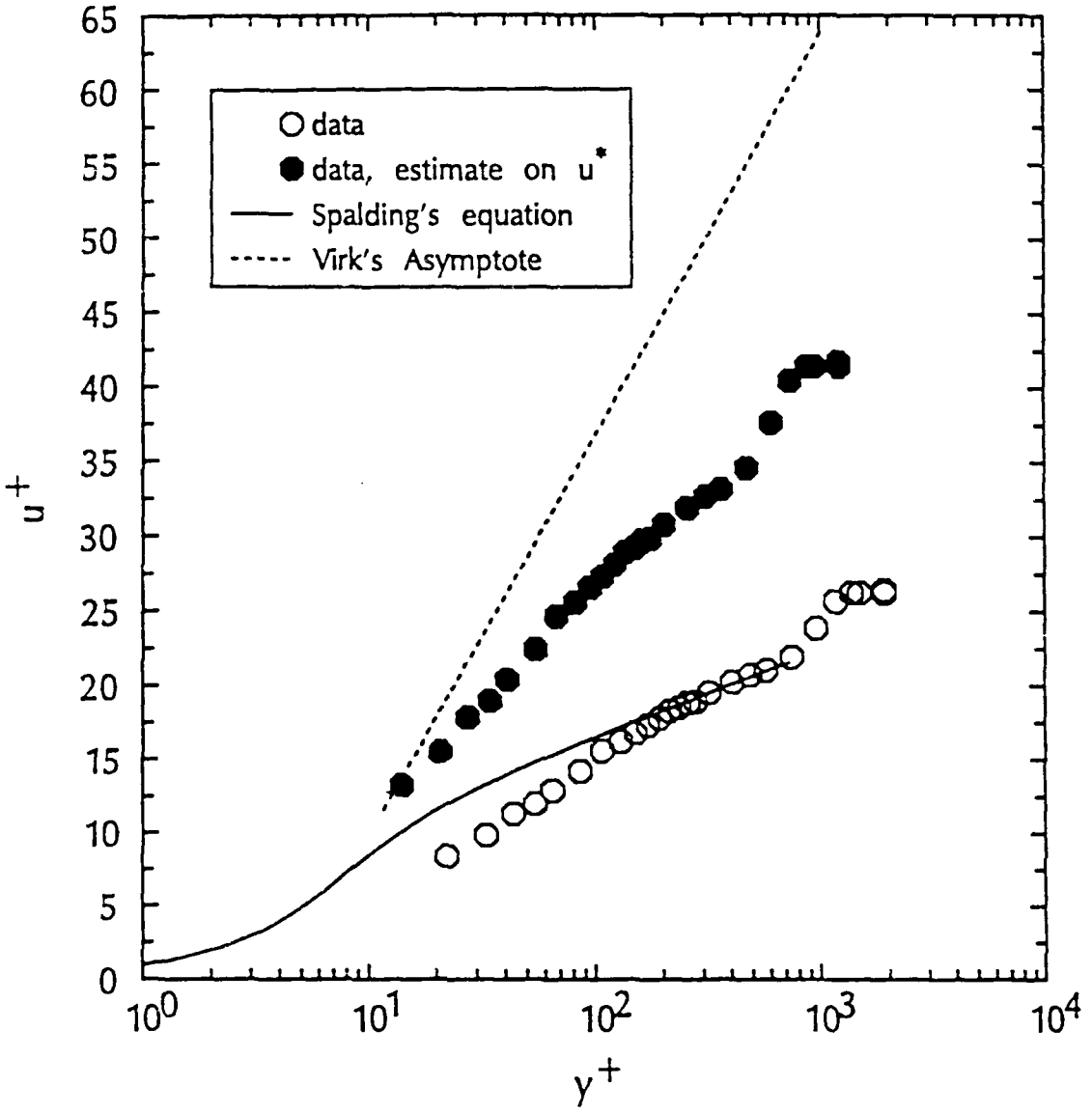

Figure 3.5. Inner variable plot of the mean streamwise velocity profile in a LEBU modified TBL at $\xi = 19.5$, $5Q_s$ polymer injection

u^* than used for the open symbols can be made. Theoretical estimates of the maximum skin friction reduction for dilute polymer solutions in pipe flow have been extended to external flat plate boundary layers. Virk *et al.* (1970) present a formulation for the predicted maximum skin friction reduction coefficient that is possible in dilute uniform polymer solution flat plate TBL flows as a function of Reynolds number. Granville (1972) presents the same type of data in graphical form. Based on these predictions, a 60% reduction in the skin friction was used as an approximation at the present location of $\xi = 19.5$ to nondimensionalize the solid symbol results in figure 3.5. Given that Fontaine *et al.* (1990) have measured 50% integrated drag reductions with a large drag balance for the present polymer injection rate and freestream velocity, and that the near wall region has polymer concentrations of 100 to 450 WPPM at this location, 60% drag reduction at this location near the slot seems reasonable. However, the present data are found to approach the asymptote condition but are not on or near the asymptote for all but the smallest y value above the wall.

There are several reasons why the solid symbol data do not lie on the asymptote condition. First, both the asymptote and the predicted maximum drag reduction presented by Virk *et al.* (1970) and Granville (1972) are based on pipe flow results and have not been shown to be accurate for flat plate TBLs. The flow in the present investigation is slot injected polymer at high concentration. The concentration at the wall for the data in figure 3.5 exceeds 400 WPPM. Such high concentrations produce less skin friction reduction in pipe flows than optimum dilute concentrations. Also, y^+ was normalized using pure water values of ν. Smaller y^+ values (near the wall), representing a shift of the data towards Virk's asymptote, would be observed if the larger kinematic viscosity values of polymer solutions were used for normalization. But, ν is very difficult to estimate for polymer solutions because of the values dependence on the shear rate and

the variable concentration. At $\xi = 19.5$, the mean polymer concentration has decreased with increasing distance from the wall to approximately 100 WPPM by $y^+ = 100$. At this concentration, viscometer results indicate that the shear viscosity is, roughly, a factor of 2 larger than with water alone.

Examination of the solid symbol data in figure 3.5 shows a remnant log region between $y^+ = 300$ and 400 may still be present. There is a positive ΔB shift of this remnant log region from the open symbol results, but the slope appears to be greater. This discrepancy in the slope could be due to the small number of data points that are actually in the log region remnant. Also, the viscosity gradient not accounted for in the nondimensionalization of y^+ could change the slope.

Plots of the momentum thickness, θ, versus ξ are shown in figures 3.6 and 3.7 without and with polymer injection, respectively. There is a large increase in θ at $\xi = 19.5$ for the LEBU modified TBL over the standard case in both figures which is due to the device drag, but otherwise the growth rate of θ downstream of the LEBUs has been reduced considerably. Similar trends are noted by Guezennec and Nagib (1985) in a LEBU modified TBL. For a zero pressure gradient flat plate TBL flow, the drag depends solely on $d\theta/dx$, thus the ratios of slopes yields and integrated estimate of the skin friction reduction over the length of the flat plate. Anders and Watson (1985) found a mild pressure gradient on the wall due to the LEBUs that extended approximately 3 boundary layer thicknesses downstream of the LEBU devices and concluded that the effects of the imposed pressure field on the turbulent-wall boundary layer is of limited extent and magnitude. Thus, the integrated estimate of the skin friction reduction over the length of the flat plate is not affected by the mild pressure gradient confined to immediately downstream of the LEBU devices. Using the least squares curve fit to the data in figures 3.6 and 3.7, the average

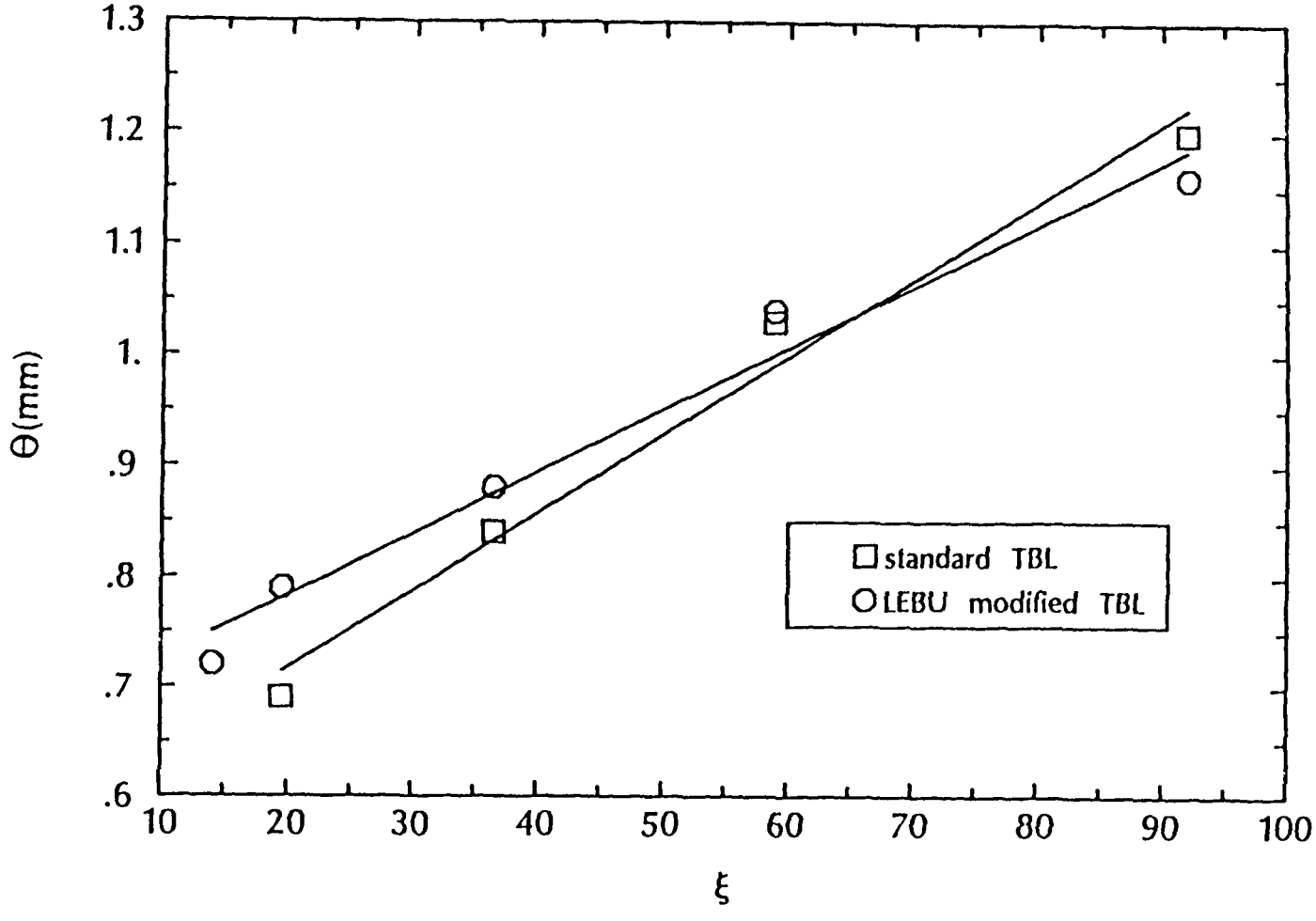

Figure 3.6. Momentum thickness versus nondimensionalized downstream distance from leading edge of upstream LEBU, no injection

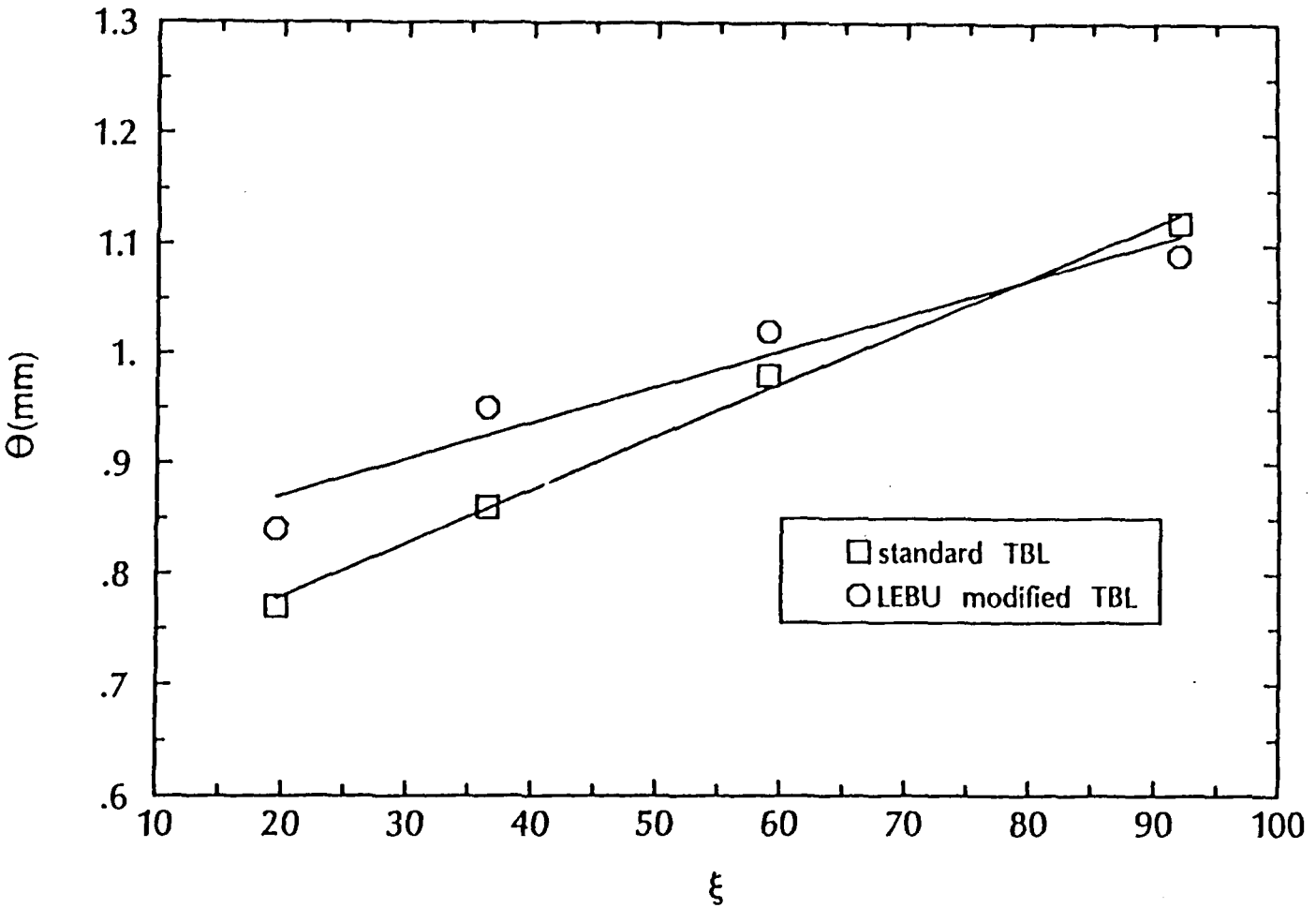

Figure 3.7. Momentum thickness versus nondimensionalized downstream distance from leading edge of upstream LEBU, $5Q$, polymer injection

skin friction reduction in the test section due to the LEBUs was approximately 20%. Also, the integrated skin friction reduction for polymer injection into a standard TBL of Fontaine *et al.* (1990) was approximately 31%. Finally, the integrated skin friction for polymer injection into a LEBU modified TBL was approximately 53%, which is additive of the two individual drag reducing techniques. Note that these estimates are made on the skin friction only, and do not include device or support drag. Also this approach gives only a rough estimate of the average over the length of the test section but the trends are supported by the rest of the data. To check the validity of these estimates, an integrated skin friction reduction of 19.5% was determined from figure 3.4 for a LEBU modified TBL without polymer injection over the same downstream distance. This compares very well with the 20% skin friction reduction found based on $d\theta/dx$. However, drag balance measurements by Fontaine *et al.* for the no LEBU 5 Q_s 500 WPPM polyox injection at $U_e = 4.6m/s$ observed C_f reduction near 50%.

Figure 3.8 is a plot of the displacement thickness, δ^*, versus ξ, with and without injection. This plot exhibits similar types of behavior as the momentum thickness in that the displacement thickness in the LEBU modified TBL without injection is initially thicker than that of the standard TBL of Fontaine *et al.* (1990), but the growth rate, $d\delta^*/dx$, has been reduced. By the last downstream measurement location, δ^* in the LEBU modified TBL is slightly smaller than in the standard TBL. Again, the trends are consistent to results of Guezennec and Nagib (1985). Polymer injection into both TBLs increases δ^* over the respective no injection values by an amount which is proportional to the amount of polymer near the wall. Otherwise, the behavior of δ^* between both TBLs is very similar as without polymer injection.

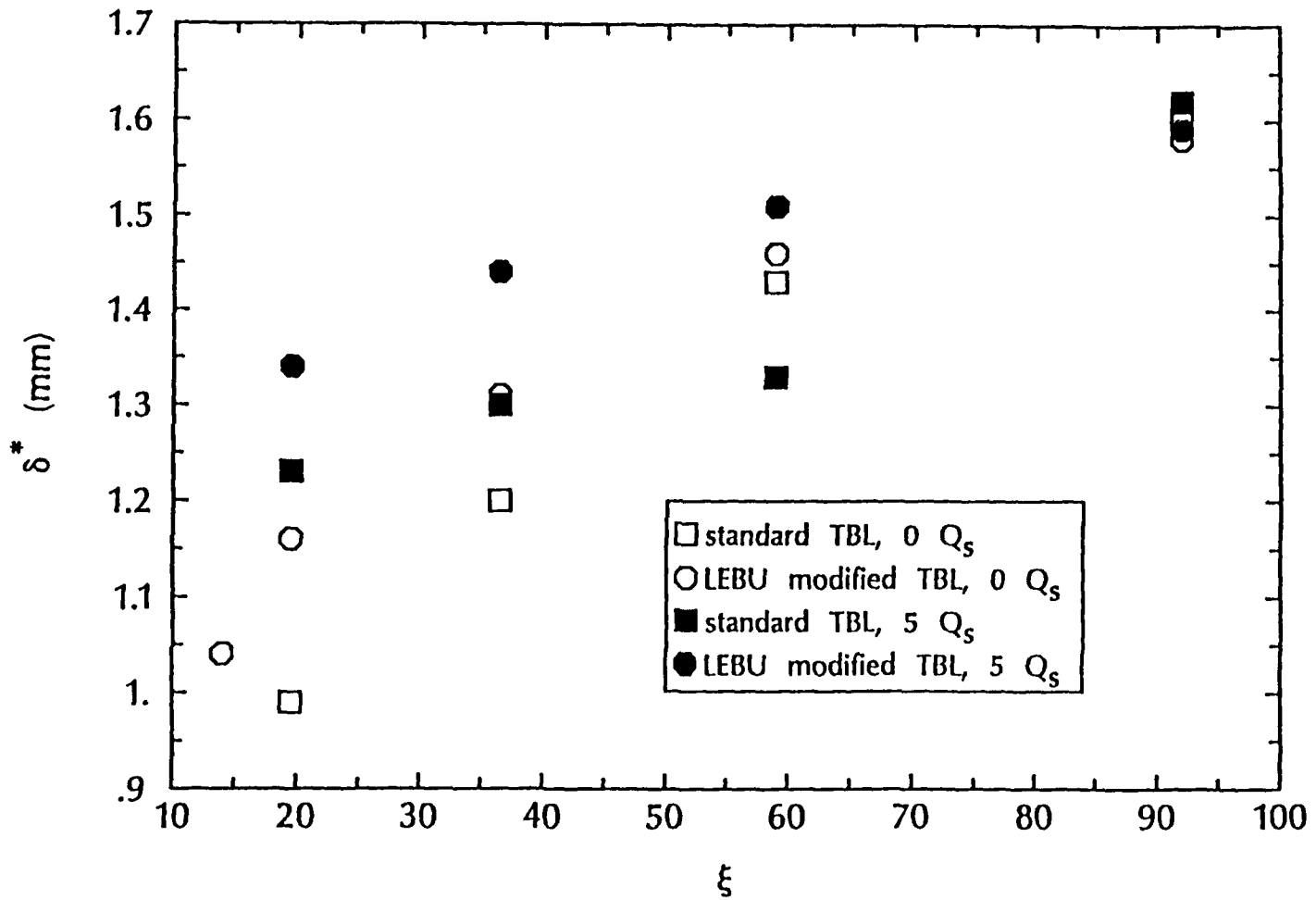

Figure 3.8. Displacement thickness versus nondimensionalized downstream distance from leading edge of upstream LEBU

3.1.2 Turbulence Profile Data

The downstream development of the turbulence intensity profiles without and with polymer injection are shown in figures 3.9, 3.10, and 3.11 for $\xi = 19.5$, 36.4, and 92.0, respectively. Open and closed symbols represent LEBU modified TBL data with no injection and with $5Q_s$ polymer injection, respectively. The solid and dashed lines are standard TBL data of Fontaine *et al.* (1990) with no injection and with $5Q_s$ polymer injection, respectively.

3.1.2.1 Turbulence Intensity Profiles with No Polymer Injection

The LEBU modifications to the upstream turbulence levels are most significant without polymer injection. At $\xi = 19.5$, figure 3.9, there are large reductions in the u rms velocity component of the LEBU modified TBL with no polymer injection from the wall to approximately $y/\delta^* = 4.2$. The v rms velocity component of the LEBU modified TBL with no polymer injection show reductions from the wall to approximately $y/\delta^* = 3.0$, but above $y/\delta^* = 3.0$, the v rms velocity component is larger than the standard TBL data. Figure 3.10 shows that the v rms profiles with no polymer injection have relaxed to the standard TBL profiles of Fontaine *et al.* (1990), but there are still reductions in the u rms LEBU profiles. Figure 3.11 at $\xi = 92.0$ indicates that the effects of the LEBUs on the turbulence intensity with no polymer injection in the present investigation extend further downstream than reported by Guezennec and Nagib (1990) who observed that the u' fluctuations return almost completely to a standard TBL case by $\xi = 45$, and the v' fluctuations are only slightly lower at the same location. Riedy and Mautner (1986) and Chang and Blackwelder (1990)

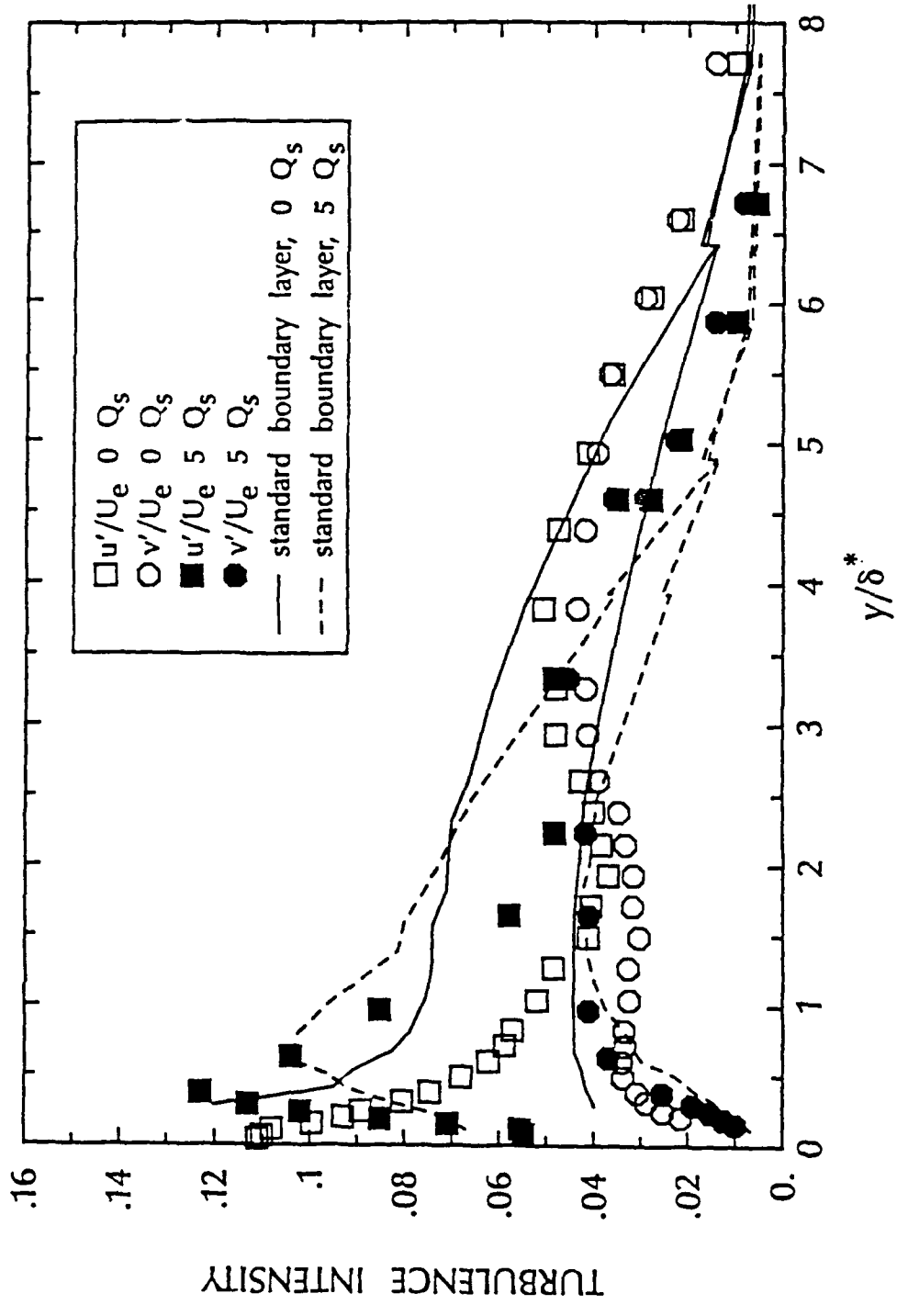

Figure 3.9. Turbulence intensity profiles for a standard and LEBU modified TBL at $\xi = 19.5$

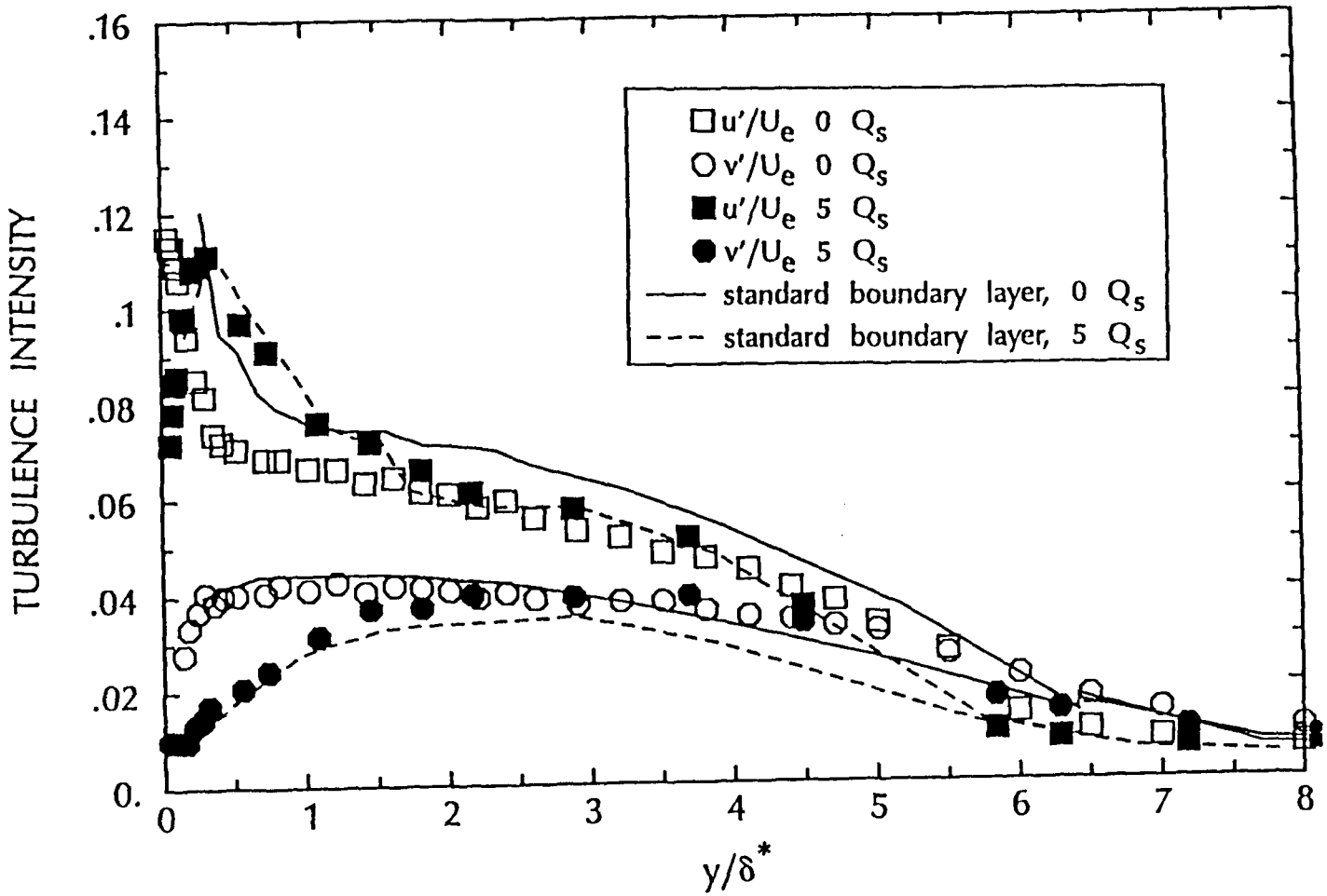

Figure 3.10. Turbulence intensity profiles for a standard and LEBU modified TBL at $\xi = 36.4$

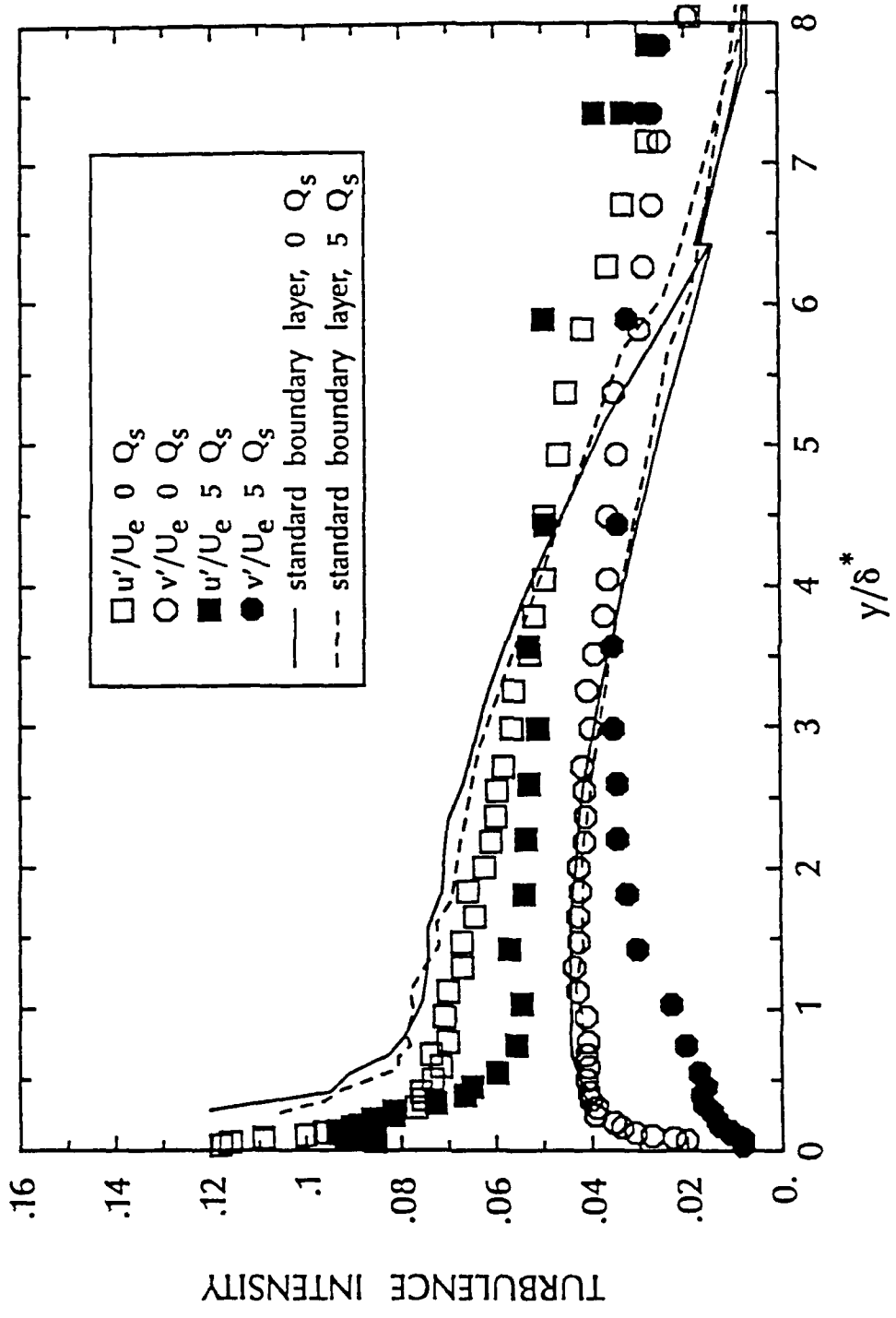

Figure 3.11. Turbulence intensity profiles for a standard and LEBU modified TBL at $\xi = 92.0$

report similar results to Guezennec and Nagib, and Trigui and Guezennec (1990) found slight effects on the u' fluctuations as far downstream as $\xi = 85$.

3.1.2.2 Turbulence Intensity Profiles with Polymer Injection

The turbulence intensities in the LEBU modified TBL data with polymer injection are much lower near the wall than with LEBUs alone and similar to the standard TBL of Fontaine *et al.* (1990) with polymer injection over the entire downstream measurement locations. There is a peak in the u' fluctuations slightly away from the wall, ranging from approximately $y/\delta^* = 0.6$ at $\xi = 19.5$ to $y/\delta^* = 0.25$ at $\xi = 92.0$ for polymer injection in the LEBU modified TBL. Also, the peak streamwise turbulence levels decrease from $u'/U_e > 0.12$ at $\xi = 19.5$ to $u'/U_e < 0.1$ at $\xi = 92.0$. Without the LEBUs, this peak intensity is lower at $\xi = 19.5$ and increases slightly, as ξ increases, approaching the unmodified TBL. The peak in the streamwise turbulence intensity away from the wall is characteristic of profiles where a substantial layer of polymer exists near the wall, as shown by Fontaine *et al.* (1990). The u and v rms profiles with polymer injection develop differently from each other. The effects of polymer on the u rms profiles in both TBLs are observed immediately and relax for increasing downstream distance, whereas the effects of polymer in the v rms profiles take some distance to fully develop, consistent with Fontaine *et al.* (1990). The effects persist further downstream with the LEBUs than without, as observed in figure 3.11.

Figures 3.9 and 3.10 show that the polymer injection data for each TBL do not coincide with the corresponding no injection data in the outer boundary layer. This is because δ^* for each profile was used to normalize y. Figure 3.8 shows larger δ^* values for polymer injection in both TBLs at $\xi = 19.5$ and 36.4,

which shifts the data toward the wall. But by $\xi \approx 92.0$, figure 3.11, the polymer injection data for each TBL does coincide with the corresponding no injection data in the outer boundary layer because there is not much of a difference in δ^* in figure 3.8 at this location due to polymer injection. Also, note that all of the δ^* values in figure 3.8 at $\xi = 92.0$ are approximately equal. Thus the higher turbulence intensity levels in the LEBU modified TBL over the standard TBL in figure 3.11 are real effects and are not due to differences in δ^* used for normalization.

3.1.2.3 Reynolds Stress Results

Figures 3.12 and 3.13 show the Reynolds stress profiles at $\xi = 36.4$ and 92.0, respectively, for a standard TBL of Fontaine *et al.* (1990) and LEBU modified TBL. The Reynolds stress levels without polymer injection in the LEBU modified TBL are considerably lower than in the standard TBL throughout the entire TBL at $\xi = 36.4$. At $\xi = 92.0$, the LEBU modified no injection levels are still lower close to the wall and are comparable to the polymer only modifications. The LEBU modified Reynolds stress levels with polymer injection are much lower than for either LEBUs alone or for the standard TBL with polymer injection below $y/\delta^* = 2.5$ at $\xi = 36.4$. The distance from the wall that the Reynolds stress data with polymer breaks away from the data without polymer is approximately the same with and without LEBUs. The Reynolds stress reduction with polymer injection in a LEBU modified TBL is still very pronounced at $\xi = 92.0$, figure 3.13. Fontaine *et al.* (1990) argue that the Reynolds stress profiles in the standard TBL with polymer injection are similar to the v' profiles in that the Reynolds stress is suppressed outside of the high concentration polymer layer near the wall. This trend is also observed in the LEBU data.

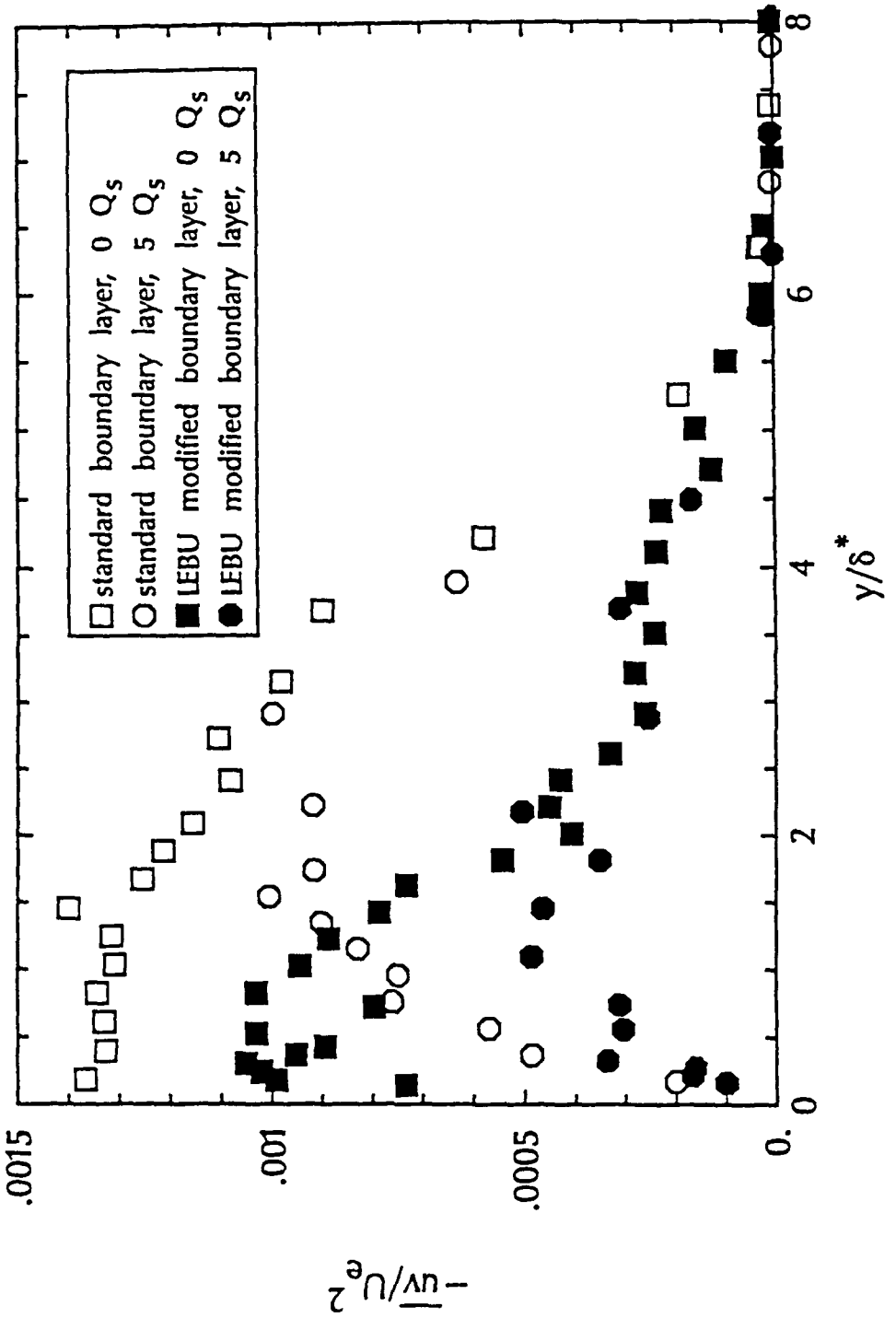

Figure 3.12. Reynolds stress profiles for a standard and LEBU modified TBL at $\xi = 36.4$

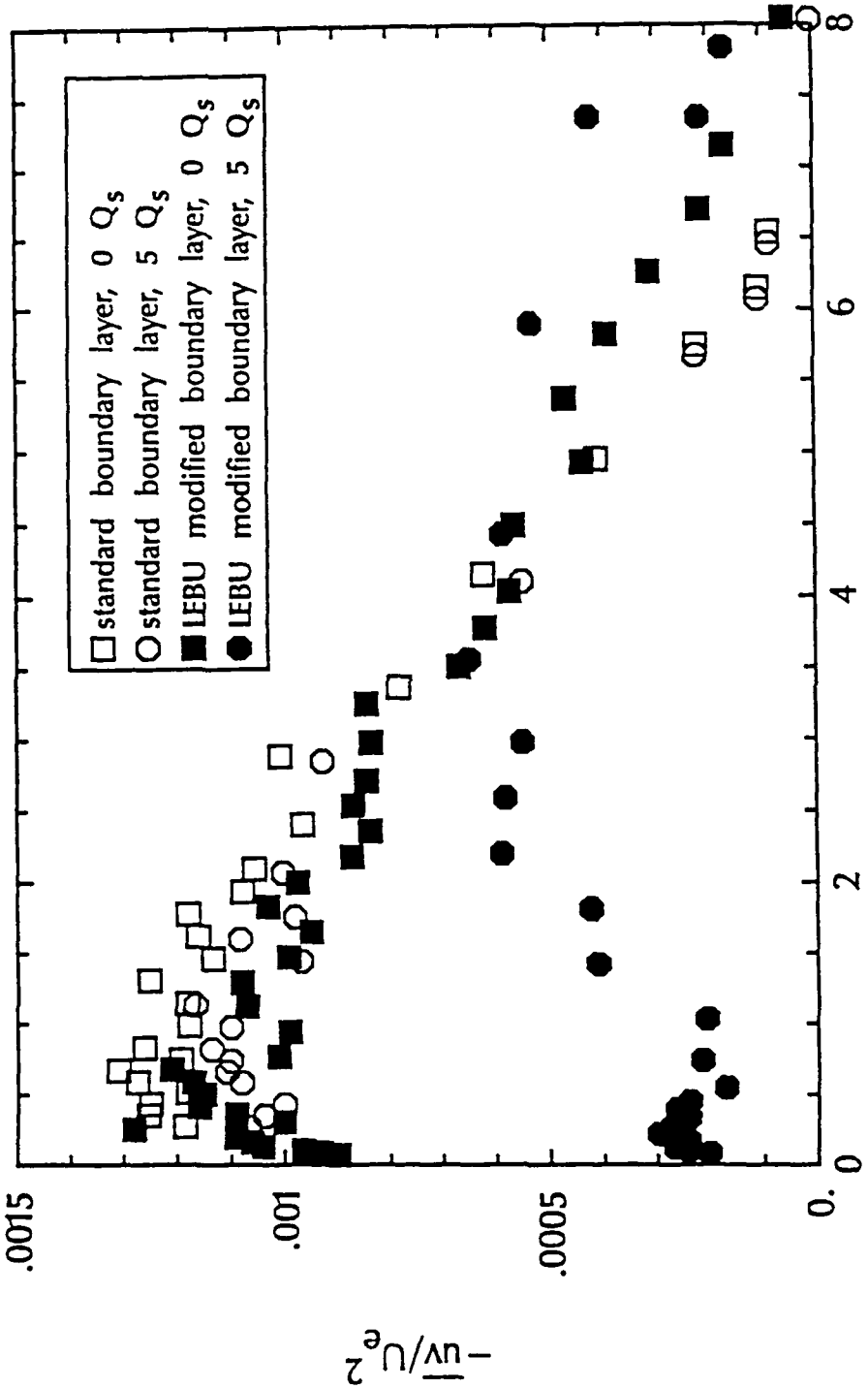

Figure 3.13. Reynolds stress profiles for a standard and LEBU modified TBL at $\xi = 92.0$

3.1.2.4 Higher Order Moments

It is instructive to look at higher order moments of the velocity data. Figures 3.14, 3.15, and 3.16 are plots of u skewness (3^{rd} order moment) versus y/δ^* for a standard and LEBU modified TBL with no injection at $\xi = 19.5$, 36.4, and 92.0, respectively. Arrows on the x-axis mark the height of the LEBU devices normalized with the local displacement thickness. At $\xi = 19.5$, figure 3.14, the effects of the LEBU wake are clearly evident. Below $y/\delta^* = 2.0$, the LEBU modified TBL u velocity data are *more negatively skewed* than the standard TBL velocity data of Fontaine *et al.* (1990), but above $y/\delta^* = 2.0$, the LEBU modified TBL data have larger skewness values. Note that at approximately $y/\delta^* = 2.0$, where the LEBU modified TBL skewness data cross the standard TBL data, both components of the turbulence intensity profiles have a local minimum in figure 3.9. At $\xi = 36.4$, figure 3.15, the LEBU modified TBL data have slightly larger skewness values above the LEBU devices. Finally at the furthest downstream measurement location, figure 3.16, the u skewness values of the LEBU modified TBL are slightly lower than the standard TBL data below the LEBUs, but above the devices, the skewness values of the LEBU modified TBL are again larger.

These same types of trends due to LEBU modifications are observed with polymer injection, except near the wall. Figure 3.17 is the same type of plot as 3.16 at $\xi = 92.0$ but with polymer injection. Here there is a dip in the LEBU modified profile at approximately $y/\delta^* = 0.4$. This dip was typical of both TBLs where a concentrated layer of polymer existed near the wall. The magnitude of the dip decreased and the location moved closer to the wall as the polymer layer became less concentrated.

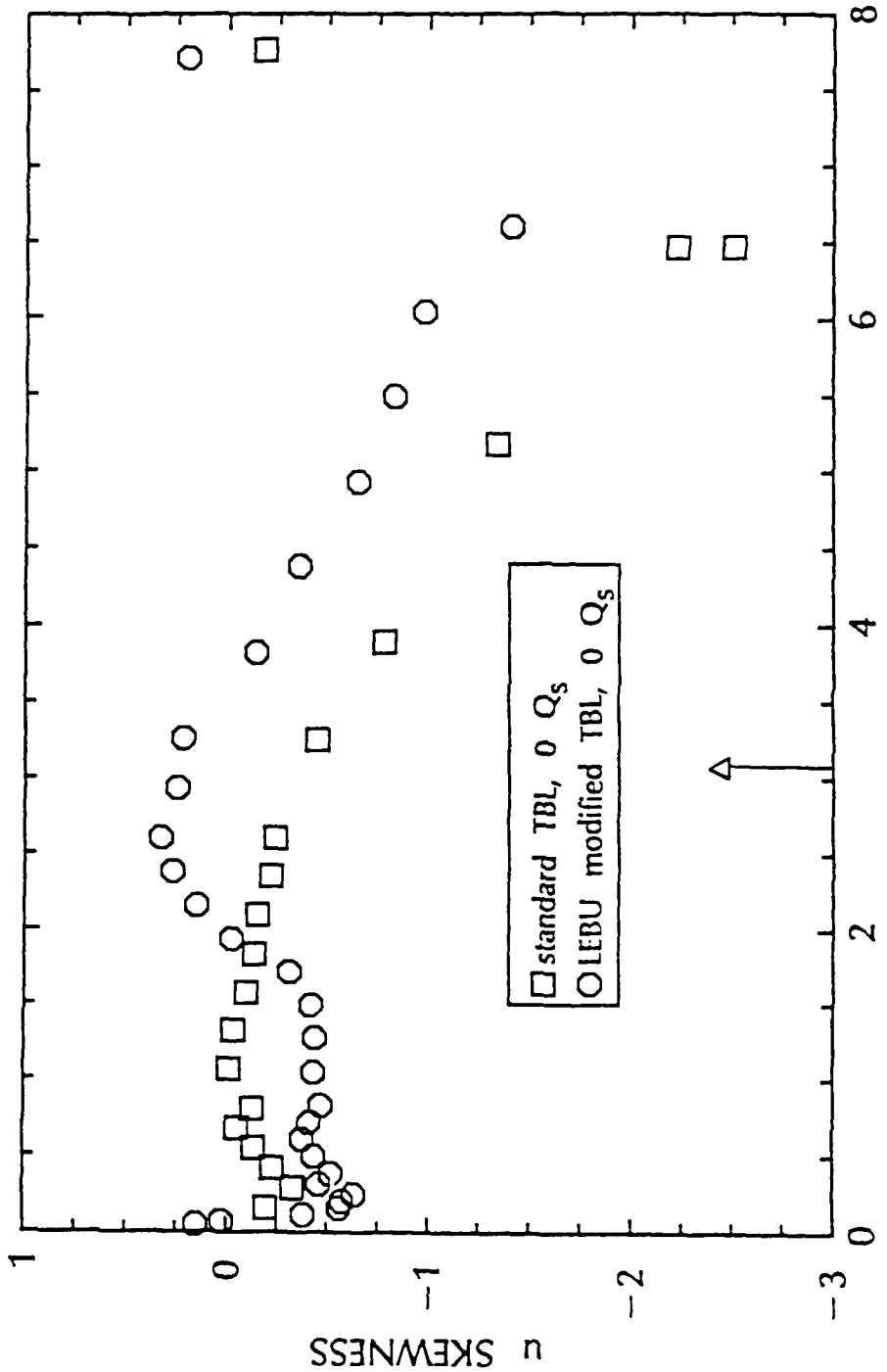

Figure 3.14. Mean streamwise velocity skewness profiles for a standard and LEBU modified TBL at $\xi = 19.5$, no injection

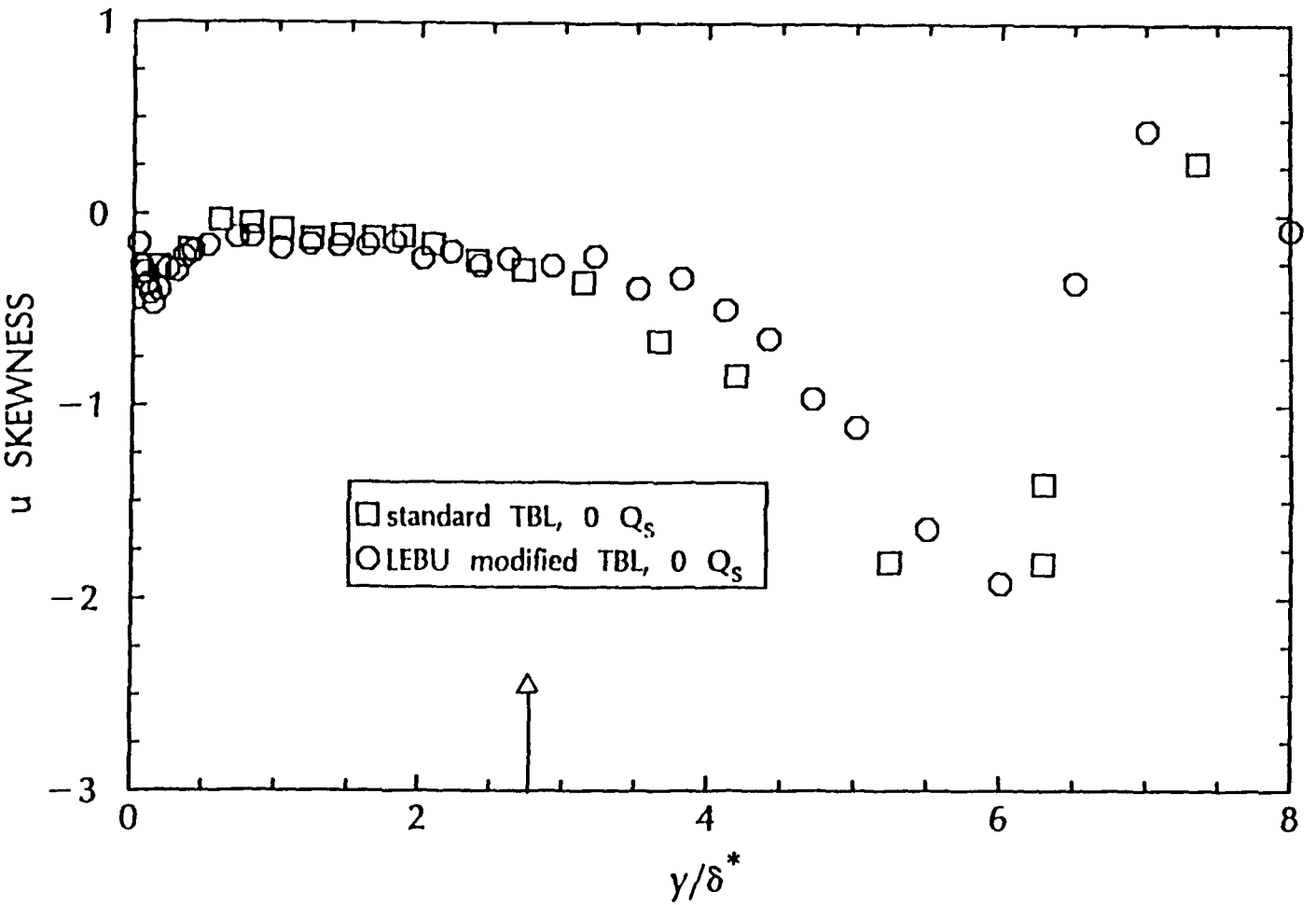

Figure 3.15. Mean streamwise velocity skewness profiles for a standard and LEBU modified TBL at $\xi = 36.4$, *no injection*

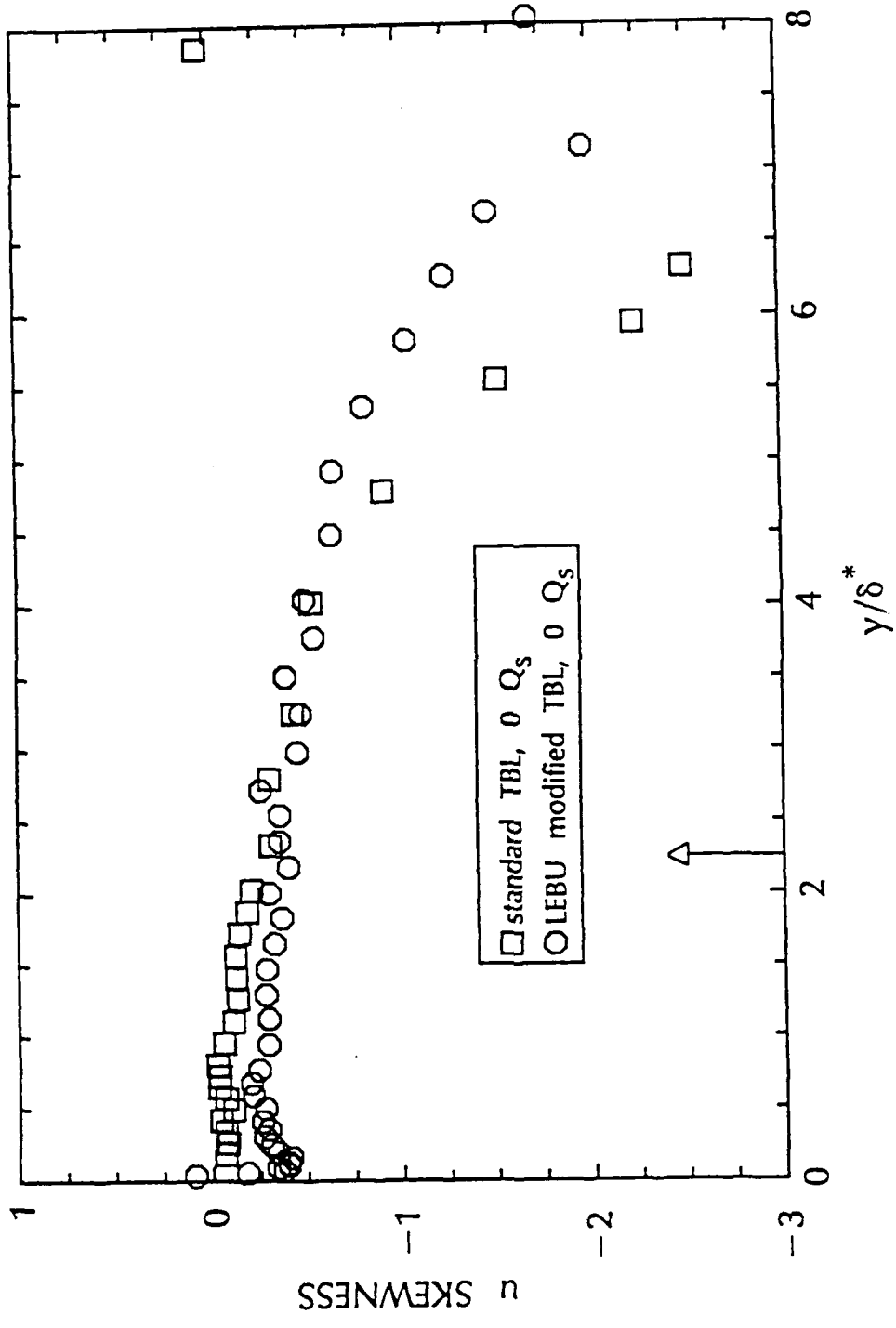

Figure 3.16. Mean streamwise velocity skewness profiles for a standard and LEBU modified TBL at $\xi = 92.0$, no injection

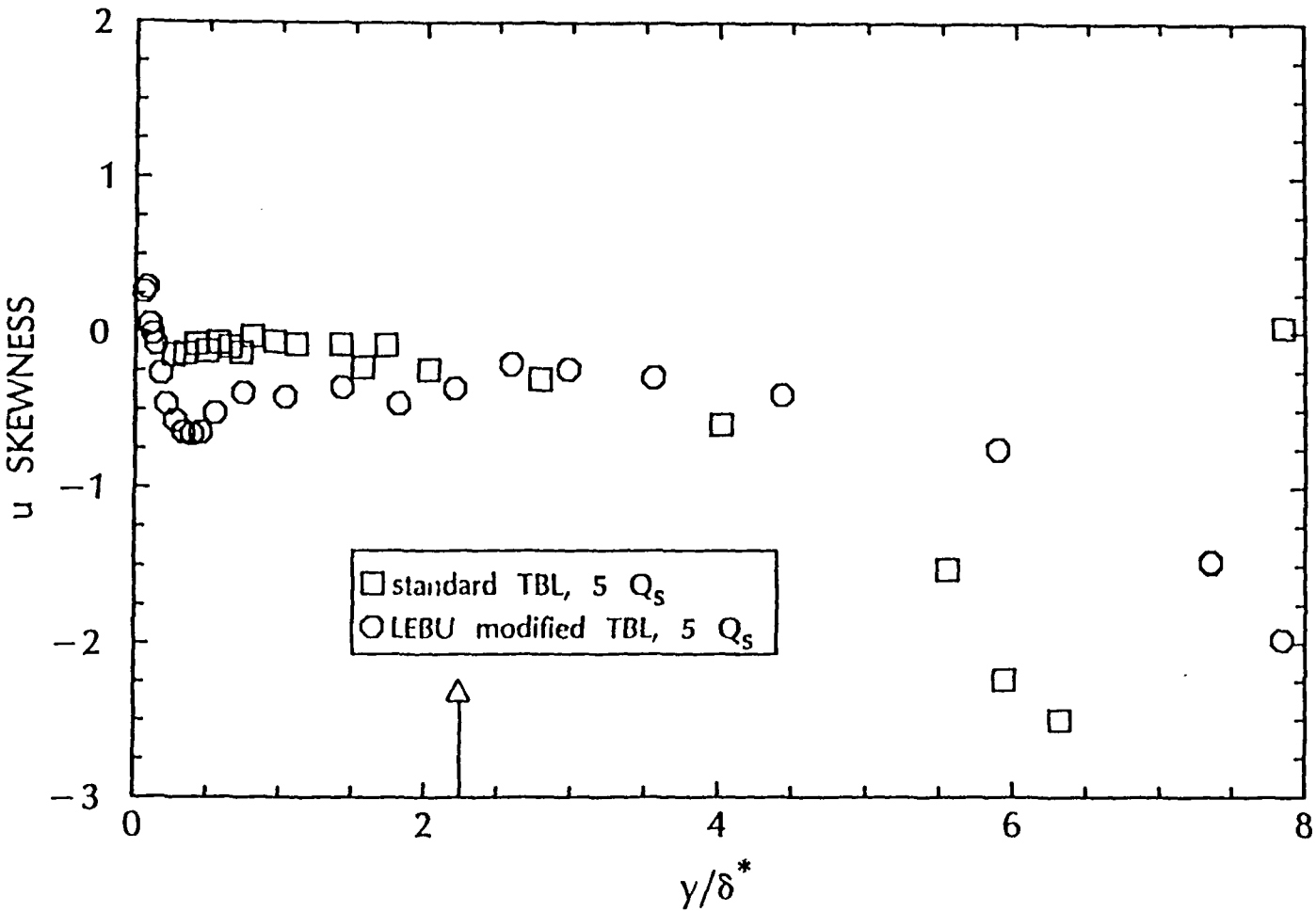

Figure 3.17. Mean streamwise velocity skewness profiles for a standard and LEBU modified TBL at $\xi = 92.0$, $5Q_s$ polymer injection

Plots of v skewness versus y/δ^* at $\xi = 19.5$ and 36.4 are given in figures 3.18 and 3.19 , respectively, with no polymer injection. The v skewness profile is altered over the entire boundary layer by the LEBUs at $\xi = 19.5$, and the effects of the LEBU wake are clearly evident by the large dip in the data. The LEBU location is indicated by the arrow on the y/δ^* axis. The minimum v skewness value occurs approximately at the location of the LEBU devices. By $\xi = 36.4$, the LEBU modified skewness profile is similar to standard TBL data of Fontaine *et al.* (1990) except for a decrease above the LEBUs. Note that the v component velocity is positively skewed in the outer boundary layer before returning to a Gaussian value in the freestream. This trend is opposite to that noticed earlier in the u skewness profiles. Also, the v skewness peak at the LEBU location is negative, which is opposite to the u skewness peak at the LEBU location.

The trends observed in v skewness with polymer injection are nearly the same as those without injection except near the wall. Similar to the u skewness profiles, the v skewness profiles exhibit a dip near the wall when a concentrated layer existed, as shown in figure 3.20 at $\xi = 36.4$. Also similar to the u skewness profiles, the magnitude of the dip decreased and the location moved closer to the wall as the polymer layer became less concentrated. The v skewness of the LEBU modified TBL in figures 3.19 and 3.20 show a sudden jump at the wall above a Gaussian value of zero and then a decrease below zero away from the wall.

Figures 3.21 and 3.22 are plots of u kurtosis (4^{th} order moment) versus y/δ for a standard and LEBU modified TBL with no injection at $\xi = 19.5$ and 36.4, respectively. The local 99% boundary layer thickness, δ, was used to nondimensionalize to get a better feel where the edge of the boundary layer is. The two figures indicate that the LEBU modified TBL is less intermittent than the standard TBL Fontaine *et al.* (1990). The lower, broader peak at the edge

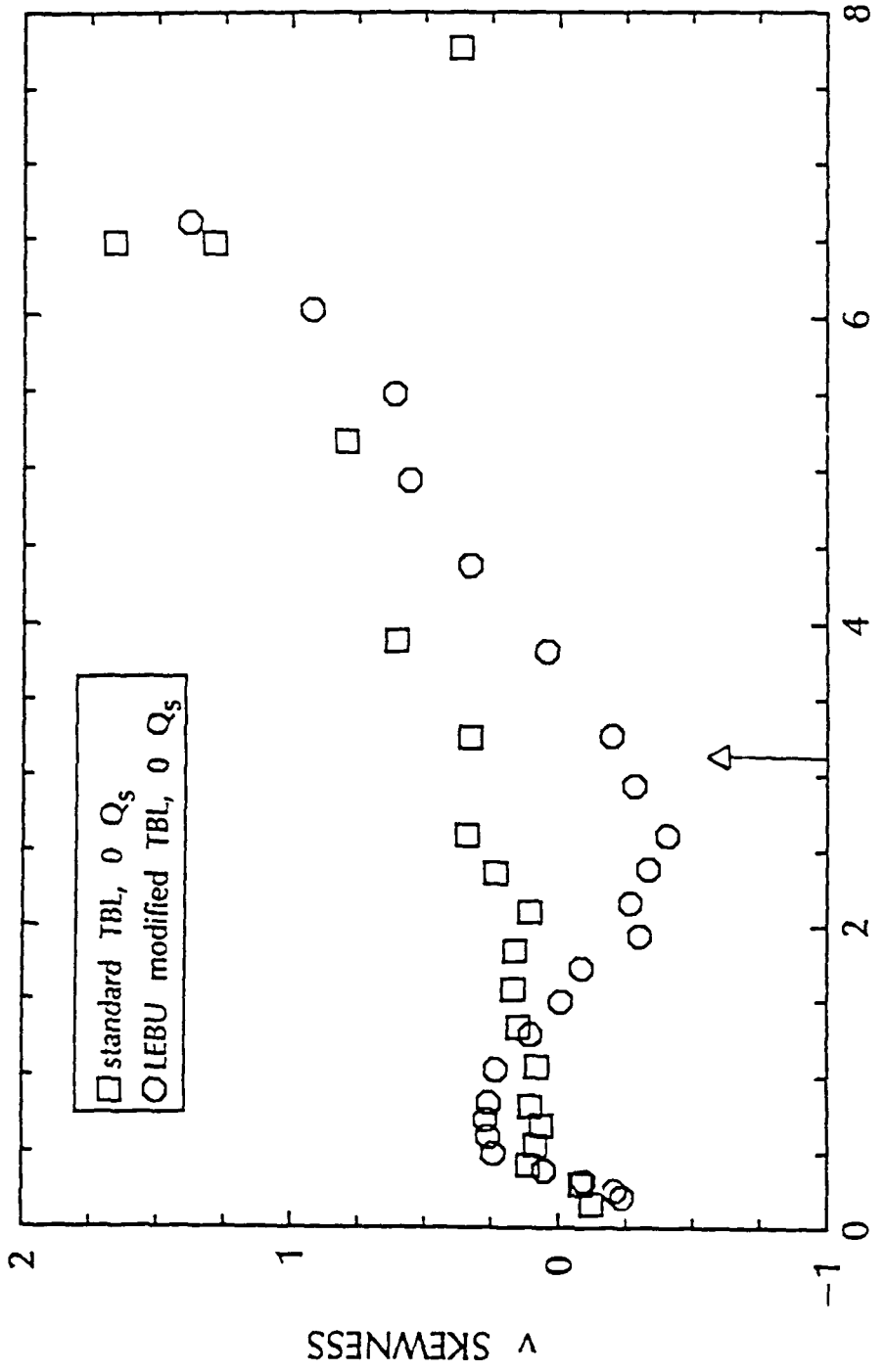

Figure 3.18. Mean vertical velocity skewness profiles for a standard and LEBU modified TBL at $\xi = 19.5$, no injection

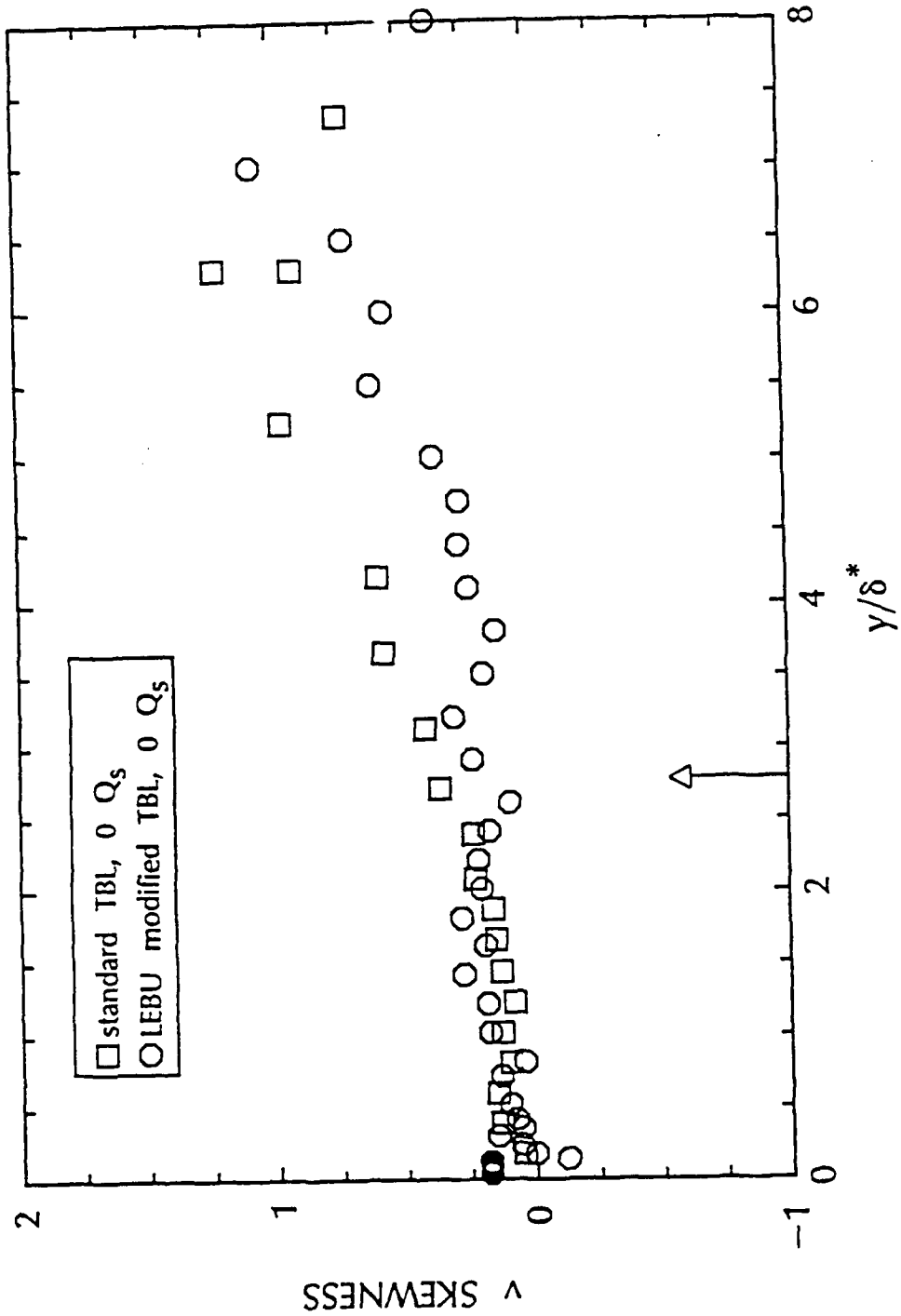

Figure 3.19. Mean vertical velocity skewness profiles for a standard and LEBU modified TBL at $\xi = 36.4$, no injection

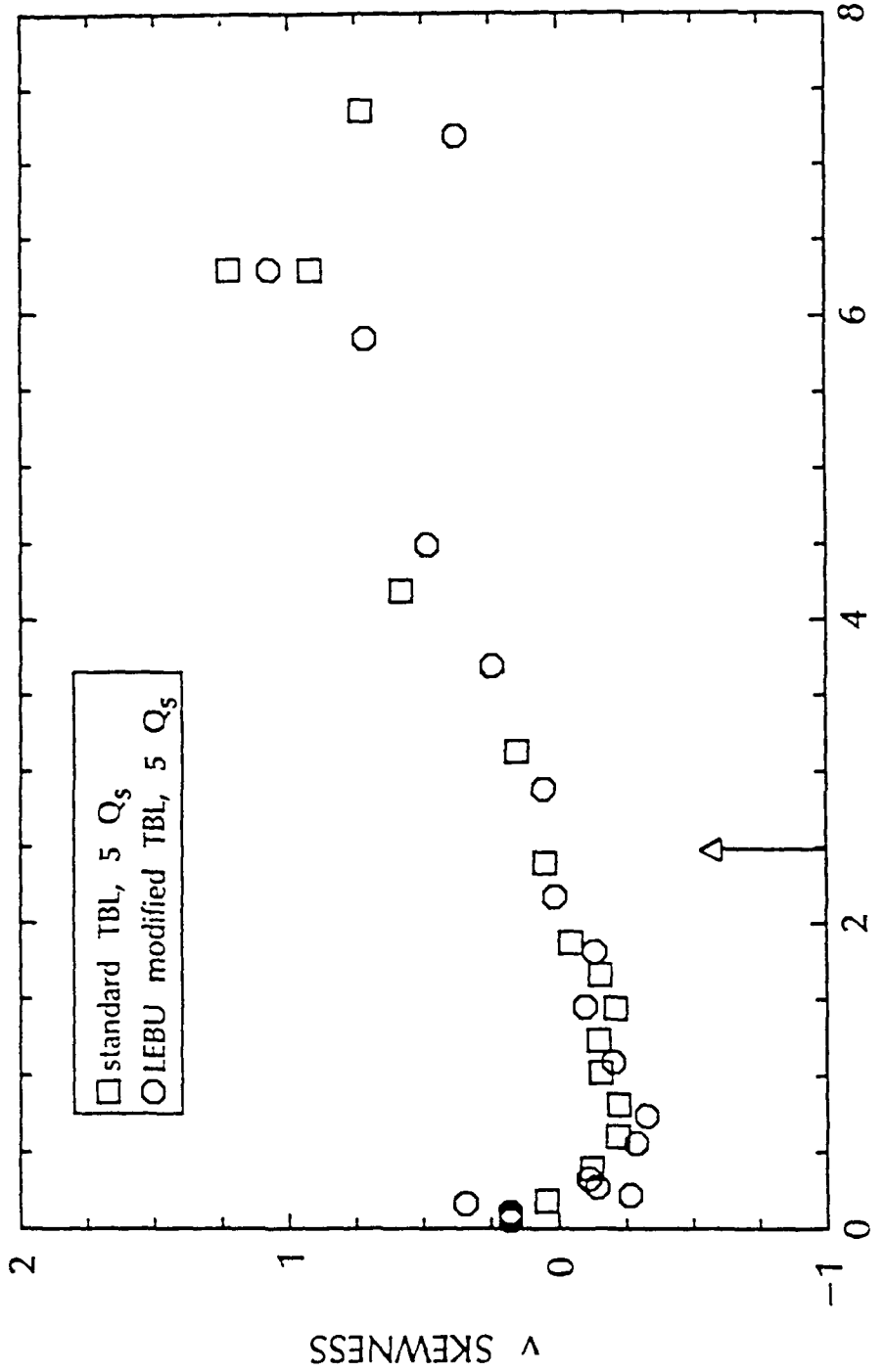

Figure 3.20. Mean vertical velocity skewness profiles for a standard and LEBU modified TBL at $\xi = 36.4$, $5Q_s$ polymer injection

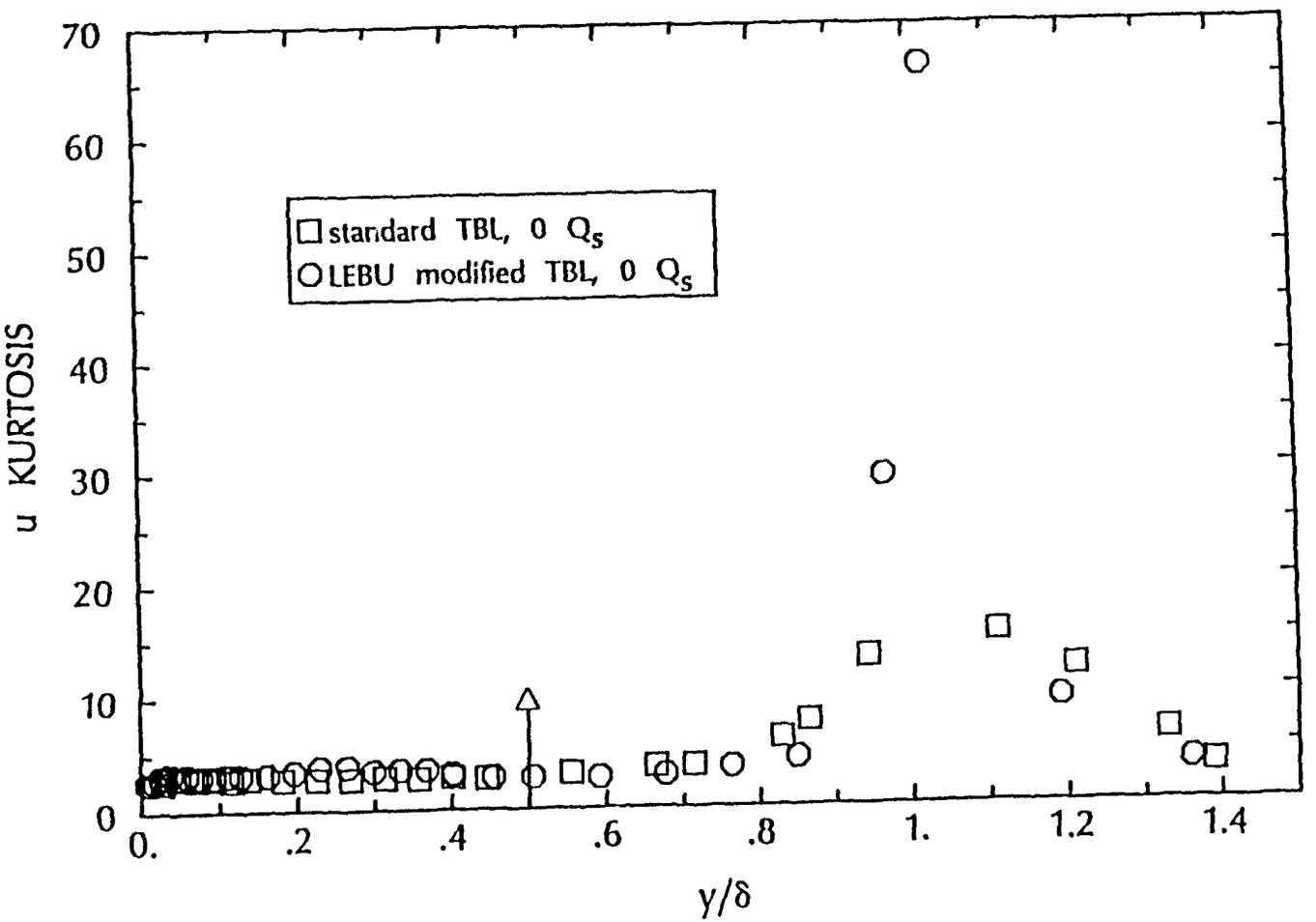

Figure 3.21. Mean streamwise velocity kurtosis profiles for a standard and LEBU modified TBL at $\xi = 19.5$, no injection

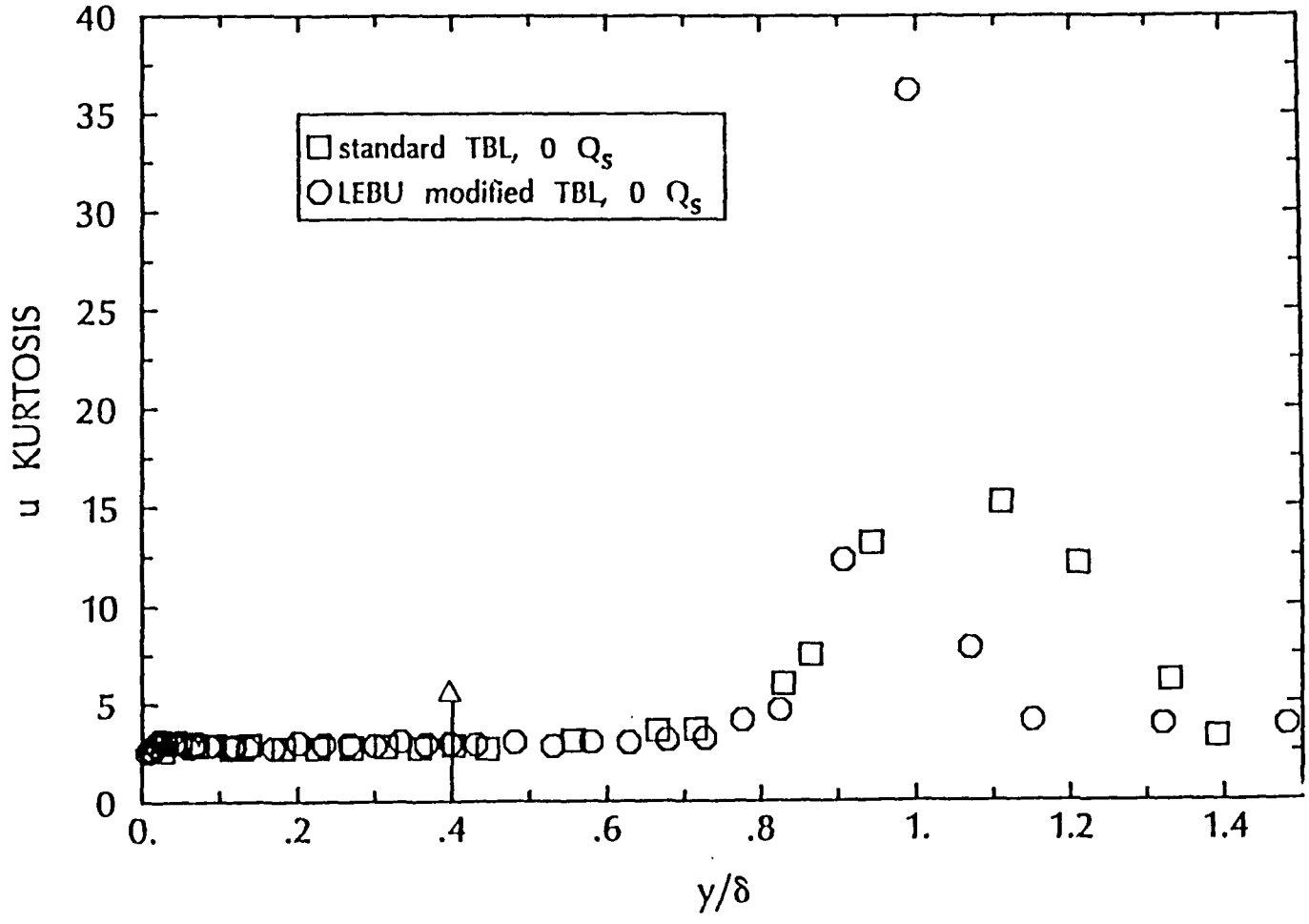

Figure 3.22. Mean streamwise velocity kurtosis profiles for a standard and LEBU modified TBL at $\xi = 36.4$, no injection

of the standard TBL suggests a large intermittent region; while the much larger, sharper peak in the LEBU modified TBL suggests a less convoluted edge. This is consistent with the flow visualization findings of Corke *et al.* (1984) and Savill and Mumford (1988). These trends are also typical of the u kurtosis profiles with polymer injection, except for an increase in kurtosis observed near the wall when a concentrated layer exists.

The peaks in the v kurtosis profiles are seen to be about the same with and without LEBUs in magnitude and form and both TBLs show an increase in kurtosis near the wall. Figure 3.23 shows v kurtosis at $\xi = 19.5$ with no injection. The increase in the v kurtosis with polymer is even more evident than that of the u kurtosis without polymer injection near the wall. At $\xi = 92.0$ with polymer injection (figure 3.24) there is a large deviation of the LEBU modified TBL v kurtosis data from the standard result near the wall, indicating a substantial layer of polymer exists on the wall in the LEBU modified TBL.

3.2 Concentration Profile Data

3.2.1 Water Injection

Figures 3.25 [standard TBL data taken from Brungart (1990)] and 3.26 show the maximum local injected water concentration normalized with the injection concentration as a function of the downstream distance from the injection slot, x, for the standard and LEBU modified TBL, respectively. Both sets of data were taken by different investigators, but the facility, flat plate, injection slot, freestream velocity, and injection rates were identical in both cases. The 10 Q_s injection data were not available at several locations for the standard TBL, thus for consistency, neither figure shows any 10 Q_s data. These

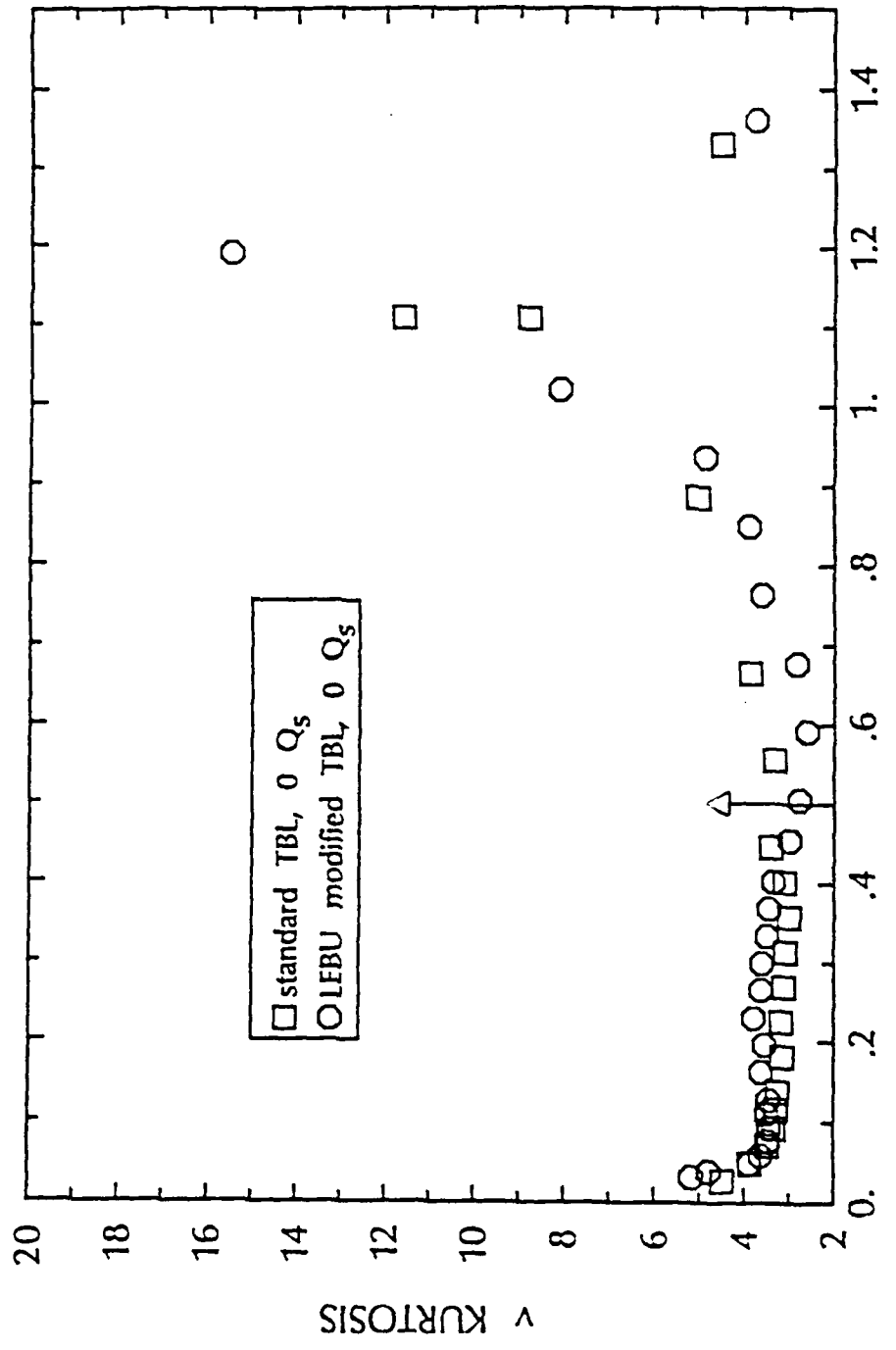

Figure 3.23. Mean vertical velocity kurtosis profiles for a standard and LEBU modified TBL at $\xi = 19.5$, no injection

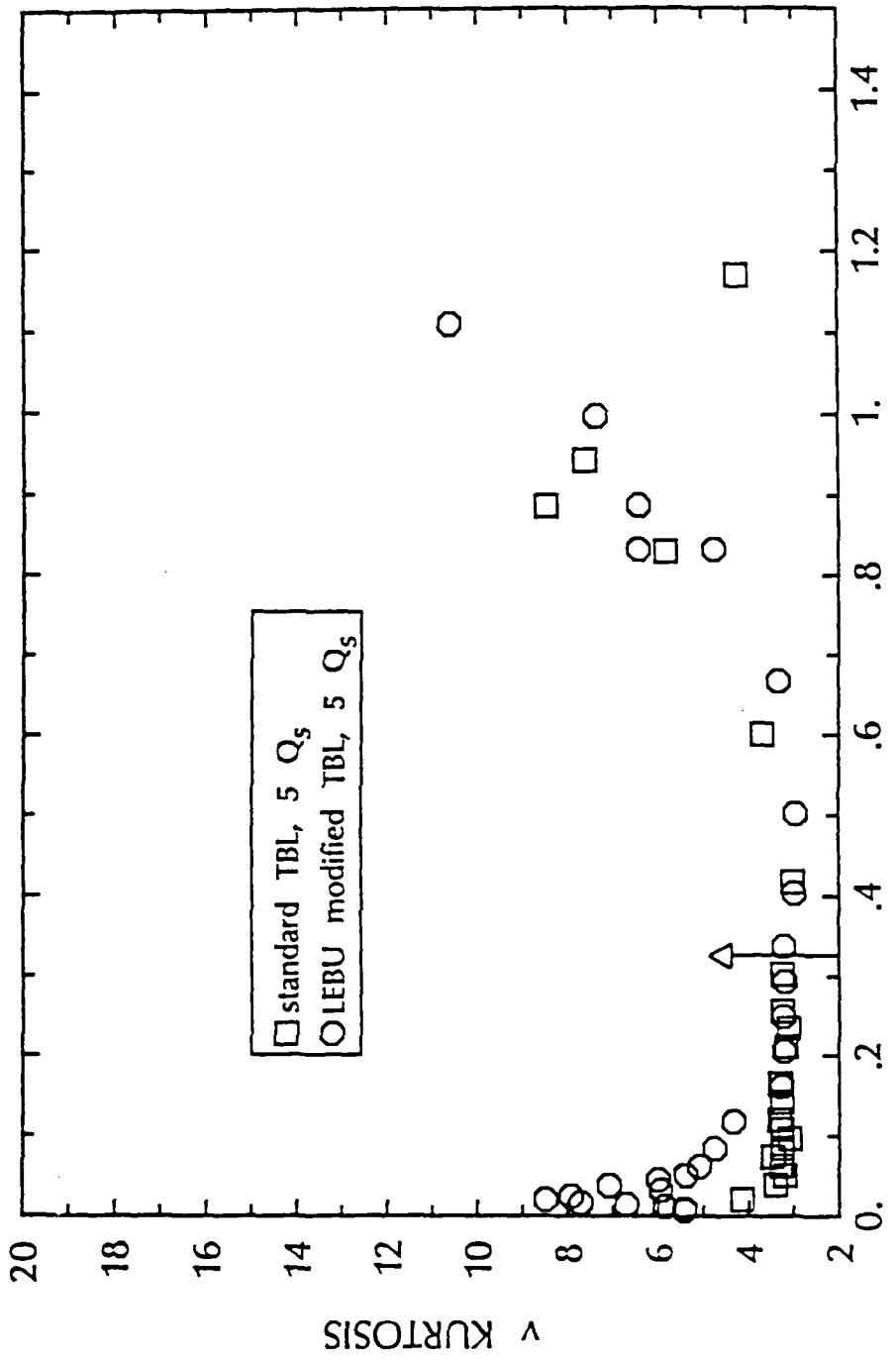

Figure 3.24. Mean vertical velocity kurtosis profiles for a standard and LEBU modified TBL at $\xi = 92.0$, $5Q_s$ polymer injection

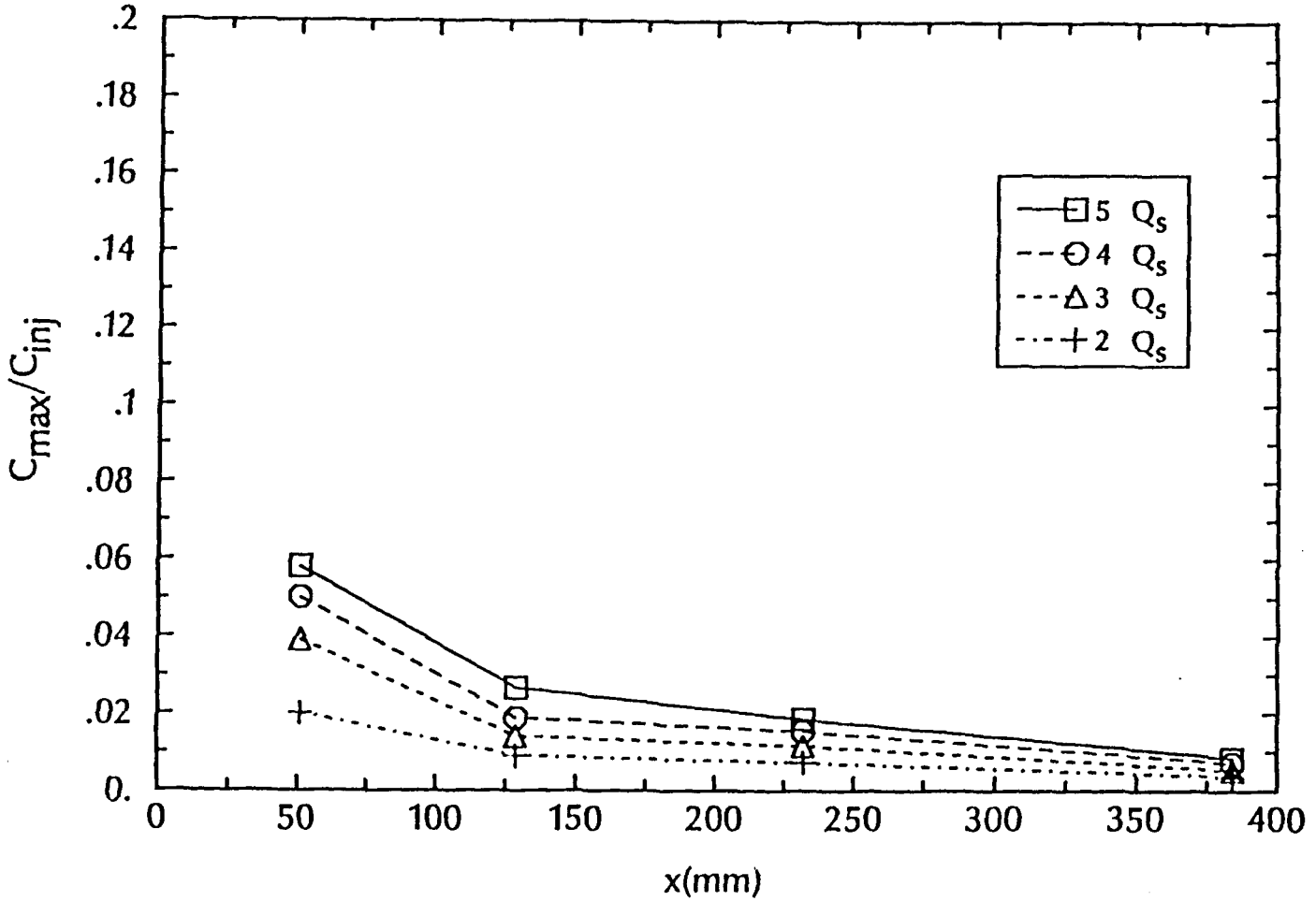

Figure 3.25. Maximum water concentration versus streamwise distance from the slot in a standard TBL [data taken from Brungart (1990)]

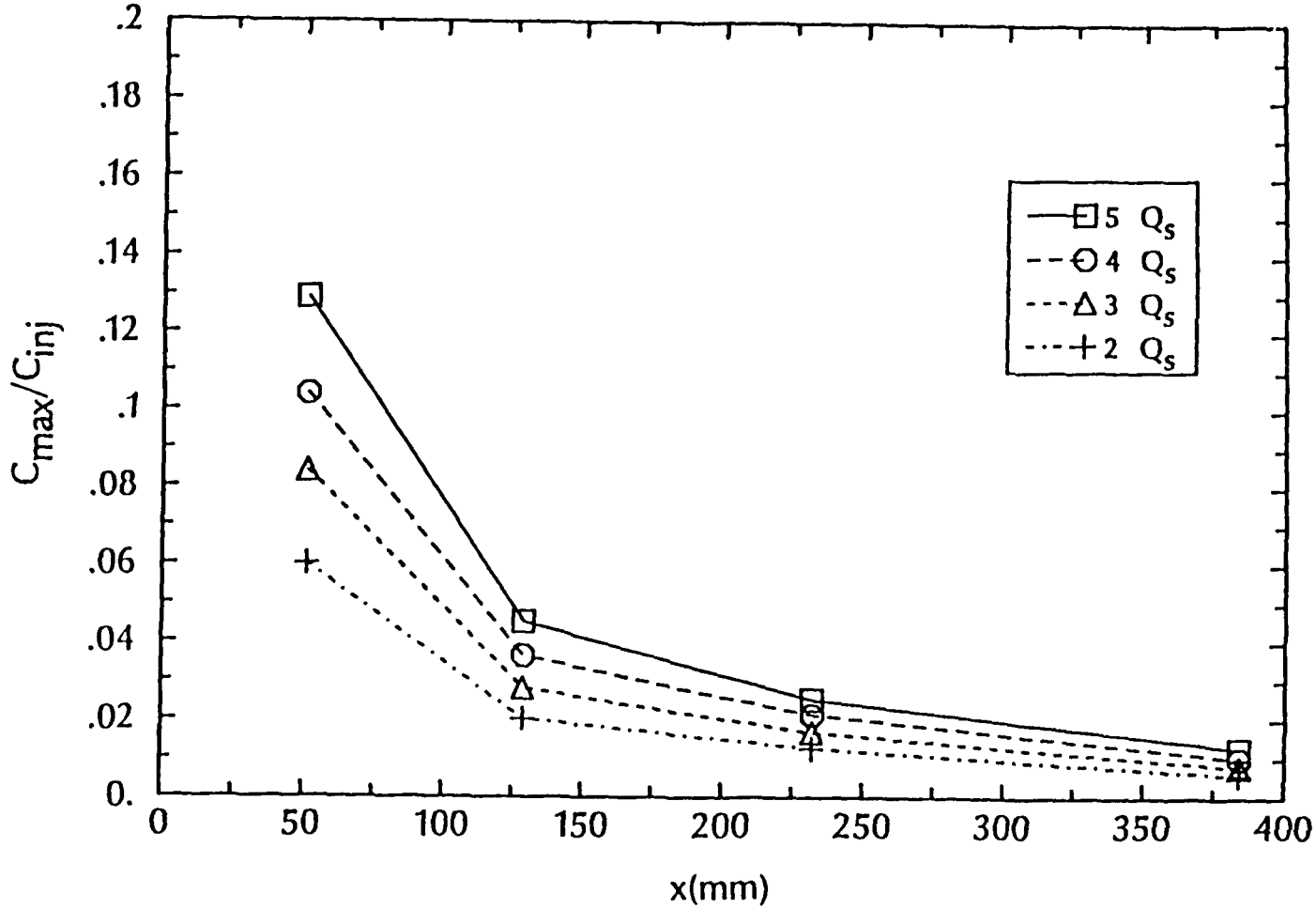

Figure 3.26. Maximum water concentration versus streamwise distance from the slot in a LEBU modified TBL

two figures show that the maximum local injected water concentration is much larger at $x = 50.8\ mm$ for the LEBU modified TBL for all injection rates. At $x = 128.6mm$, the maximum local injected water concentration is still slightly larger for the LEBU modified TBL. Beyond this point, the passive contaminant has diffused throughout both TBLs and the magnitude of the potential differences in the local concentrations are limited due to the low values.

A comparison of the diffusion of water in a LEBU modified TBL to the results of Poreh and Cermak (1964) for the diffusion of a passive contaminant from a line source in an unmodified TBL is shown in figure 3.27. Here, λ is the height above the wall at which the concentration decreases to 50% of its local maximum value. Normalization of λ in figure 3.27 is by the local boundary layer thickness, δ_{local}, of the unmodified TBL. The downstream distance is normalized with the average boundary layer thickness, δ_{avg}, between the injection slot and x. The solid line in the figure represents Poreh and Cermak's (1964) passive contaminant results. The figure shows that the LEBUs initially diminish the diffusion of water, but by $x/\delta_{avg} = 20.7$ (or $\xi = 36.4$) the 50% thickness has returned to the case of a passive contaminant in a standard TBL. Comparison with figure 3.1 indicates that the diffusion of water has returned to the standard case faster than the mean velocity profiles, which returned to the standard by $\xi = 58.9$. This is consistent to the observations of Chang and Blackwelder (1990) and Trigui and Guezennec (1990) for the diffusion of heat, another passive contaminant, in a LEBU modified TBL. Water injection data from Brungart *et al.* (1990) in a standard TBL correspond exactly to Poreh and Cermak's (1964) results. Figure 3.27 also shows that, as with the standard TBL, there is no dependence of λ/δ_{local} on the injection rate.

Poreh and Cermak (1964) define four downstream diffusion zones of a scalar quantity ejected from a steady line source within a two-dimensional turbulent boundary layer as follows:

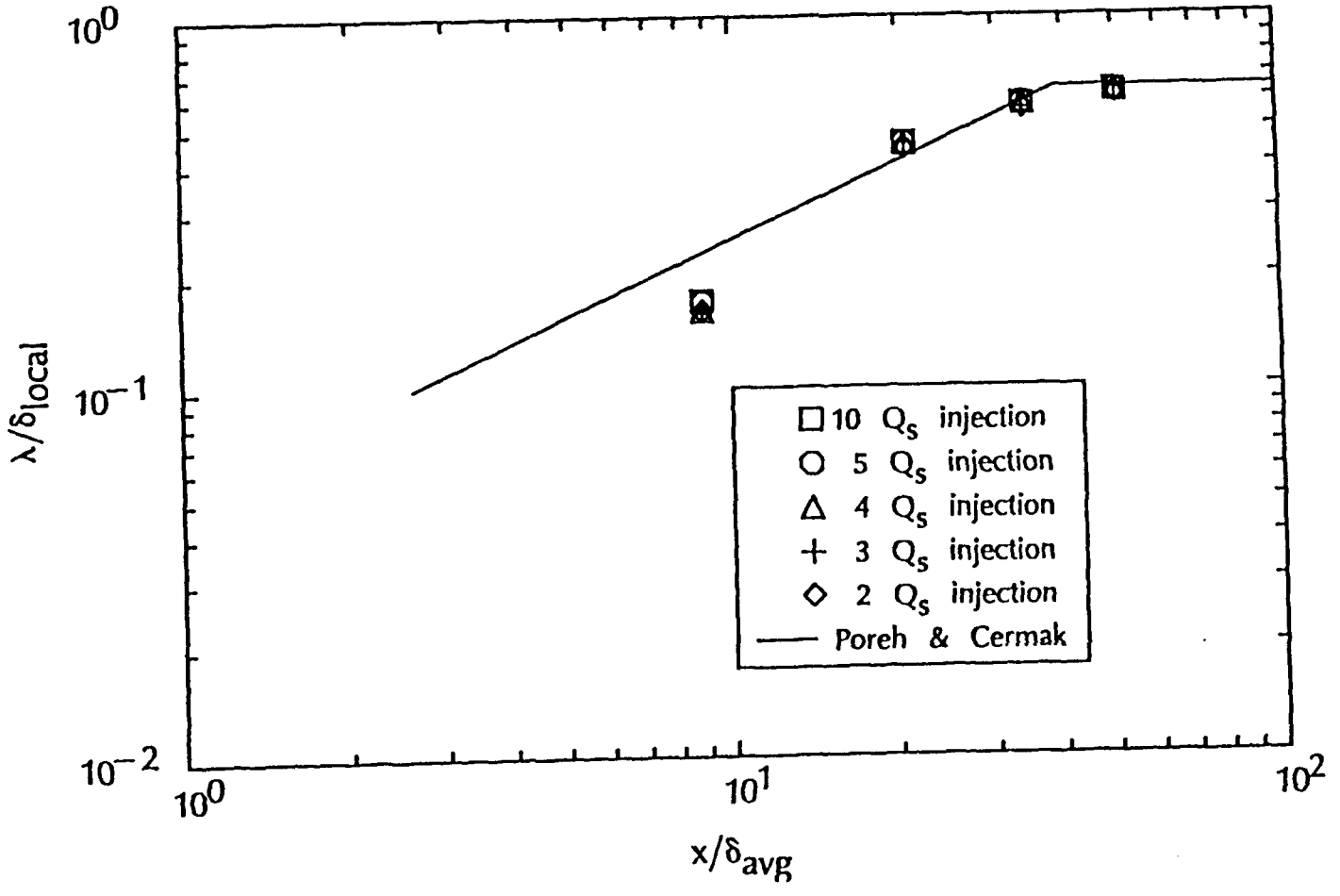

Figure 3.27. Comparison of diffusion of water in a LEBU modified TBL to the results of Poreh and Cermak (1964) for the diffusion of a passive contaminant in a standard TBL

1) Initial Zone - A concentrated layer of injection fluid exists near the wall and large velocity and concentration gradients are characteristic of this region.
2) Intermediate Zone - The diffusion layer is submerged in the boundary layer but is much thicker than the viscous sublayer. Also, the rate of growth of the diffusion layer is larger than the boundary layer.
3) Transition Zone - The diffusion layer has grown such that the intermittent outer edge of the viscous boundary layer has begun to retard the growth of the diffusion layer and has changed the shape of the concentration profiles
4) Final Zone - The diffusion and boundary layer growth rates are the same.

The data in figure 3.27 span what Poreh and Cermak (1964) define as the intermediate and transition diffusion zones and the final zone is closely approached at the most downstream location.

Morkovin (1965) determined empirical curves for mean concentration profiles of a passive contaminant in a standard TBL for the intermediate and final diffusion zones. The mean concentration profile for the intermediate diffusion zone is:

$$C/C_{max} = e^{-0.693(y/\lambda)^{1.5}} \tag{3.3}$$

and the mean concentration profile for the final diffusion zone is:

$$C/C_{max} = e^{-0.693(y/\lambda)^{2.15}} \tag{3.4}$$

Water injection data in a standard TBL from Brungart *et al.* (1990) are in excellent agreement with these empirical relations. But, the present water injection data in a LEBU modified TBL deviate from equation (3.3) at the upstream

most measurement location. Figure 3.28 is a plot of y/λ versus C/C_{max} at $\xi = 19.5$ ($x/\delta_{avg} = 8.8$), and the solid line is equation (3.3). Morkovin's curve is not representative of the present data. The form of the water data corresponds well with that observed with polymer just at the point that there is not much of a layer at the wall and the 50% diffusion layer thickness is increasing rapidly with streamwise distance. By the next measurement location, $\xi = 36.4$ ($x/\delta_{avg} = 20.7$), the water injection data in a LEBU modified TBL corresponds very well to equation (3.4), as shown in figure 3.29. Note that Poreh and Cermak (1964) define this location as the intermediate zone, but correspondence to Morkovin's exponential curve show final zone characteristics. Downstream of $\xi = 36.4$, all of the water injection mean concentration profiles in a LEBU (and standard) TBL were similar to figure 3.29 in that they agree very well to Morkovin's empirical curve of the final diffusion zone.

The downstream development of the standard deviation profiles of the water injection concentration data in a LEBU modified TBL are shown in figures 3.30, 3.31, 3.32, and 3.33 at $\xi = 19.5$, 36.4, 58.9, and 92.0, respectively. Here, y^+ has been nondimensionalized with standard TBL pure water values of ν and u^*. These values are used for nondimensionalization of y^+ in all subsequent figures where needed. The standard deviation profiles have a peak which decreases and moves away from the wall for increasing streamwise distance from the slot, but the location of the peak above the wall at a given station is not injection rate dependent. These trends are very similar to the water injection results in a standard TBL of Brungart (1990).

Figures 3.34 and 3.35 are the water injection data skewness and kurtosis profiles for the same conditions at $\xi = 36.4$. Notice that these two figures show no dependence on the injection rate. Also, the skewness profile starts near zero and proceeds negative before returning towards the Gaussian value of zero. The

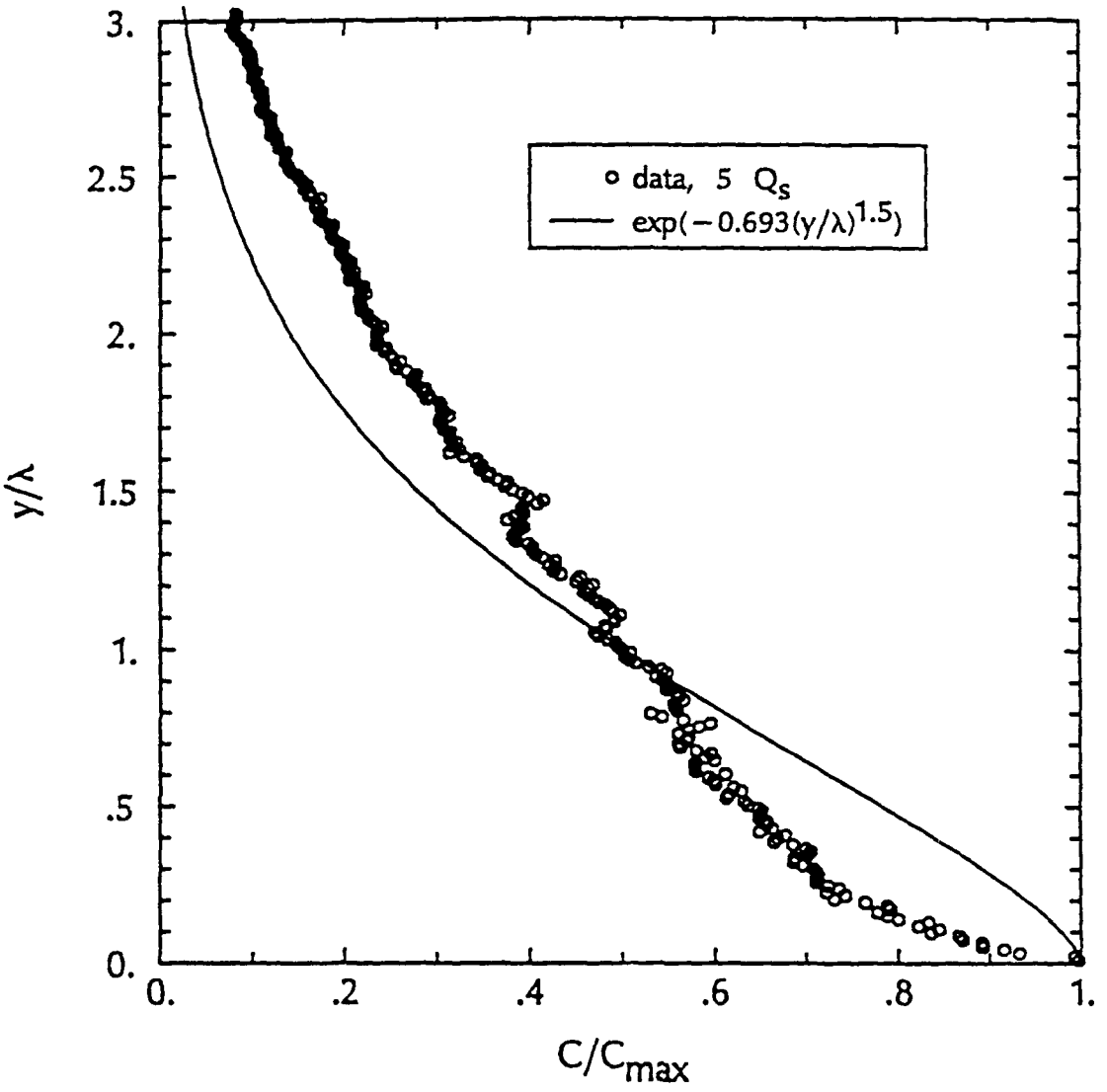

Figure 3.28. Comparison of mean water concentration profile in a LEBU modified TBL at $\xi = 19.5$ to Morkovin's (1965) exponential curve in the intermediate diffusion zone

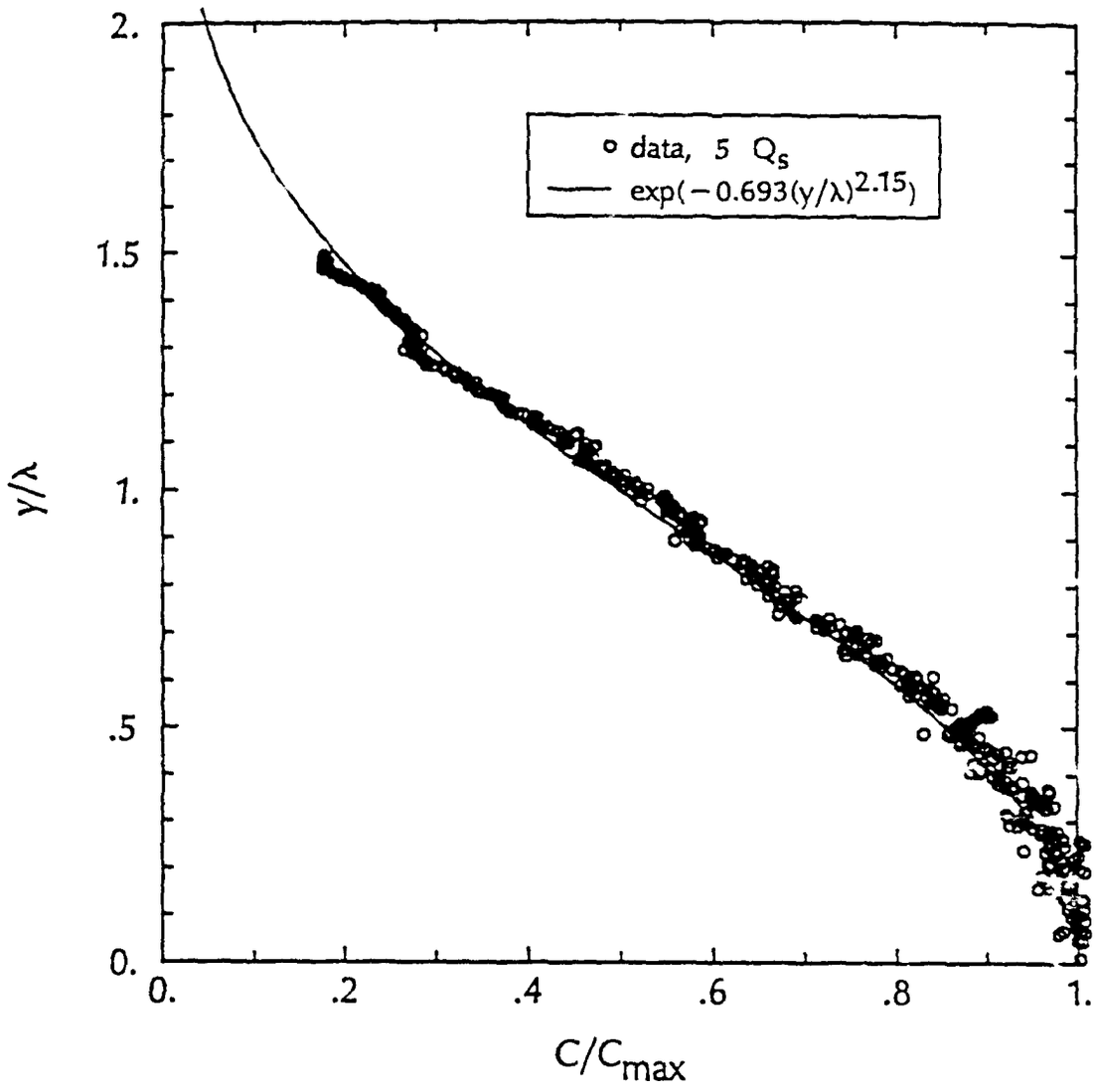

Figure 3.29. Comparison of mean water concentration profile in a LEBU modified TBL at $\xi = 36.4$ to Morkovin's (1965) exponential curve in the final diffusion zone

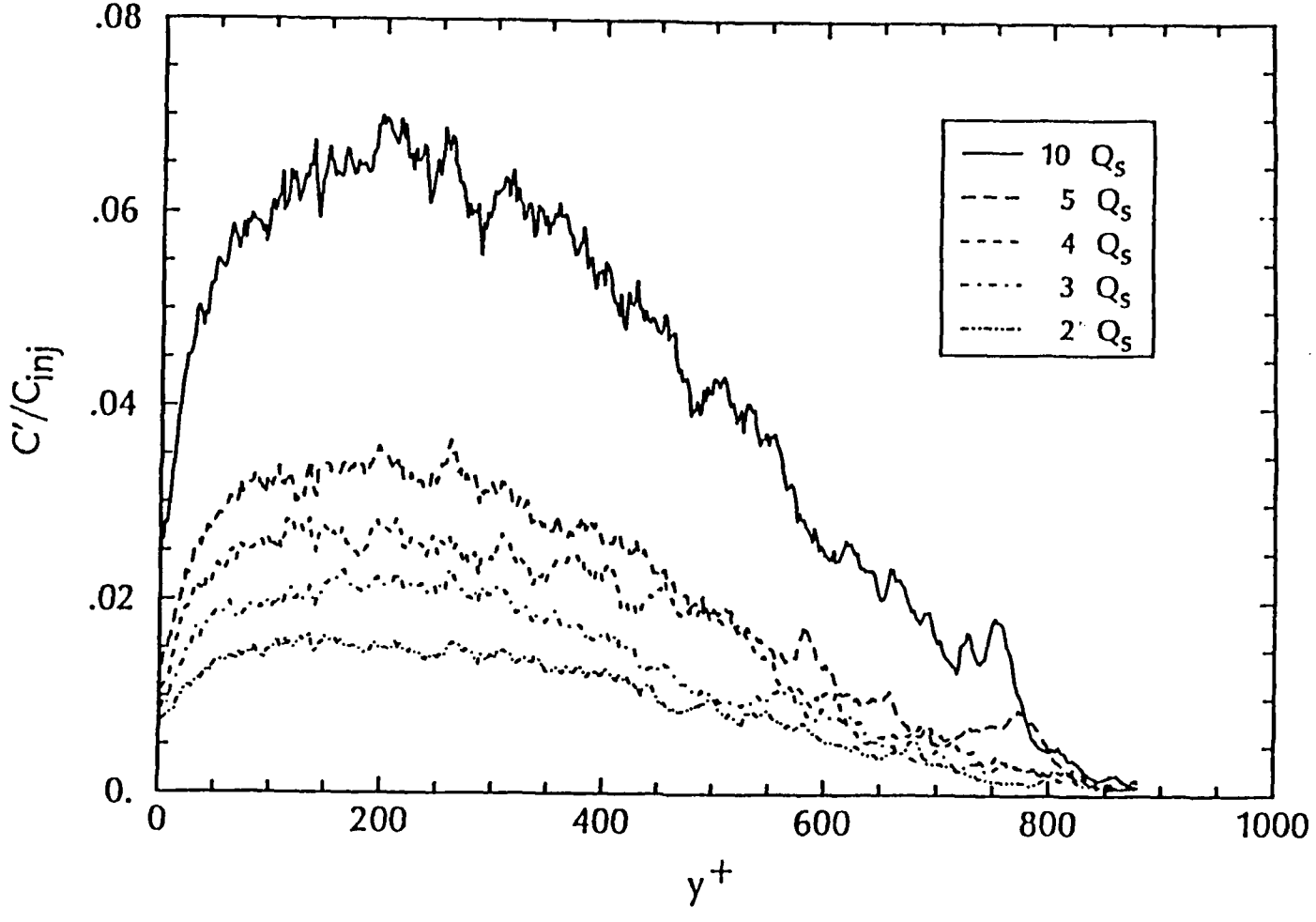

Figure 3.30. Water injection standard deviation profiles in a LEBU modified TBL at $\xi = 19.5$

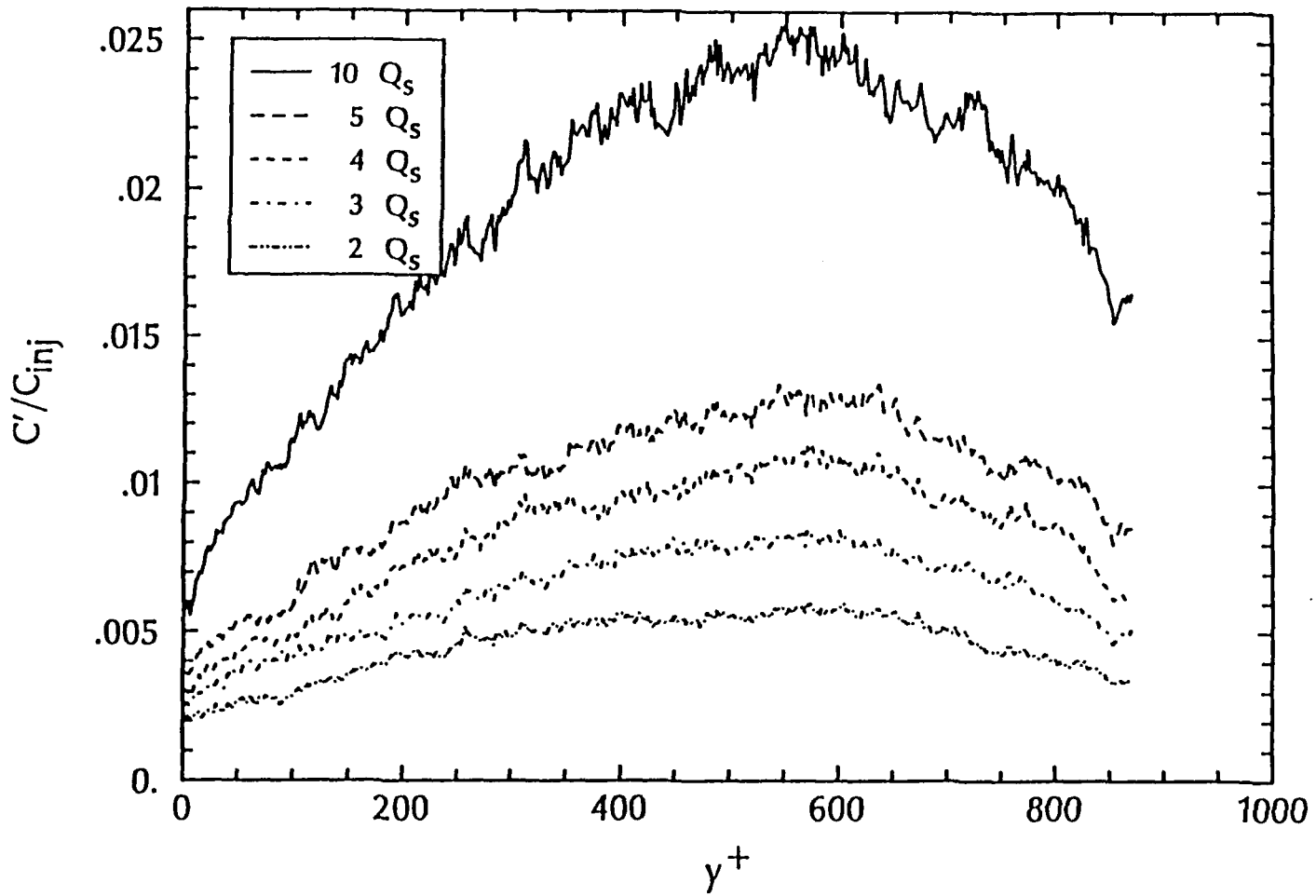

Figure 3.31. Water injection standard deviation profiles in a LEBU modified TBL at $\xi = 36.4$

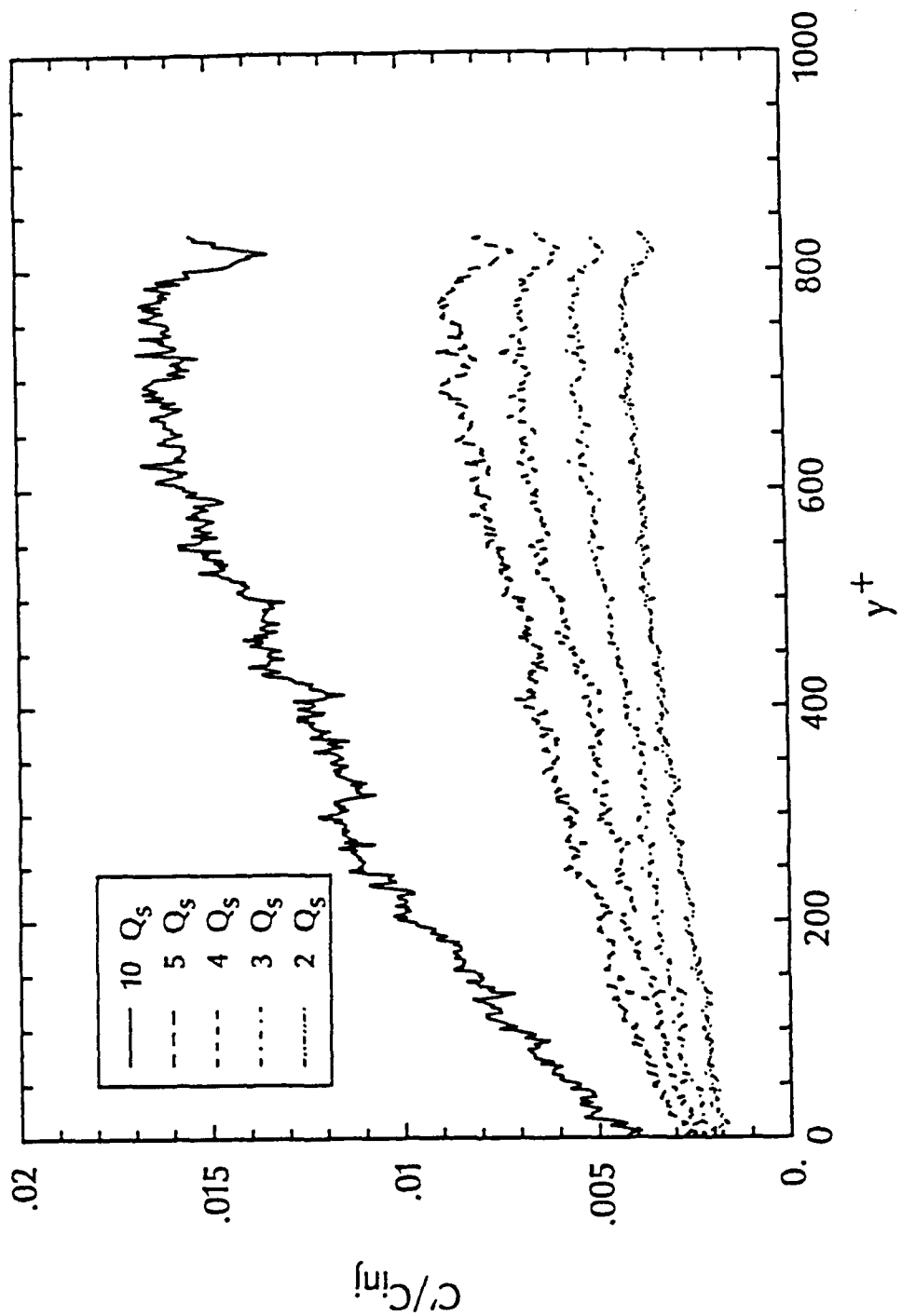

Figure 3.32. Water injection standard deviation profiles in a LEBU modified TBL at $\xi = 58.9$

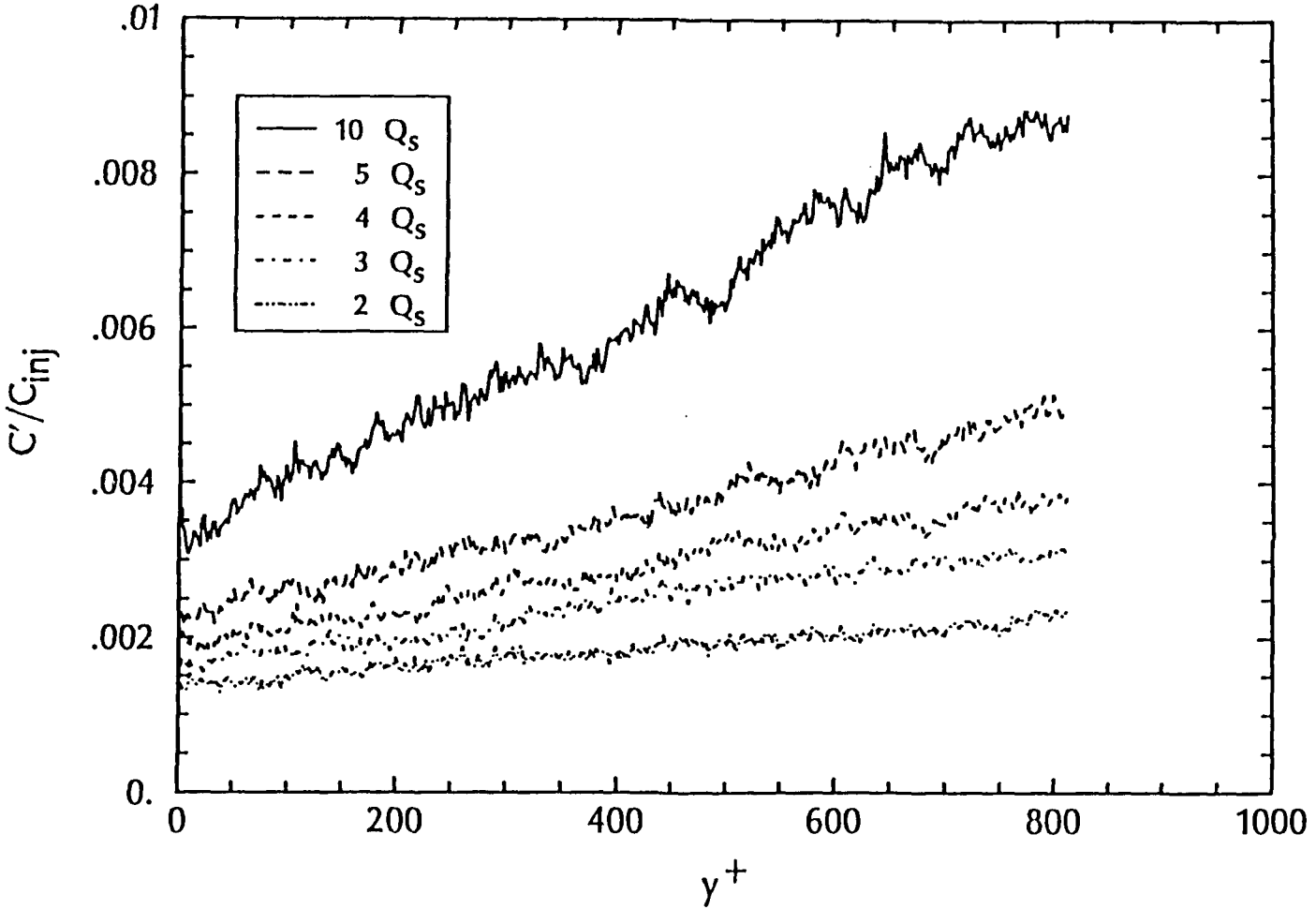

Figure 3.33. Water injection standard deviation profiles in a LEBU modified TBL at $\xi = 92.0$

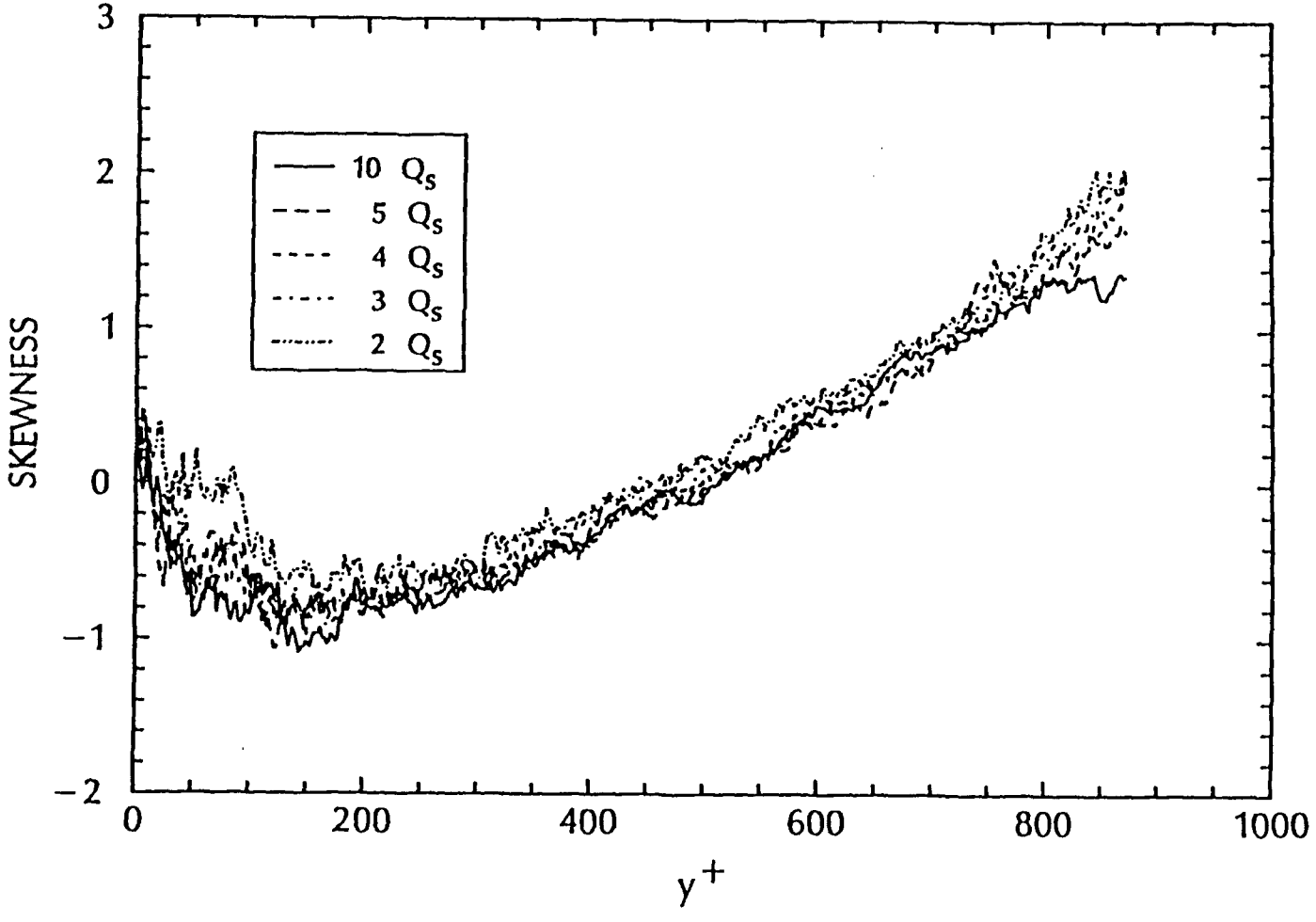

Figure 3.34. Water injection skewness profiles in a LEBU modified TBL at $\xi = 36.4$

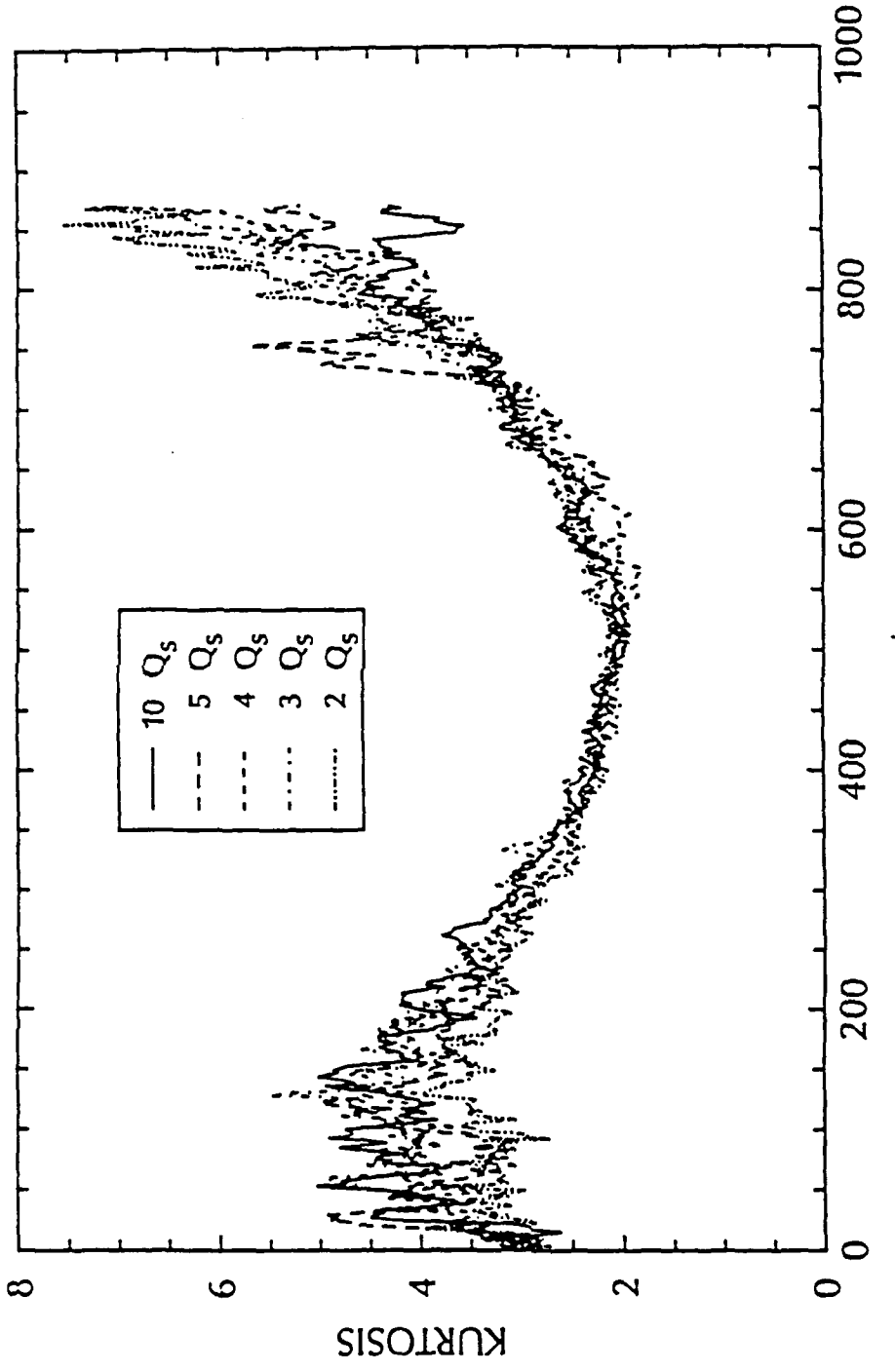

Figure 3.35. Water injection kurtosis profiles in a LEBU modified TBL at $\xi = 36.4$

profiles go through zero at approximately $y^+ = 550$. This corresponds to the location of the peak in the standard deviation profiles which is consistent to observations by Chatwin and Sullivan (1990). Chatwin and Sullivan (1990) have found many similarities in the statistical properties of concentration distributions of dispersing scalars of turbulent shear flows and have derived theoretical relationships for these properties. Also, Chatwin and Sullivan (1990) claim that the features described by the theoretical model apply regardless of the type of shear flow, dispersing scalar, or measurement technique if the resolution is high enough. The trends mentioned above for the LEBU modified TBL are very similar to the water injection results in a standard TBL of Brungart (1990). LEBUs do not seem to affect the higher order statistics of the passive contaminant data, at least downstream of $\xi = 19.5$, thereby confirming the results of Chatwin and Sullivan (1990).

3.2.2 Polymer Injection

The effects of LEBU devices on the diffusion of polymer is much greater than for water. Figures 3.36 [standard TBL data taken from Brungart (1990)] and 3.37 show the maximum normalized local polymer concentration as a function of distance from the slot for the standard and LEBU modified TBL, respectively The upstream most measurements without LEBUs were taken 25.4 mm further upstream than with the LEBUs in place because the devices interfered with the calibration process at station 1. Again, both sets of data were taken by different investigators, but everything including the polymer type and concentration were identical in both cases. There are several interesting points to be made about these figures. At the upstream most location with LEBUs, figure 3.37 at $x = 50.8$ mm, the maximum polymer concentrations are very similar for all of the

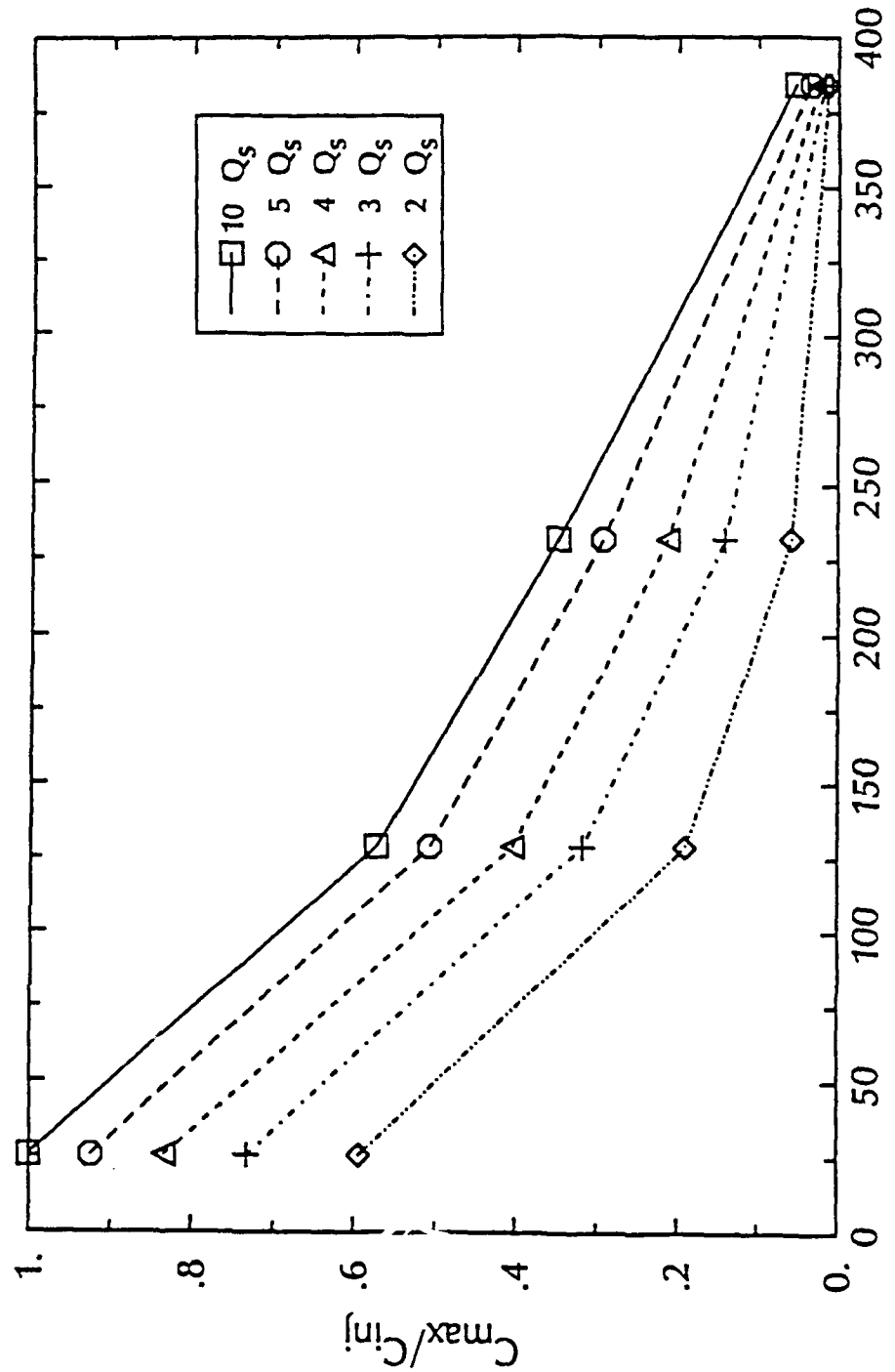

Figure 3.36. Maximum polymer concentration versus streamwise distance from the slot in a standard TBL [data taken from Brungart (1990)]

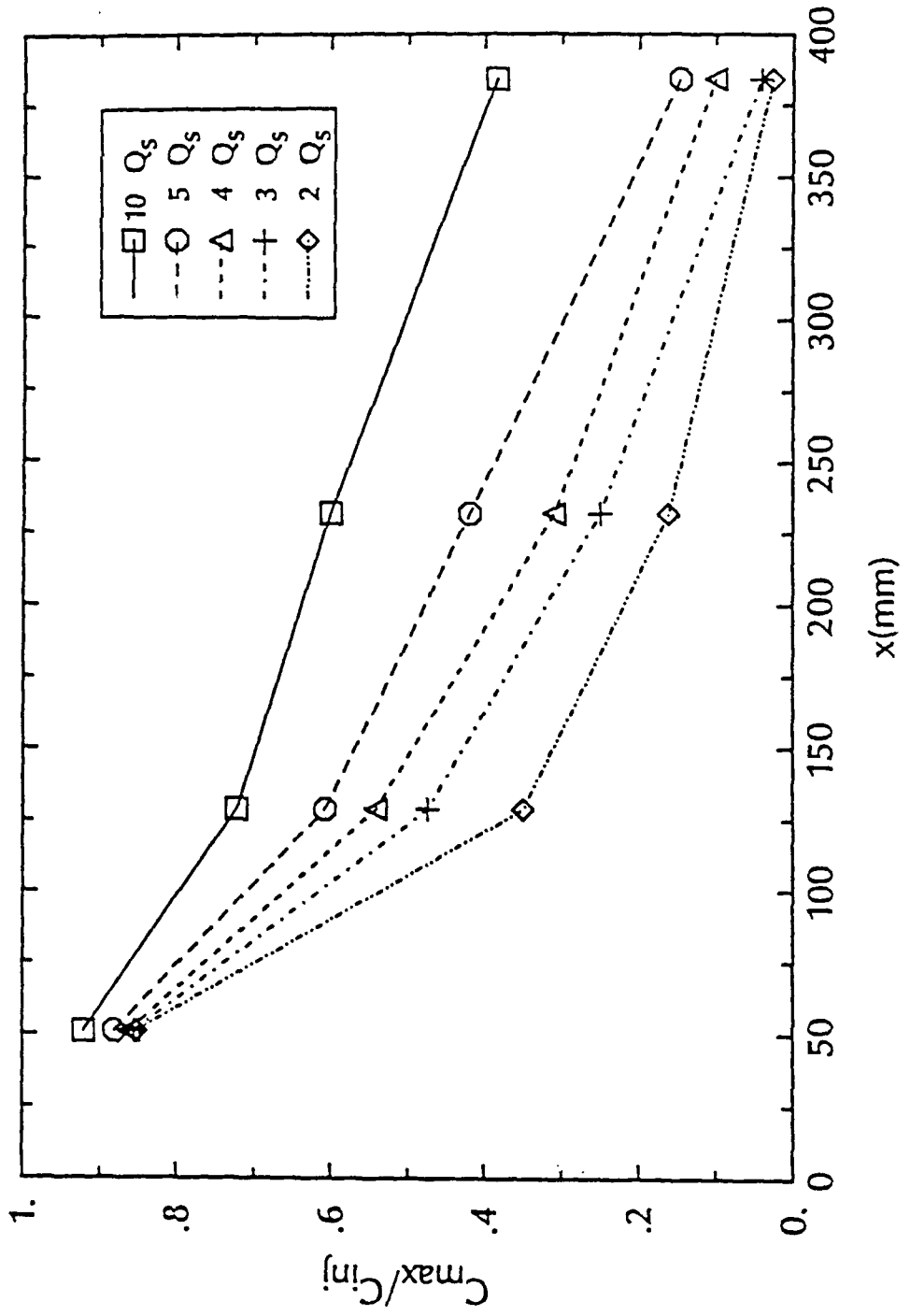

Figure 3.37. Maximum polymer concentration versus streamwise distance from the slot in a LEBU modified TBL

injection rates. This is not the case without LEBUs in figure 3.36, even at $x = 25.4\ mm$. This indicates that the LEBUs hinder the diffusion process to such an extent that the polymer concentration at the wall at $x = 50.8\ mm$ has only begun to diminish from the injection concentration at all injection rates. Another point to notice is that the maximum concentration of polymer is significantly higher at every location and injection rate in the LEBU modified TBL than in the standard TBL. At the most downstream measurement location, $x = 384.2\ mm$, approximately 39% of the $10Q_s$ injected concentration remains on the wall in the LEBU modified TBL compared to 3% or less in the standard TBL.

The mean polymer concentration profiles in the LEBU modified TBL at $x = 50.8$ (or $\xi = 19.5$) are shown in figure 3.38. A thick layer of polymer exists on the wall, and the thickness decreases with decreasing polymer injection rates.

A check on the results was performed at the downstream most measurement location. Polymer concentration data were obtained with the LEBUs present, then the water tunnel was immediately drained below the test section, the devices were removed, and the tunnel was filled back up and data were then obtained with no LEBU devices present. Using the same calibration to reduce both sets of data yielded results consistent to that described above.

Figures 3.39 [data taken from Brungart (1990)] and 3.40 show the polymer mean concentration profiles at $x = 384.2\ mm$ (or $\xi = 92.0$) in a standard and LEBU modified TBL, respectively. There is a relatively flat concentration profile with an insignificant amount of polymer in the standard TBL, as shown in figure 3.39. But, there are large maximum wall concentrations for high injection rates in the LEBU modified TBL. Although the wake in the mean velocity profile caused by the LEBUs has relaxed by this location, see figure 3.1, the polymer

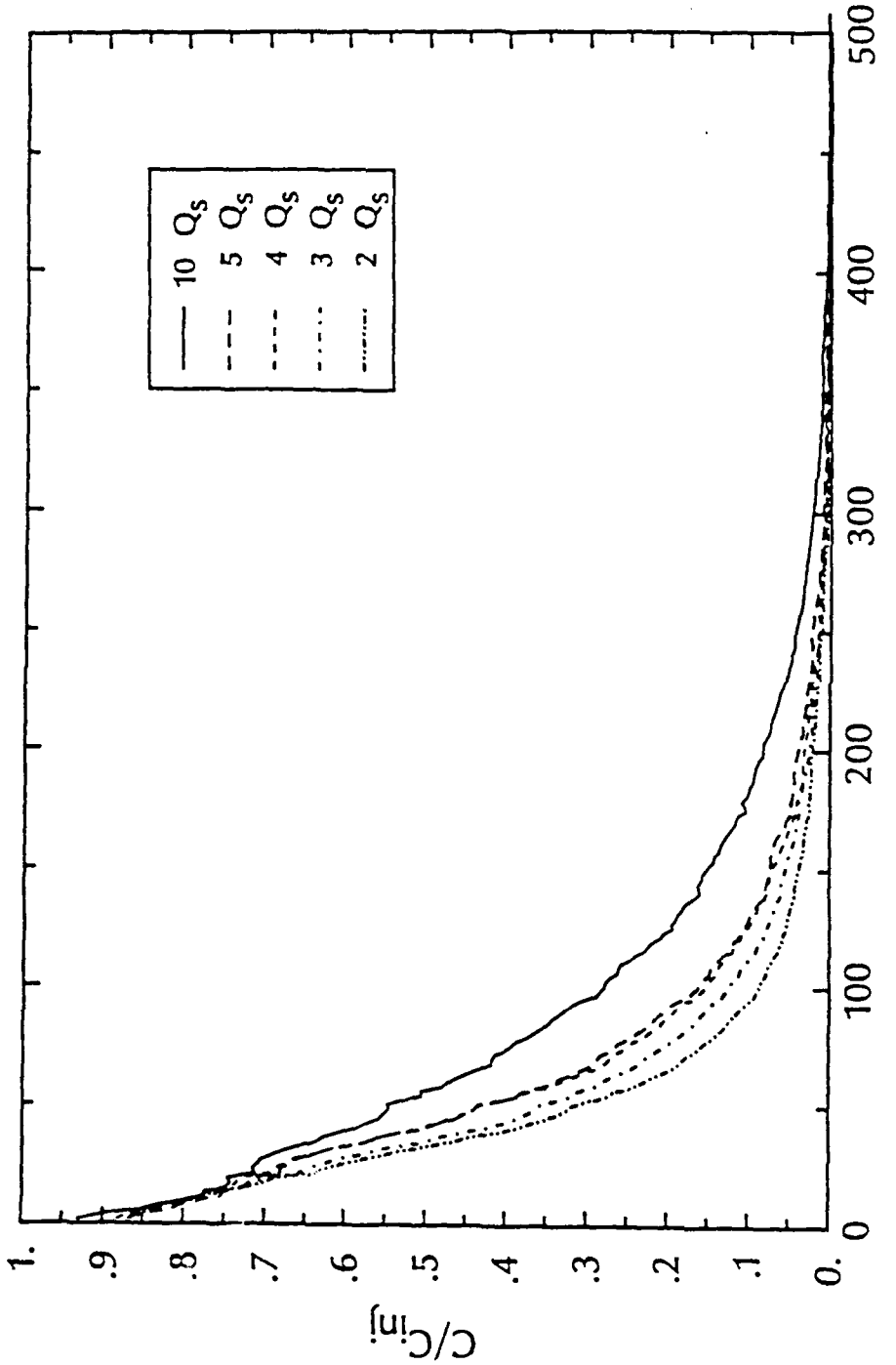

Figure 3.38. Mean polymer concentration profiles in a LEBU modified TBL at $\xi = 19.5$

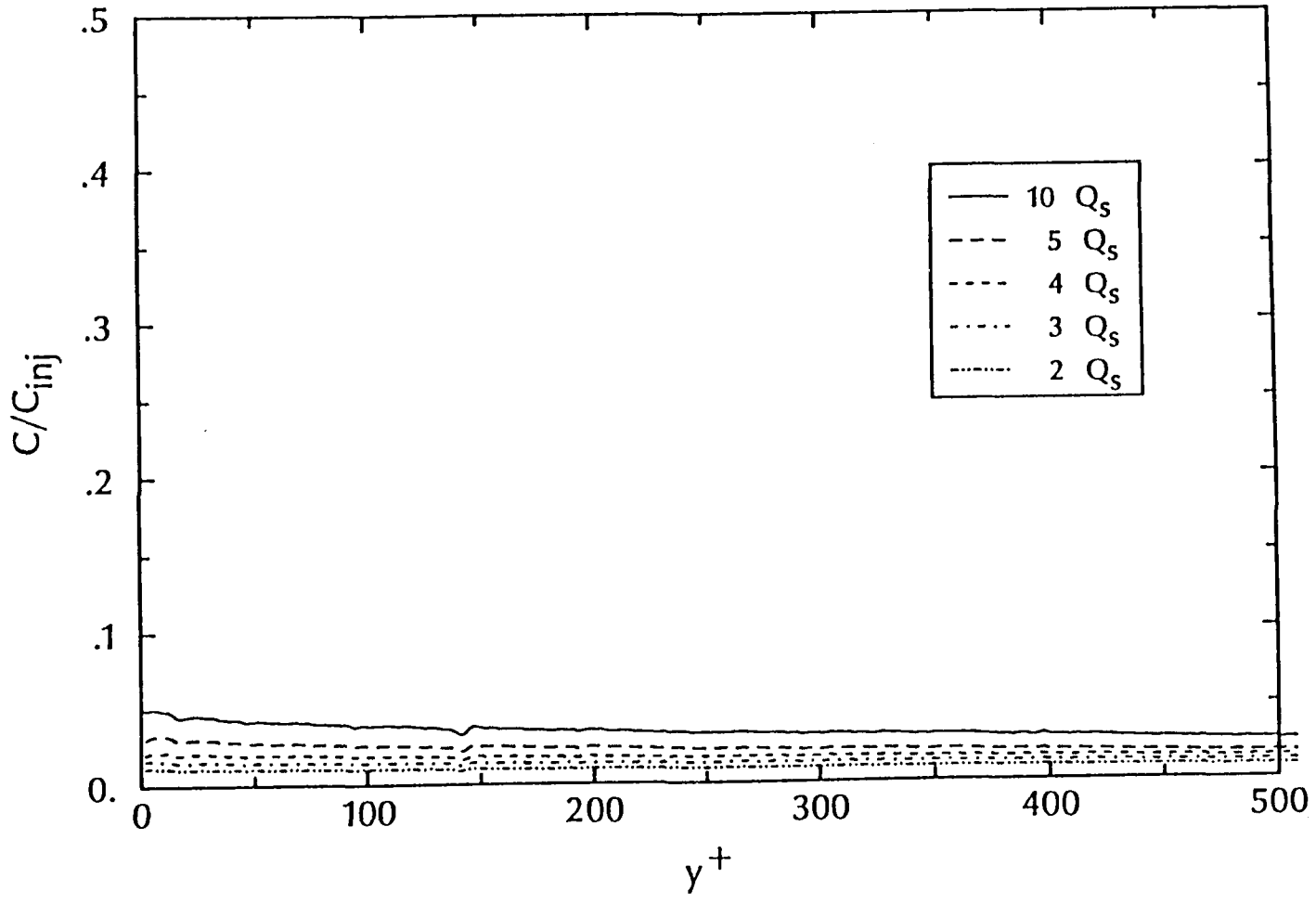

Figure 3.39. Mean polymer concentration profiles in a standard TBL at $\xi = 92.0$ [data taken from Brungart (1990)]

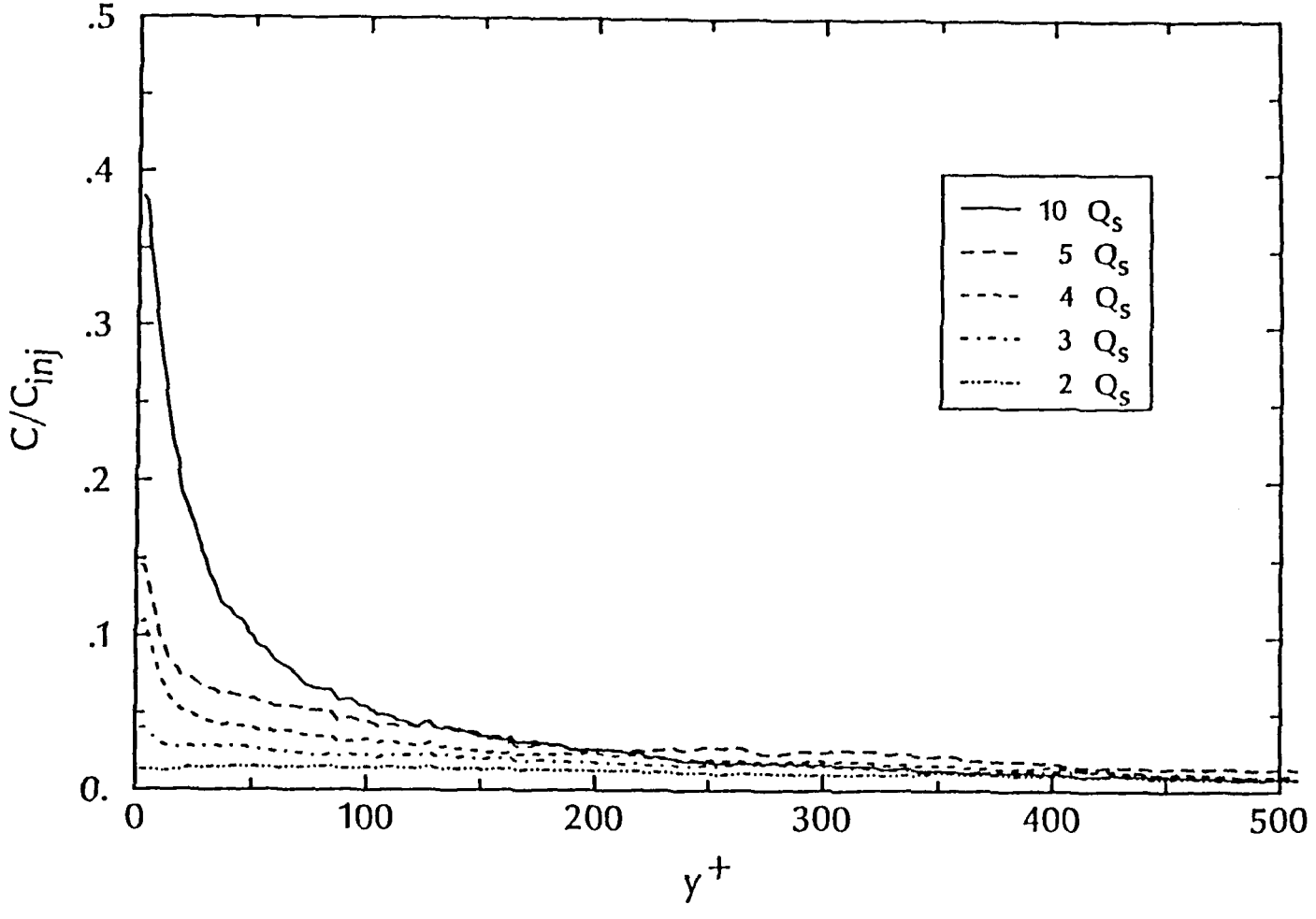

Figure 3.40. Mean polymer concentration profiles in a LEBU modified TBL at $\xi = 92.0$

mean concentration profiles are still affected to a large degree. This is a result of the integrated affect of the reduction to the diffusion rate by the LEBUs.

By examining the polymer injection data as was done with water data in figure 3.27, some insight on polymer diffusion is found. Figures 3.41 [taken from Brungart *et al.* (1990)] and 3.42 show the downstream development of the normalized 50% diffusion layer thickness for a standard and LEBU modified TBL, respectively. Both figures show similar trends in that polymer diffuses more slowly than water initially, before an abrupt transition occurs from the initial zone. But the magnitudes and locations of these occurrences are different. The value of λ in the LEBU modified TBL is slightly thinner initially, and remains thinner than that of a standard TBL. The location of the minimum value of λ, where transition between the diffusion zones occurs, is further downstream in the LEBU modified TBL. Also, transition between the diffusion zones is not as abrupt for all injection rates in the LEBU modified TBL. Another point to be made is that unlike water diffusion, there is a dependence of λ/δ_{local} on the injection rate. The 50% diffusion layer thickness is greater for higher injection rates than for the lower injection rates at the upstream locations, but between $x/\delta_{avg} = 20.7$ and 50.5 this trend reverses. For these downstream locations at the high injection rates, a large concentrated layer of polymer remains on the wall, but at the low injection rates, the polymer layer has diffused much more. This effect is consistent to Brungart *et al.* (1990) results.

Comparison of polymer injection data to Morkovin's exponential curves shows some interesting results. Figure 3.43 is a plot of y/λ versus C/C_{max} for 5 Q_s polymer injection into a LEBU modified TBL at $\xi = 19.5$. The polymer concentration data below $y/\lambda = 1.0$ lie right on Morkovin's curve for a passive contaminant in the intermediate diffusion zone Above $y/\lambda = 1.0$, there is a deviation from the curve and larger values of C/C_{max} for polymer injection are

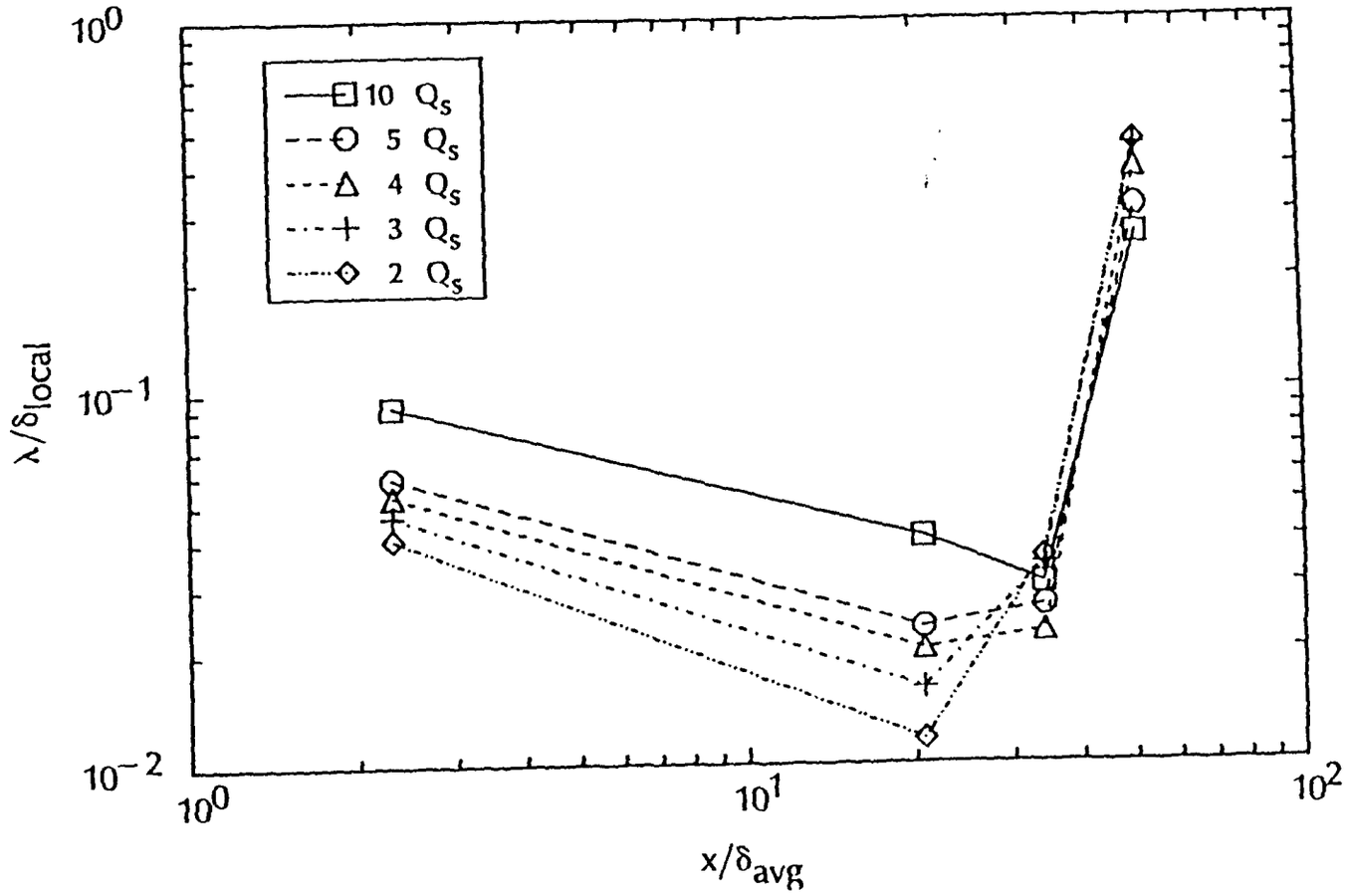

Figure 3.41. Normalized 50 percent polymer diffusion layer thickness versus downstream distance in a standard TBL [taken from Brungart *et al.* (1990)]

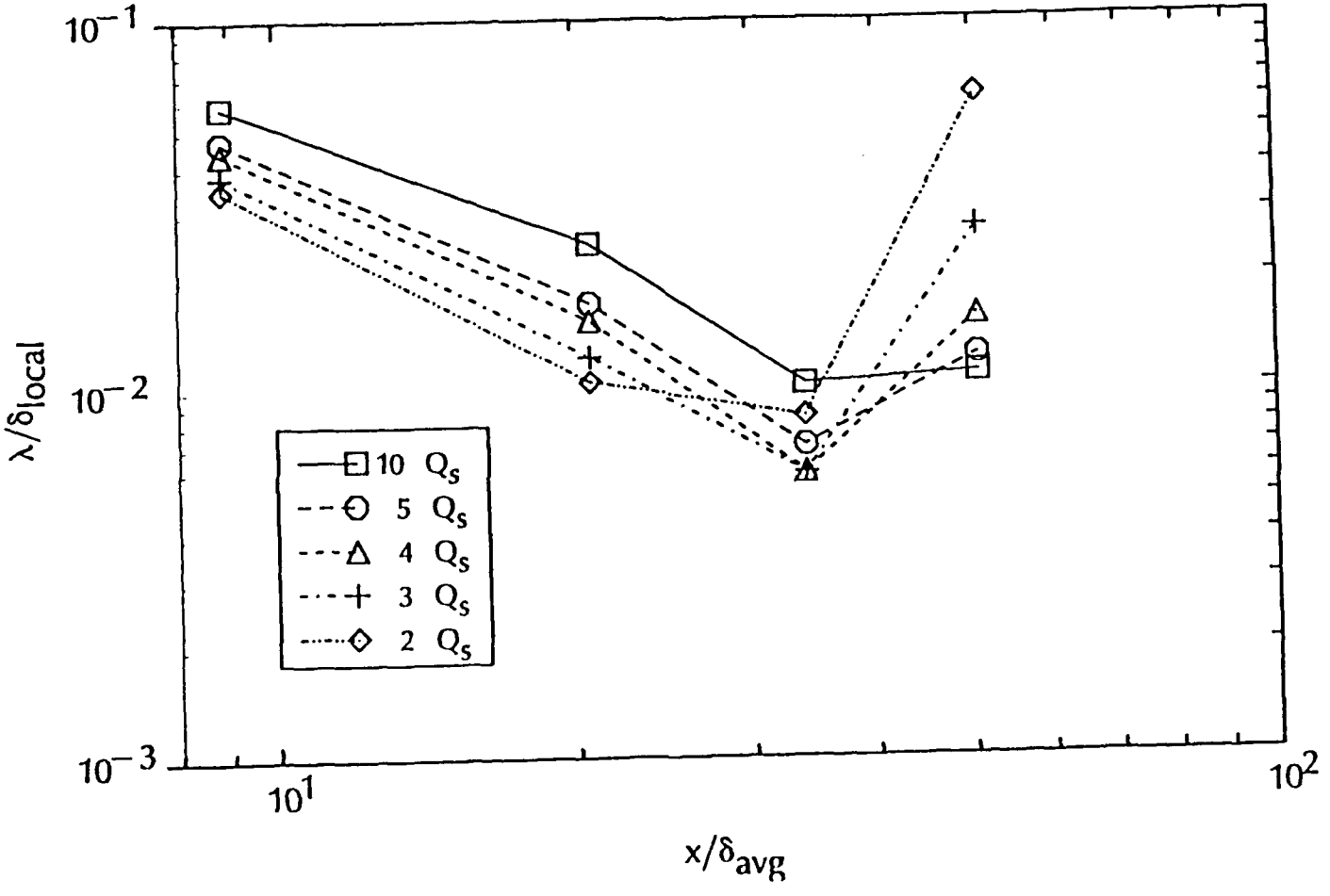

Figure 3.42. Normalized 50 percent polymer diffusion layer thickness versus downstream distance in a LEBU modified TBL

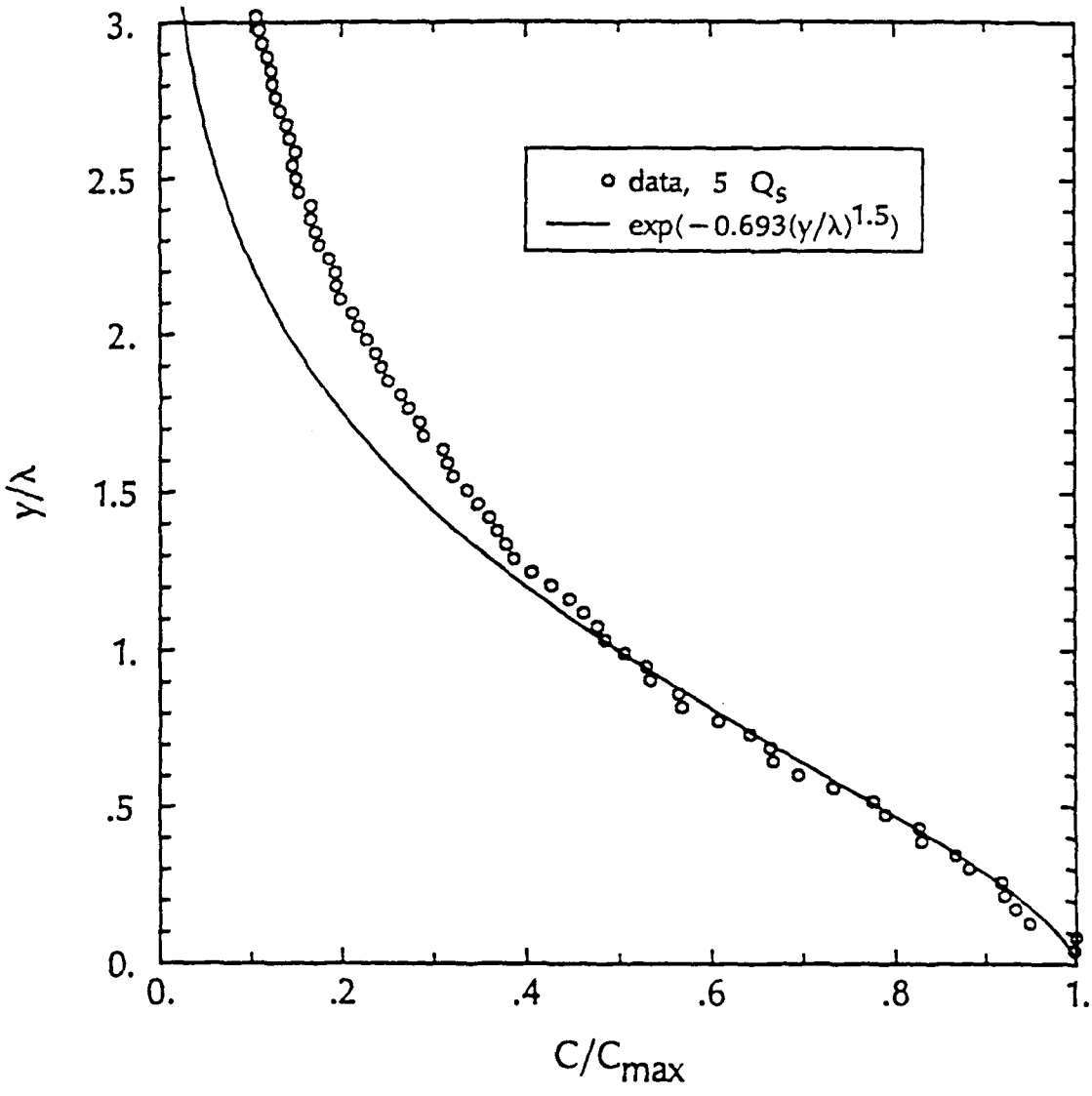

Figure 3.43. Comparison of mean polymer concentration profile in a LEBU modified TBL at $\xi = 19.5$ to Morkovin's (1965) exponential curve in the intermediate diffusion zone

observed over the passive contaminant results. These trends are very similar to Brungart's (1990) polymer injection data in a standard TBL at the most upstream measurement location, which is 25.4 mm further upstream than data in figure 3.43.

Figures 3.44, 3.45, and 3.46 are polymer injection data with standard [data taken from Brungart (1990)] and LEBU modified TBLs at $\xi = 36.4$, 58.9, and 92.0, respectively. Note that Brungart's (1990) data has a peak in C/C_{max} above $y/\lambda = 0$ which cannot be correct. This was attributed to a possible index of refraction effect of polymer, but this was not noticed in the present investigation. This error near the wall is likely the result of the calibration procedures employed by Brungart (1990) and is why the current investigation used a modified approach with a near wall calibration correction. These figures show that Morkovin's curve for a passive contaminant does not describe the diffusion of polymer. Similar trends in standard and LEBU modified TBL polymer injection data are seen in figures 3.44 and 3.45, but figure 3.46 shows large differences. Referring to standard TBL data in figure 3.41, the downstream most measurement location marks an abrupt increase in the 50% diffusion layer thickness and Brungart (1990) argues that this is the end of the initial diffusion zone. Since the 50% polymer diffusion layer is thinner in the LEBU modified TBL than in the standard boundary layer and the growth of the 50% diffusion layer thickness was not as abrupt at the same measurement location, refer to figure 3.42, the LEBU modified TBL polymer data has not reached the end of the initial zone. This is supported by figure 3.46 which shows similar trends to figures 3.44 and 3.45, but the deviation from Morkovin's curve is much greater. Note that Brungart's (1990) data in figure 3.46 is concentrated below $y/\lambda = 1.5$ because of the large value of λ used for normalization in the standard TBL at this location, and not because of any significant difference in the field of view of the measurements.

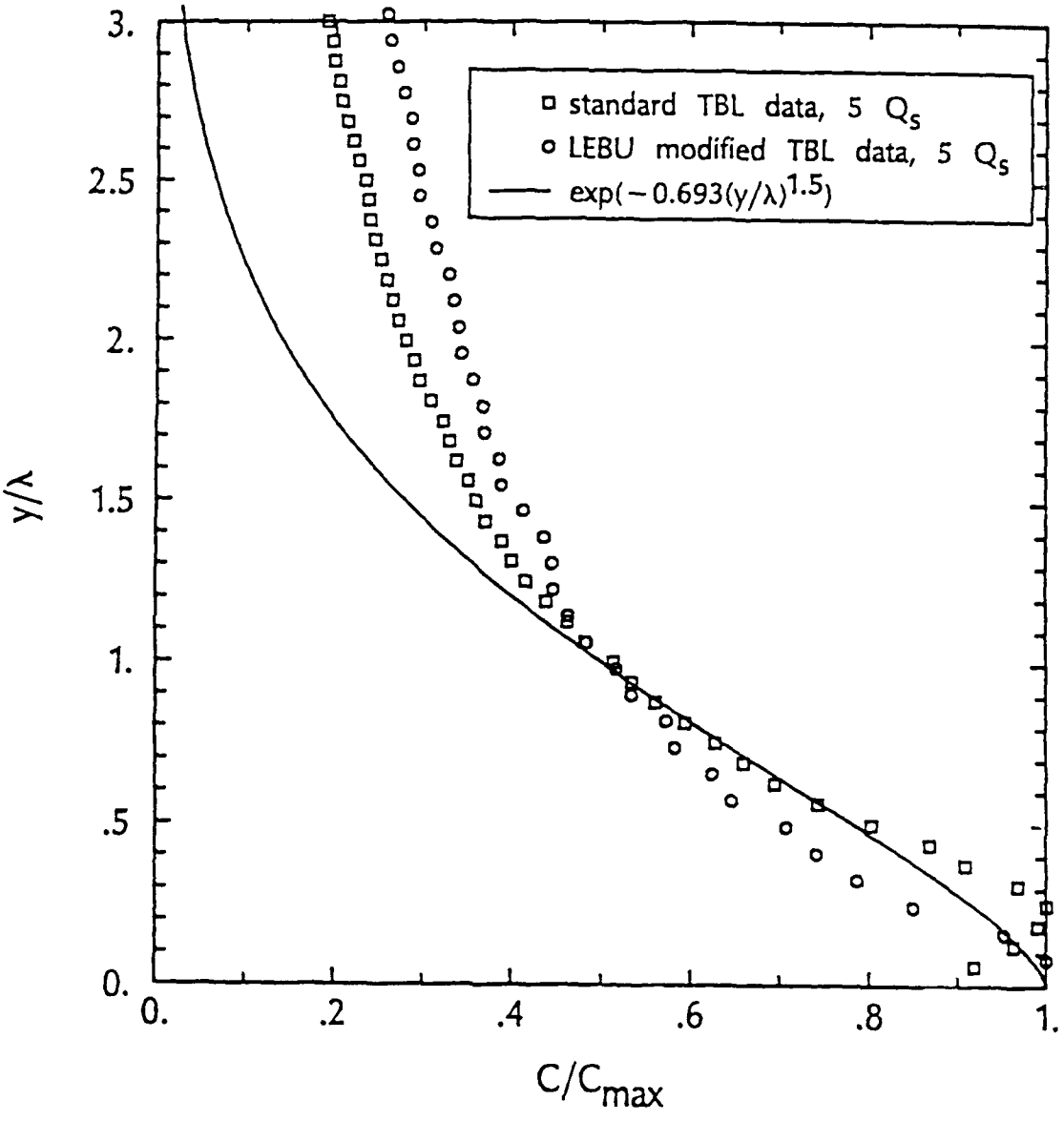

Figure 3.44. Comparison of mean polymer concentration profile in a standard [data taken from Brungart (1990)] and LEBU modified TBL at $\xi = 36.4$ to Morkovin's (1965) exponential curve in the intermediate diffusion zone

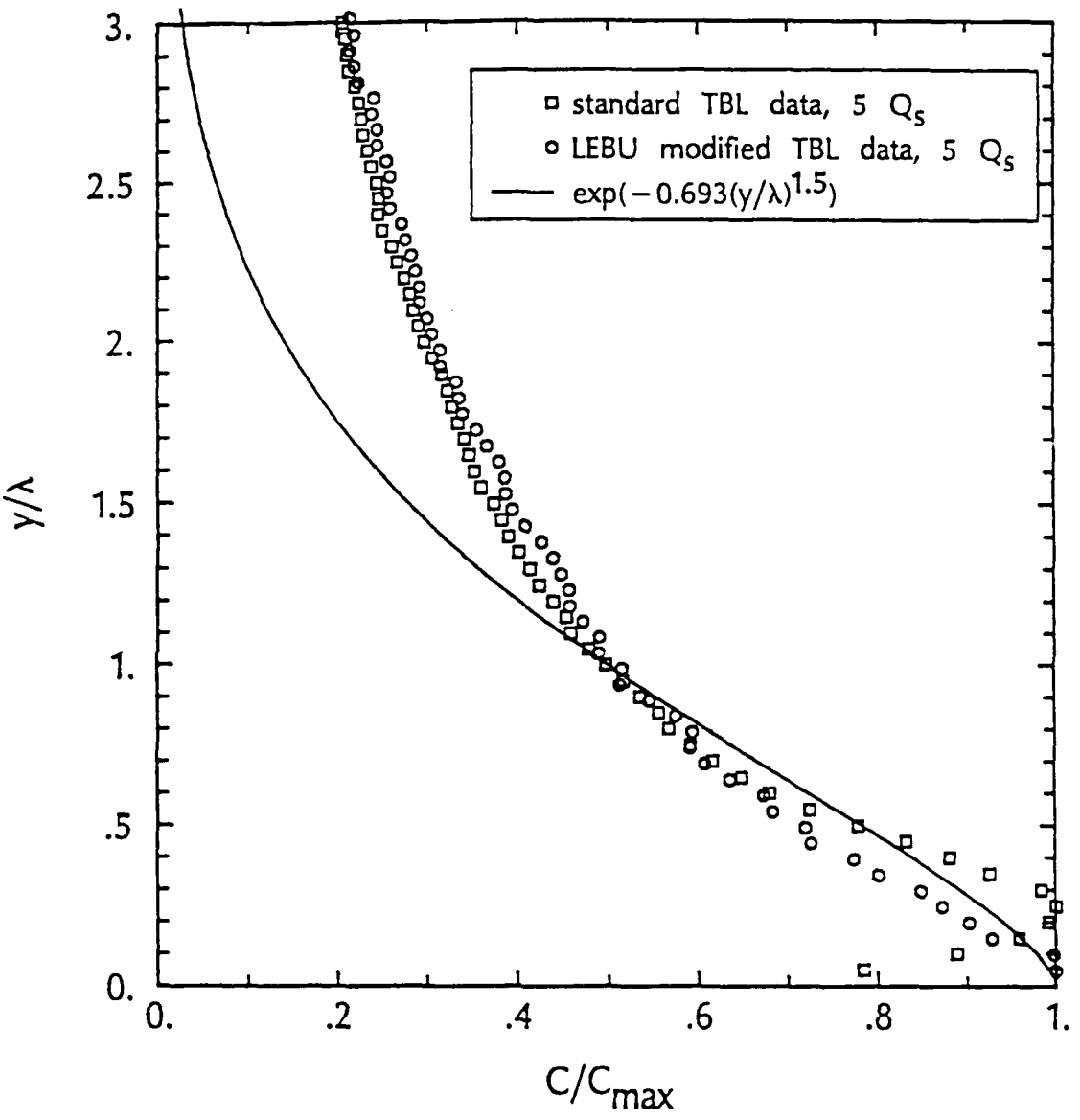

Figure 3.45. Comparison of mean polymer concentration profile in a standard [data taken from Brungart (1990)] and LEBU modified TBL at $\xi = 58.9$ to Morkovin's (1965) *exponential curve in the intermediate diffusion zone*

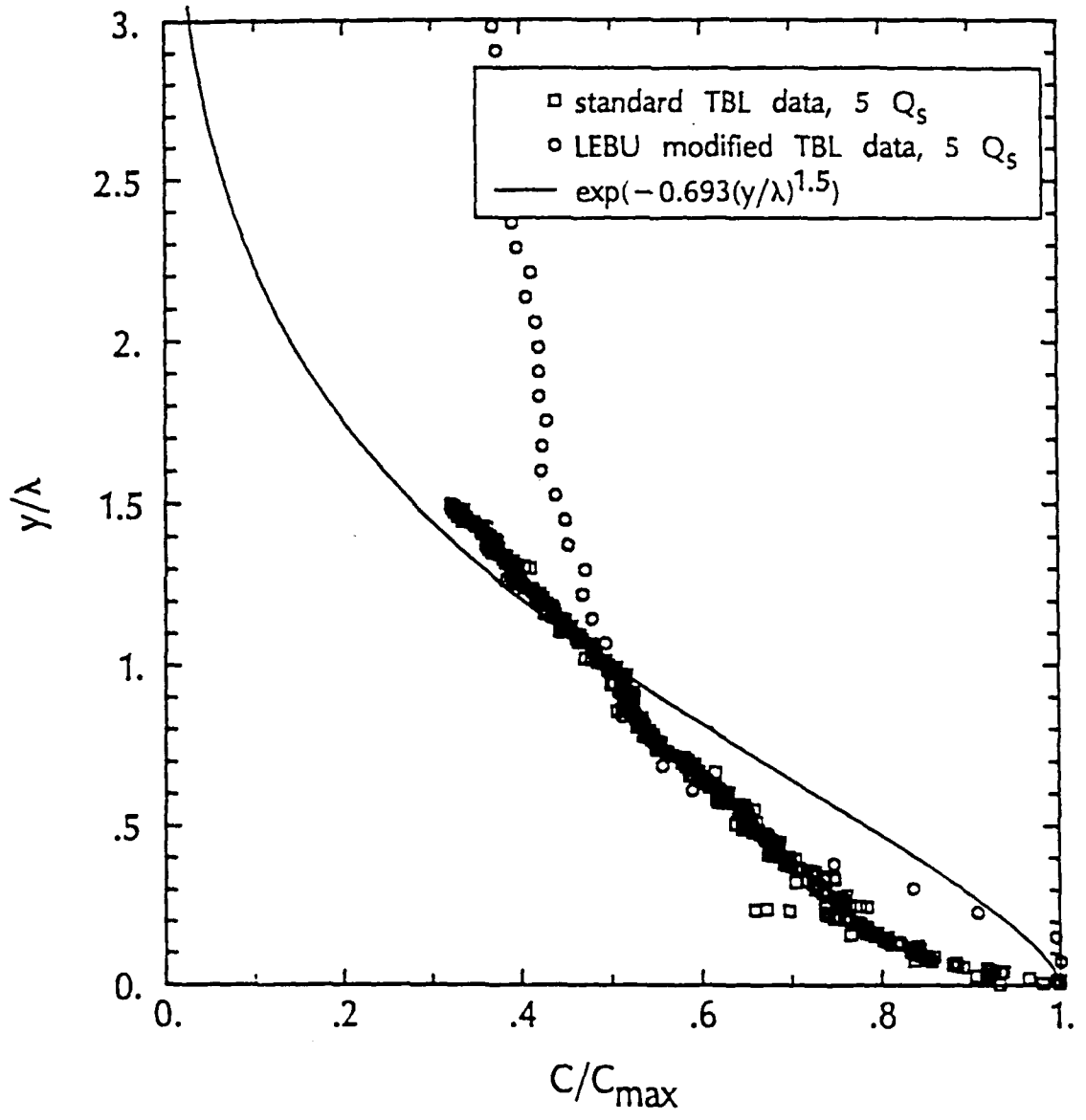

Figure 3.46. Comparison of mean polymer concentration profile in a standard [data taken from Brungart (1990)] and LEBU modified TBL at $\xi = 92.0$ to Morkovin's (1965) exponential curve in the intermediate diffusion zone

A very interesting observation is made by comparing figures 3.28 and 3.46. The water injection data in the LEBU modified TBL in figures 3.28 look very similar to the polymer injection data in the standard TBL in figure 3.46. It was argued in the previous paragraph that the polymer injection data in the standard TBL in figure 3.46 marks the end of the initial diffusion zone. Thus, a similar argument is made that the water injection data of figure 3.28 is also at the end of the initial diffusion zone. Downstream of this location, $\xi = 19.5$ ($x/\delta_{avg} = 8.8$), transition occurs between the diffusion zones and by the next measurement location, $\xi = 36.4$ ($x/\delta_{avg} = 20.7$), the water injection concentration profile in the LEBU modified boundary layer has the form expected in the final diffusion zone for a passive contaminant (refer to figure 3.29). Poreh and Cermak (1964) argue that the initial diffusion zone of a passive contaminant is very short, and Brungart *et al.* (1990) have shown in the same facility that the water injection data in a standard TBL is already in the intermediate diffusion zone by $x/\delta_{avg} = 2.3$ ($\xi = 14.0$). The major point to be made is that the LEBU devices may greatly extend the initial diffusion zone of a passive contaminant.

Intermittency profiles of the concentration data for both TBLs with polymer injection give some information on the effects of LEBUs on bursting. An ensemble of 1000 instantaneous concentration profiles at each location in both TBLs were examined to determine how often a given threshold polymer concentration was observed as a function of distance from the wall. A large number of threshold values were examined to establish if there is a range of threshold values that do not alter the results significantly. No range was found where changing the threshold had a small effect on the results. The smallest effect on the results occurred around a threshold value of $0.6C_{wall}$, thus this somewhat arbitrary value was used for the present intermittency profiles. Figures 3.47, 3.48, 3.49, and 3.50 are intermittency profiles for a standard and LEBU modified TBL with

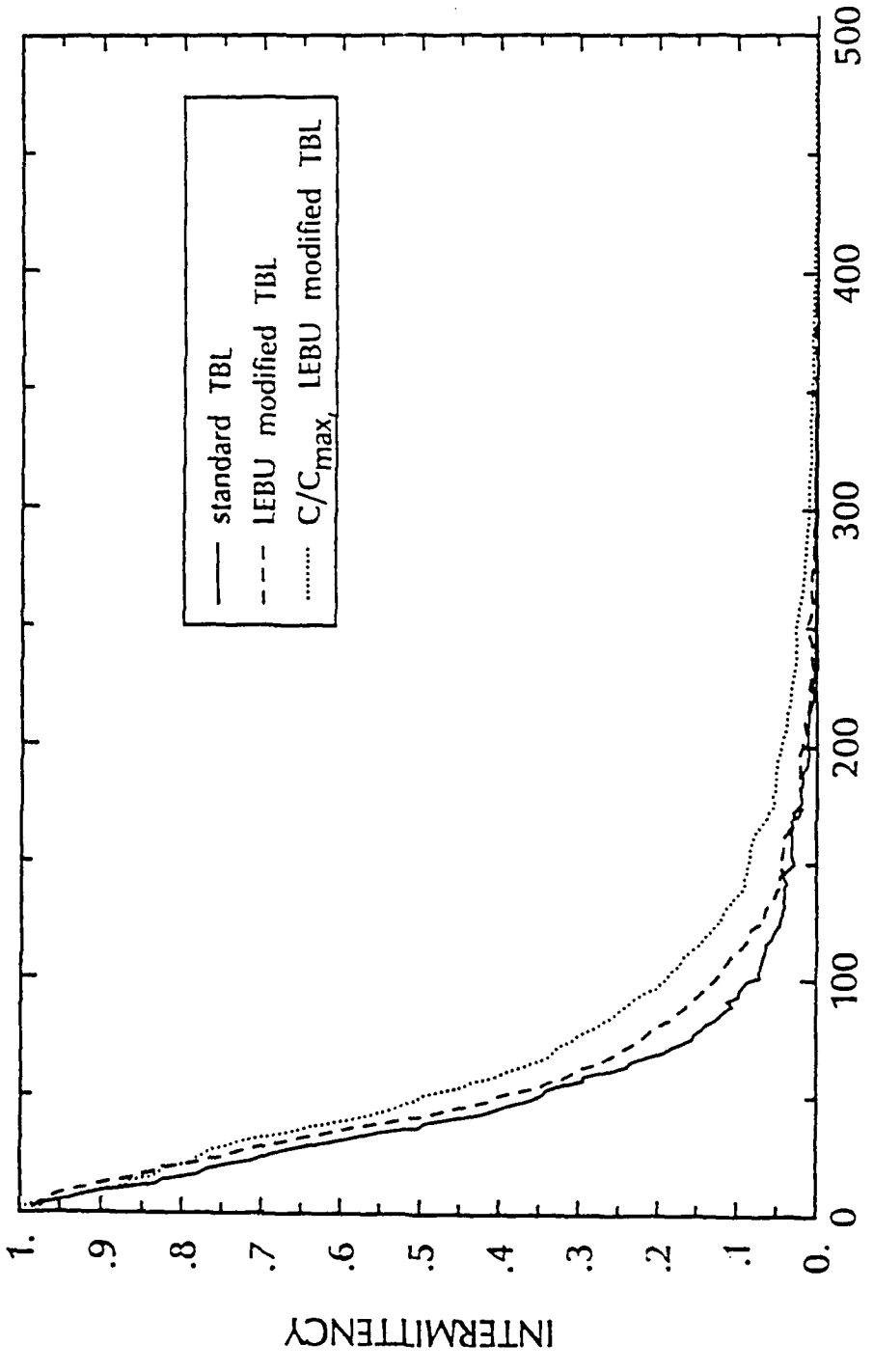

Figure 3.47. Polymer concentration intermittency profiles for a standard [data taken from Brungart (1990)] and LEBU modified TBL at $\xi = 19.5$, 5 Q_s polymer injection

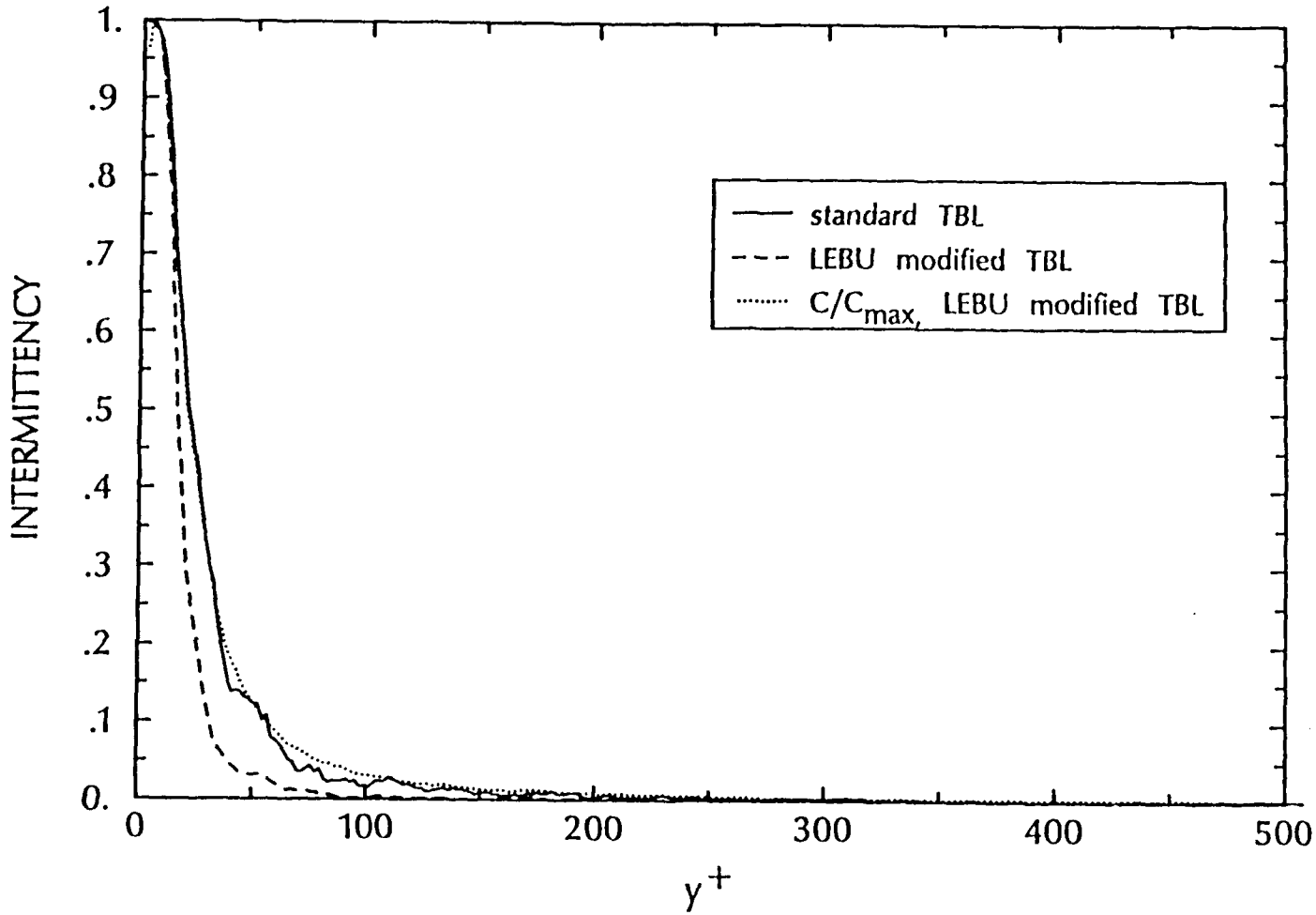

Figure 3.48. Polymer concentration intermittency profiles for a standard [data taken from Brungart (1990)] and LEBU modified TBL at $\xi = 36.4$, 5 Q, polymer injection

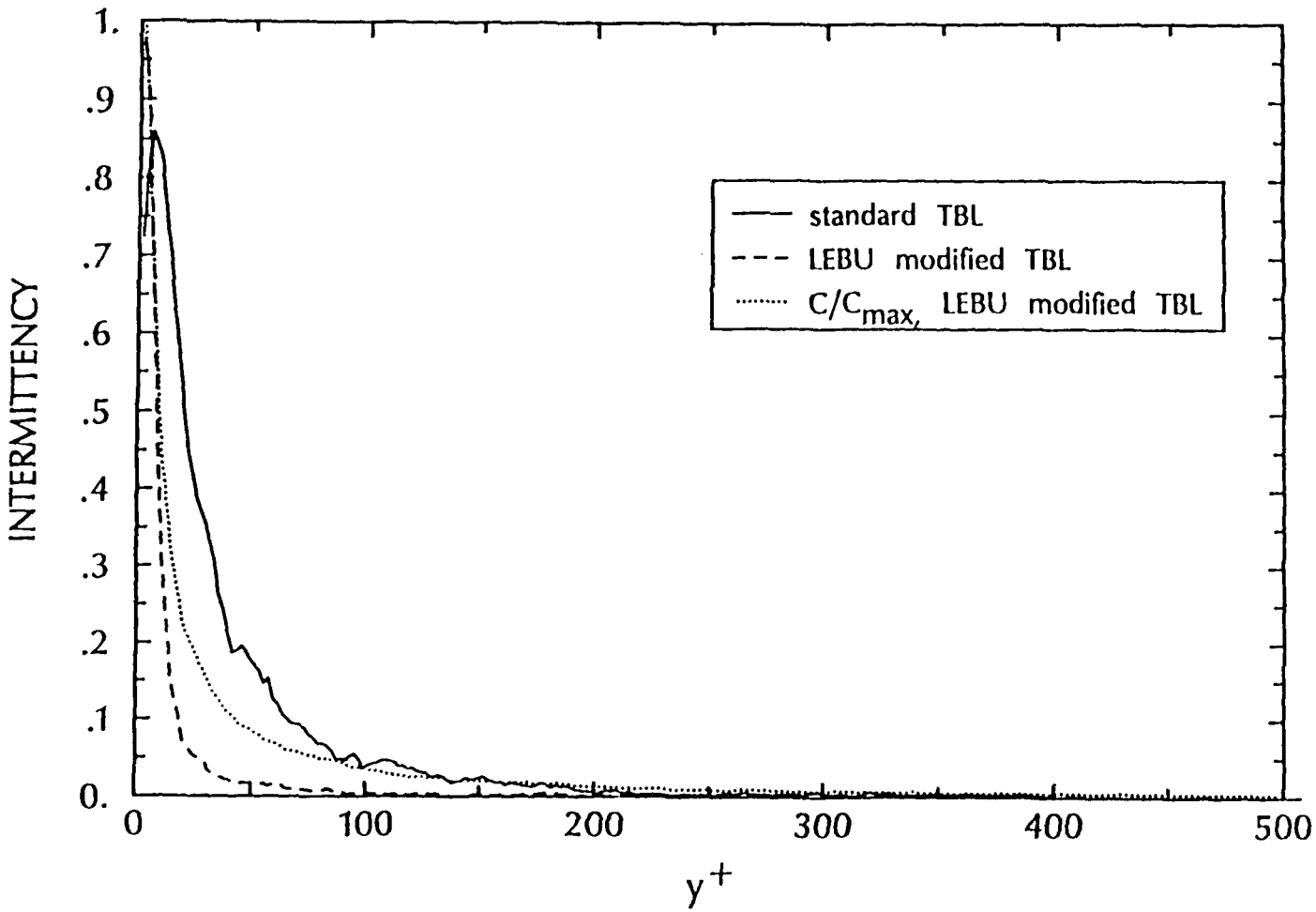

Figure 3.49. Polymer concentration intermittency profiles for a standard [data taken from Brungart (1990)] and LEBU modified TBL at $\xi = 58.9$, 5 Q_s polymer injection

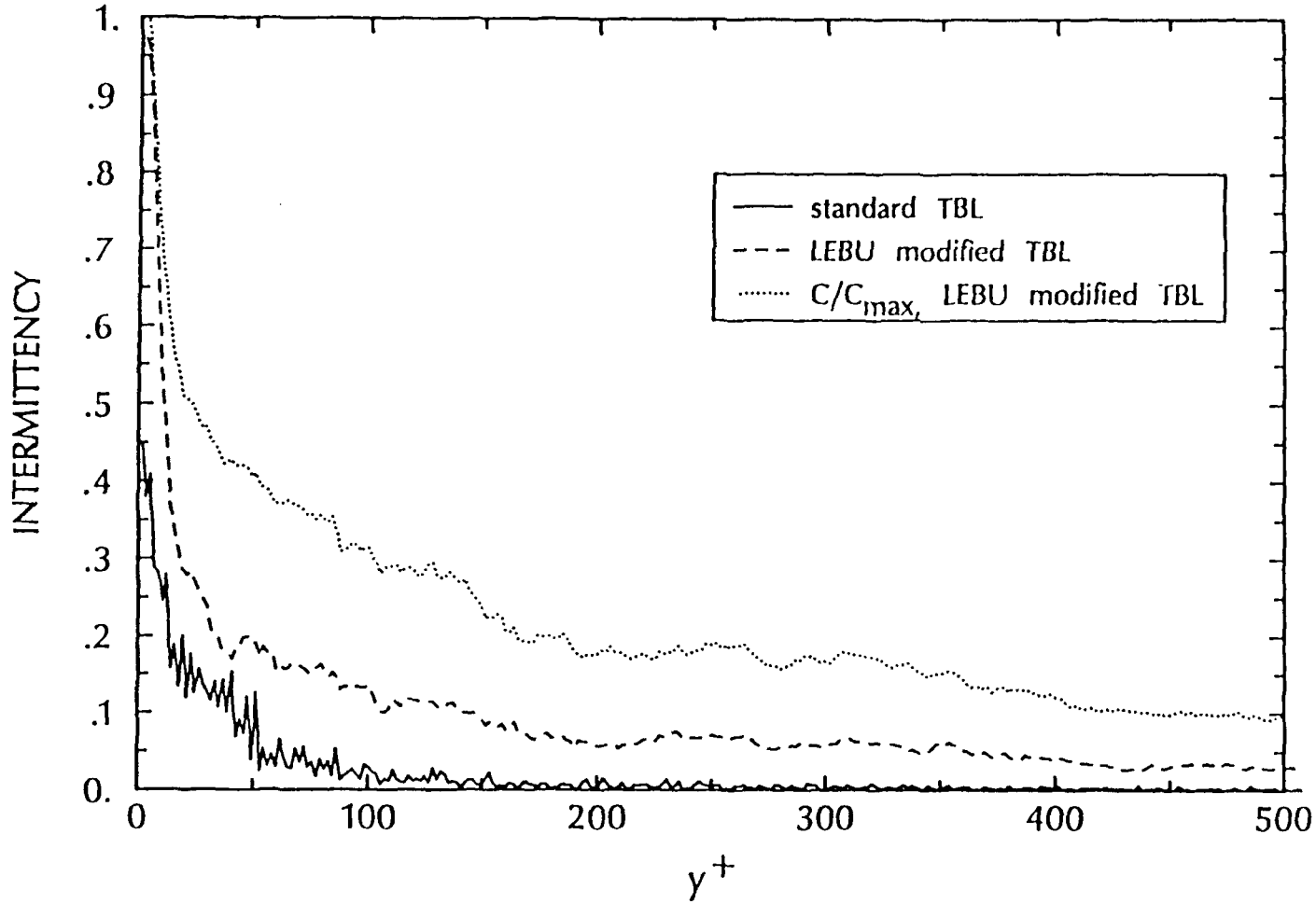

Figure 3.50. Polymer concentration intermittency profiles for a standard [data taken from Brungart (1990)] and LEBU modified TBL at $\xi = 92.0$, 5 Q_s polymer injection

polymer injection at 5 Q_s at ξ = 19.5, 36.4, 58.9, and 92.0, respectively. There are several important points to be made about these figures.

The intermittency profiles for the LEBU modified TBLs are very similar to the respective normalized mean concentration profiles, which are shown by the dotted lines in figures 3.47–3.50. Chatwin and Sullivan (1989) have shown that for the unreal case of no molecular diffusion and perfectly resolved concentration measurements, the intermittency profile is the normalized mean concentration profile, C/C_{inj}. For the dotted lines in figures 3.47–3.50, the local mean concentration has been normalized with the wall (maximum) concentration at the measurement location. This simply represents a shift of C_{inj}/C_{wall} in the curves from Chatwin and Sullivan's (1989) findings. This was done to make a direct comparison of the normalized mean concentration profiles (C/C_{wall}) to the intermittency profiles with threshold levels based on C_{wall}. Since mixing is dominated by turbulence processes and, for the present investigation, reasonably high resolution measurements are being made, it has been experimentally verified that the LIF technique, also used by Brungart *et al.* (1990), is a valid means of measuring polymer concentration profiles.

It is assumed that the lifting of concentrated filaments of polymer away from the wall is due to bursting. These lifting polymer filaments are seen in the individual instantaneous concentration profiles. Figure 3.47 shows that the intermittency profile of the standard and LEBU modified TBL are almost the same and indicate similar bursting activities at ξ = 19.5 for polymer injection. Apparently, it is hard for the LEBUs to have an affect with that much polymer on the wall, or possibly the near wall region is saturated and there is no room for an effect. That such a saturation could occur is supported by the fact that there is an asymptotic limit to the maximum drag reduction [Virk *et al.* (1970) and Granville (1972)]. Also note that in figure 3.9, the v' profiles are about

the same at $\xi = 19.5$ for 5 Q_s polymer injection both with and without LEBUs. But at $\xi = 36.4$, figure 3.48, and $\xi = 58.9$, figure 3.49, the intermittency profiles for the LEBU modified TBL have a higher peak and are narrower indicating that the bursting rates and/or strengths have been suppressed by the LEBUs, thus keeping more of the higher concentration polymer near the wall. Figure 3.50, $\xi = 92.0$, shows that although the LEBU modified TBL intermittency profile has a high peak near the wall, the polymer concentration exceeds the intermittency threshold, $0.6C_{wall}$, a noticeable fraction of the time all the way across the field of view. This is expected given the trends shown on figure 3.41 and 3.42 that show rapid increases in the 50% thickness. The concentration of polymer used for the threshold for figure 3.50, at $\xi = 92.0$, for a local comparison is only approximately $0.1C_{inj}$. Since the polymer in the standard TBL has been all but totally diffused through the TBL by this location (refer to figure 3.39) comparisons on the relative bursting activities cannot be made here.

Figure 3.51 shows the highest y value above the wall where concentrated filaments of polymer ($\geq 0.9C_{wall}$) in an ensemble of 1000 samples are observed as a function of streamwise distance. At $\xi = 19.5$, concentrated filaments of polymer extend out essentially the same distance for both TBLs. Also, the number of times these filaments are seen are approximately the same for each case. But at $\xi = 36.4$, concentrated polymer filaments extend out much further in the standard TBL. Not only do the LEBUs decrease the magnitude of the bursts at this location, the number of concentrated filaments were also seen to decrease, indicating fewer bursts. The same trend is also observed at $\xi = 58.9$. By the last measurement location, it seems that concentrated filaments extend much further out in the LEBU modified TBL, but as explained before, due to the polymer already being almost completely diffused in the standard TBL at this location, comparisons on bursting cannot be made here. Since the concentration

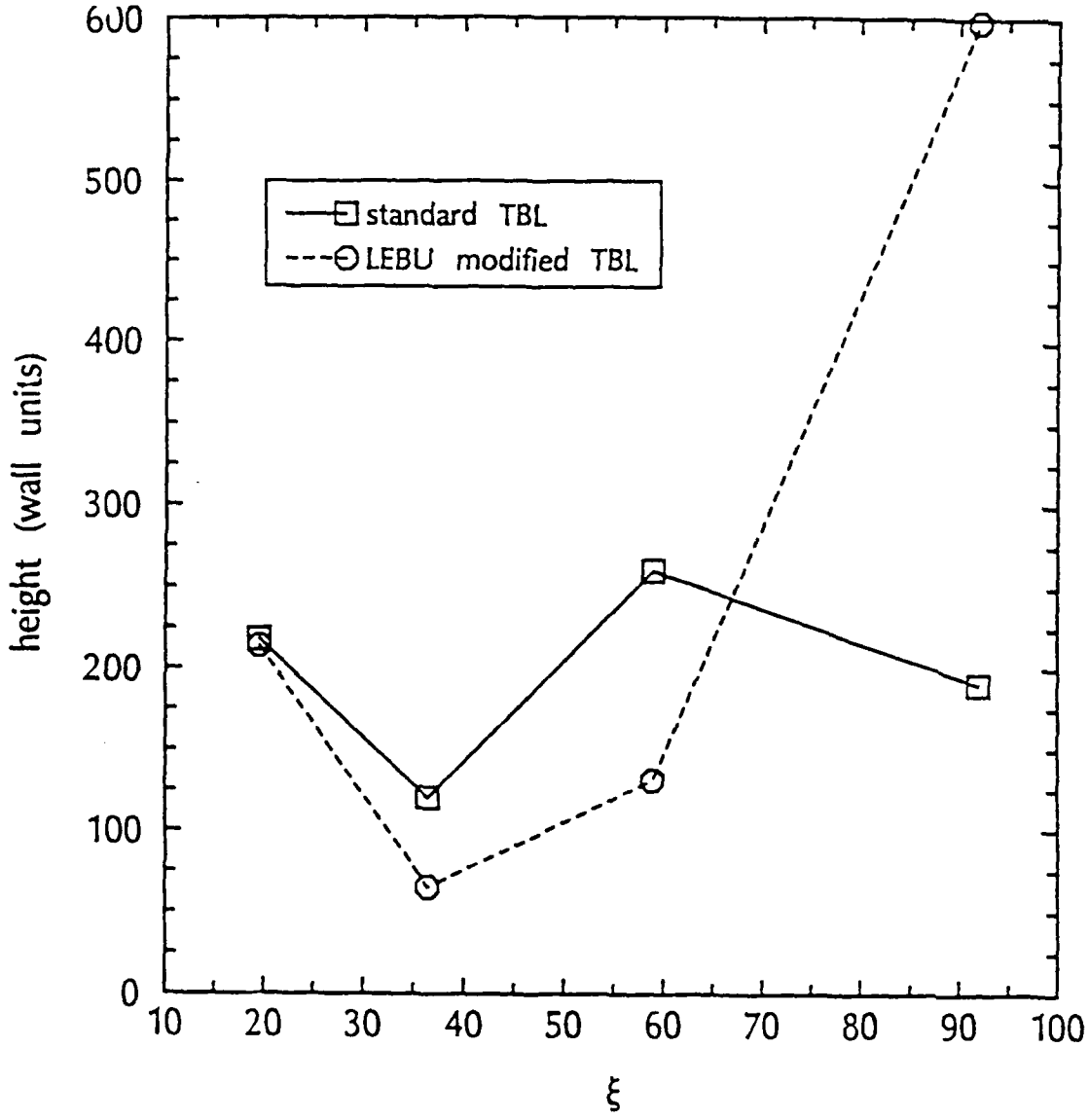

Figure 3.51. Height above the wall where concentrated filaments of polymer lift as a function of the nondimensionalized downstream distance from leading edge of upstream LEBU

gradient in the diffused case is small, there is not a large enough difference between C for a lifting filament and C_{local} to distinguish the two. The ΔC potential change is too small to resolve.

It is very instructive to look at the higher order polymer concentration profile statistics. Figures 3.52, 3.53, and 3.54 [data taken from Brungart (1990)] show standard deviation profiles of the concentration data for polymer injection into a standard TBL at $\xi = 14.0$, 58.9, and 92.0, respectively. Opposite of the trend for water injection, figures 3.52 and 3.53 show that the peak in the standard deviation profiles moves closer to the wall for increasing streamwise distance from the slot. Also, unlike water injection, the location of these peaks above the wall at a given measurement location are dependent on the injection rate. Figure 3.54 shows that the standard deviation profiles at the most downstream measurement location are similar to water, further indicating that polymer is almost completely diffused by this location in the standard TBL.

Figures 3.55, 3.56, 3.57, and 3.58 show standard deviation profiles of the concentration data for polymer injection in a LEBU modified TBL at $\xi = 19.5$, 36.4, 58.9, and 92.0, respectively. The trends in the locations of the peaks are very similar to the standard TBL data, but the LEBU modified TBL peaks reach a slightly higher magnitude at each location. Also, the profiles are much narrower than the standard TBL profiles. At $\xi = 92.0$, figure 3.58, the 10 Q_s injected polymer shows the same trends as the upstream locations, but the 5, 4, 3, and 2 Q_s data are different. The peaks are displaced further from the wall and are starting to take the form of the water injection data. This indicates the length that a layer of polymer remains on the wall increases with injection rate.

Figures 3.59, 3.60, and 3.61 show skewness profiles for polymer injection in a standard TBL at $\xi = 14.0$, 58.9, and 92.0, respectively. The same types of figures for a LEBU modified TBL are shown in figures 3.62, 3.63, and 3.64

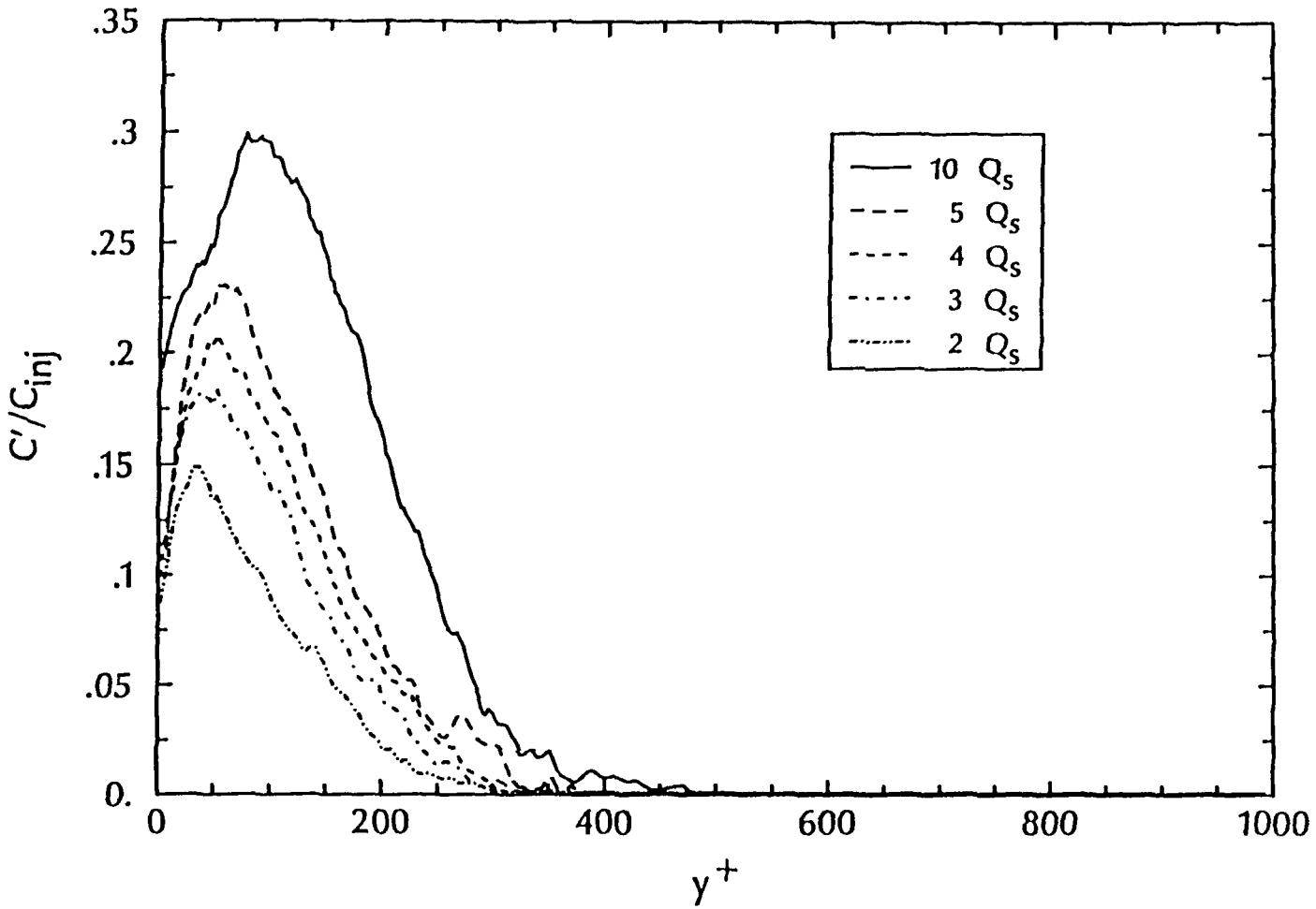

Figure 3.52. Polymer injection standard deviation profiles in a standard TBL [data taken from Brungart (1990)] at $\xi = 14.0$

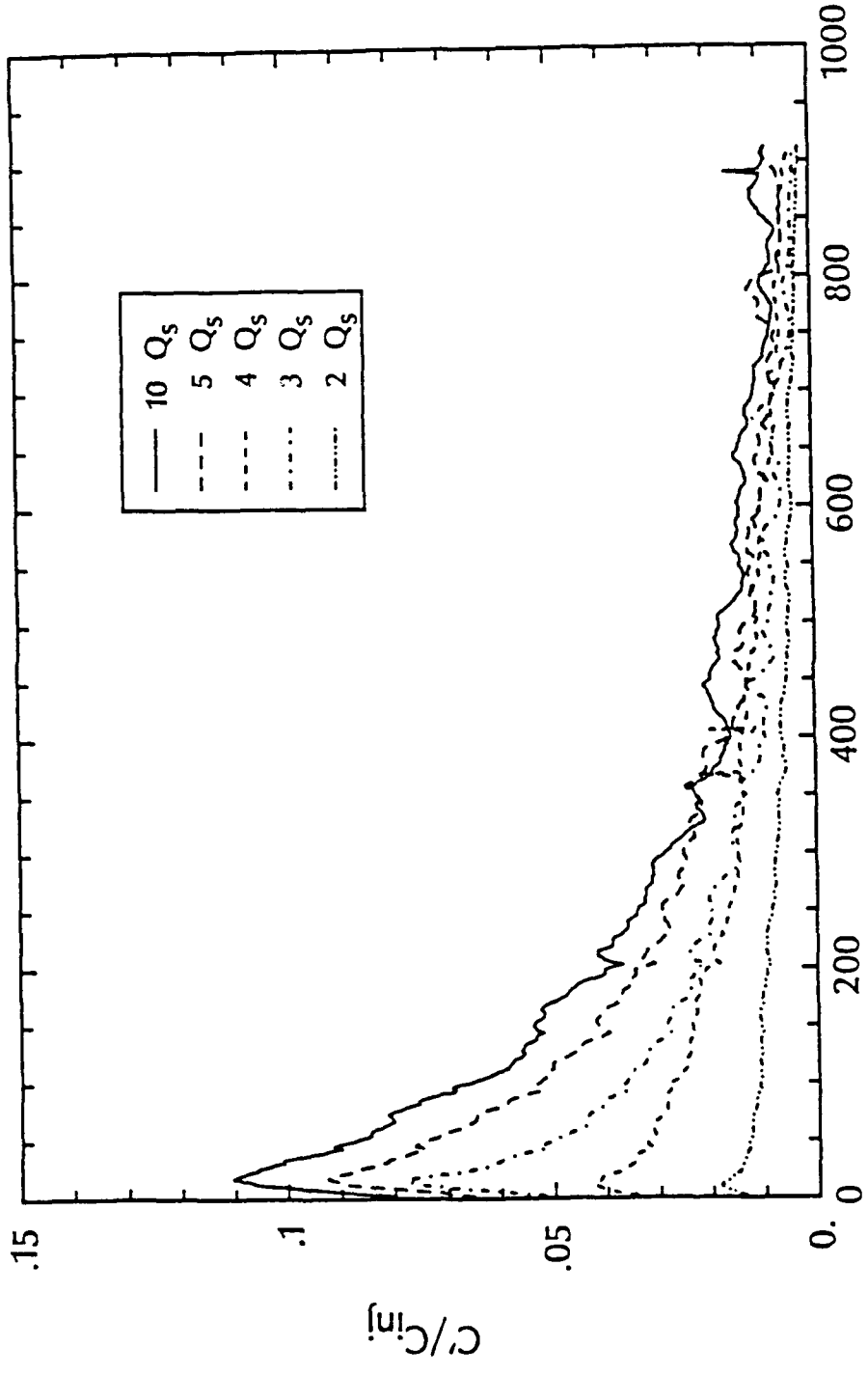

Figure 3.53. Polymer injection standard deviation profiles in a standard TBL [data taken from Brungart (1990)] at $\xi = 58.9$

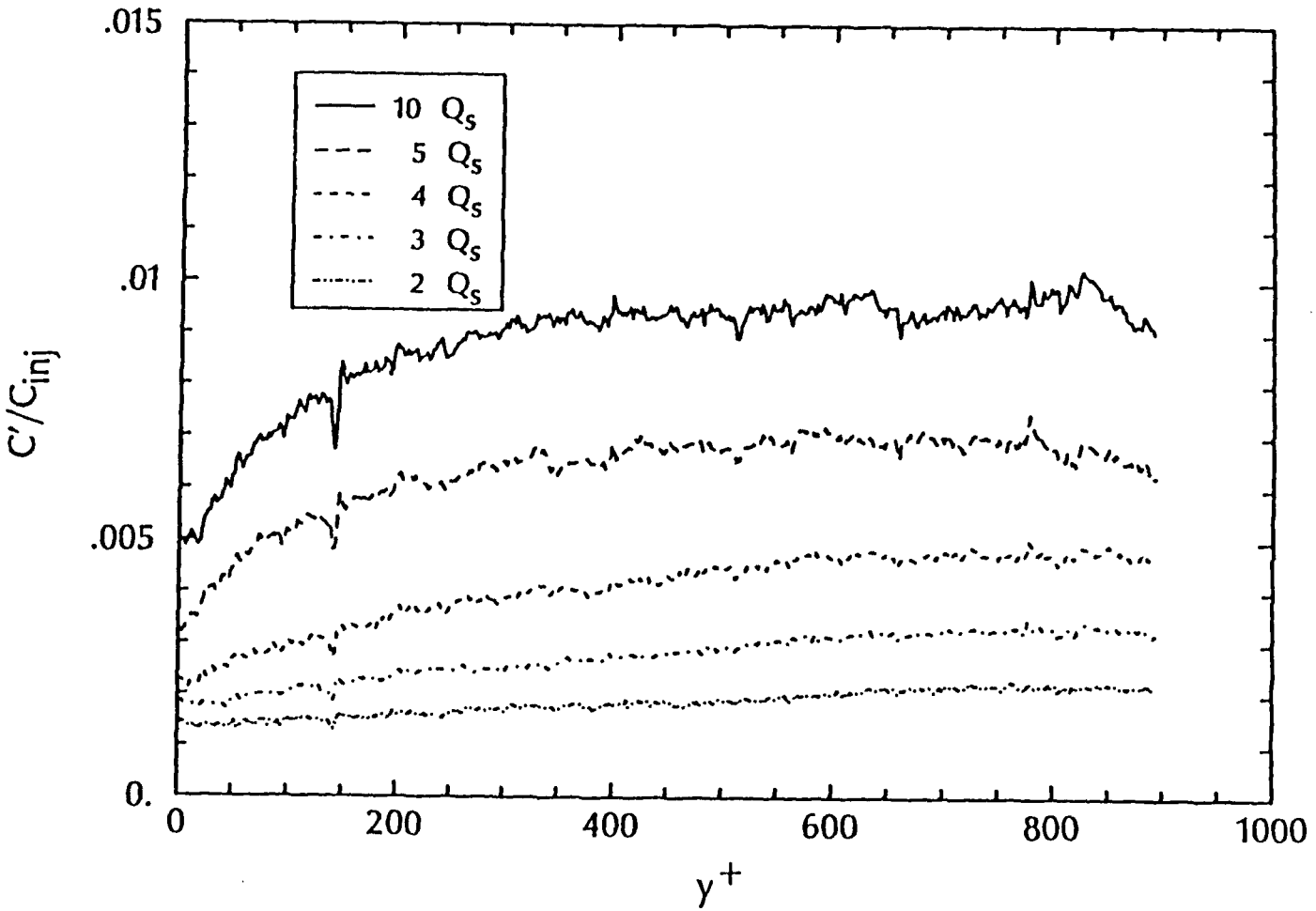

Figure 3.54. Polymer injection standard deviation profiles in a standard TBL [data taken from Brungart (1990)] at $\xi = 92.0$

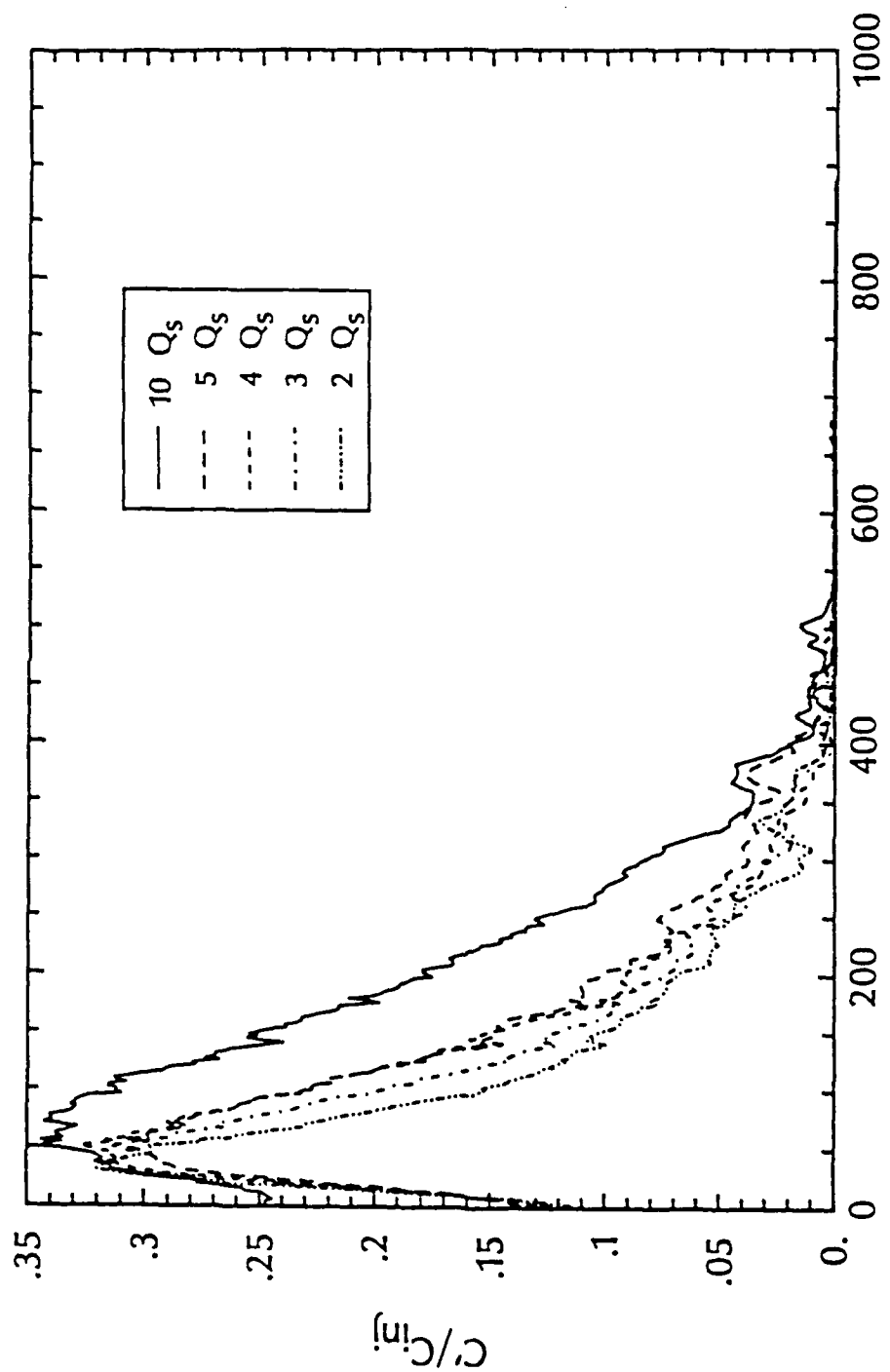

Figure 3.55. Polymer injection standard deviation profiles in a LEBU modified TBL at $\xi = 19.5$

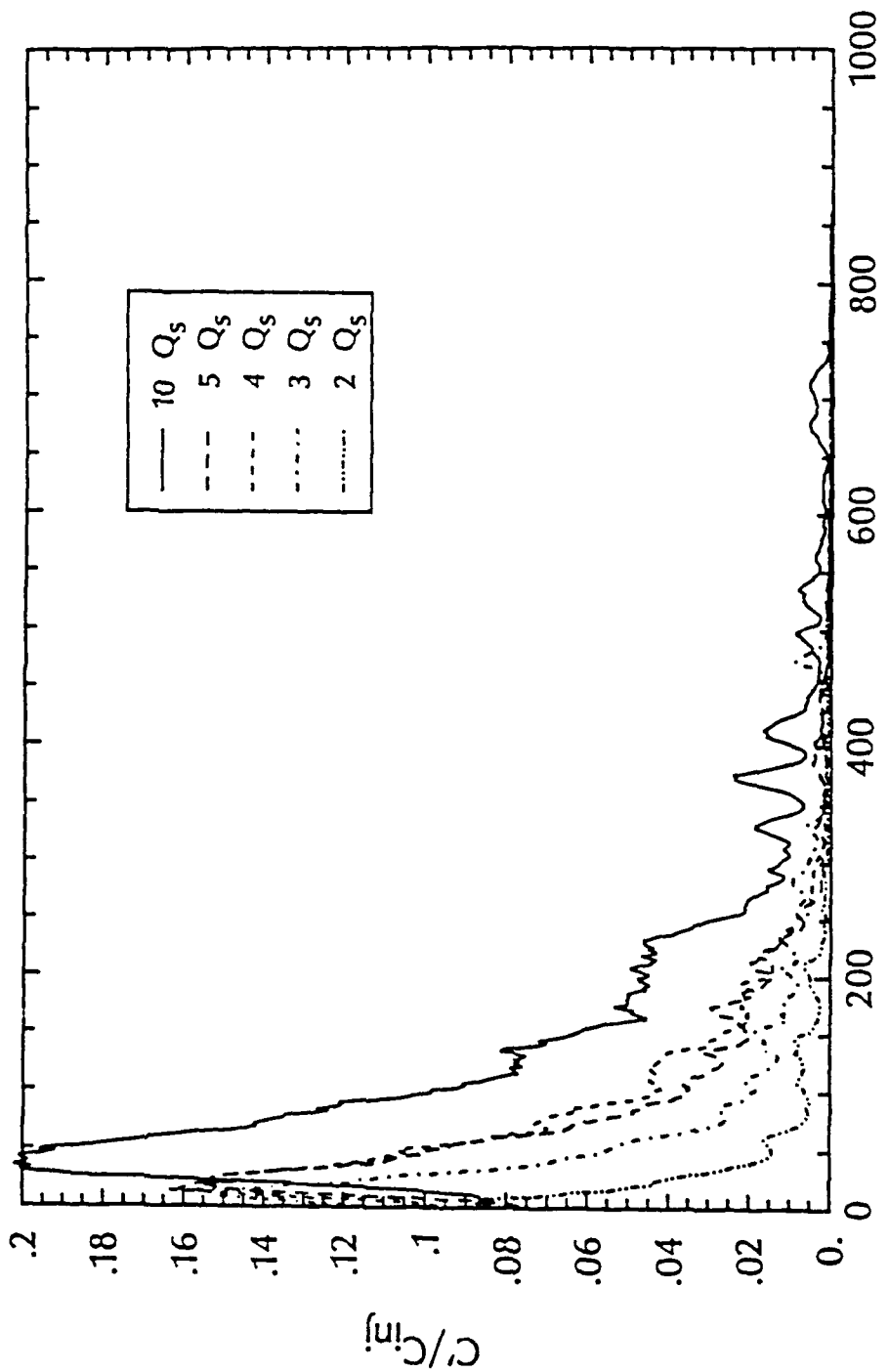

Figure 3.56. Polymer injection standard deviation profiles in a LEBU modified TBL at $\xi = 36.4$

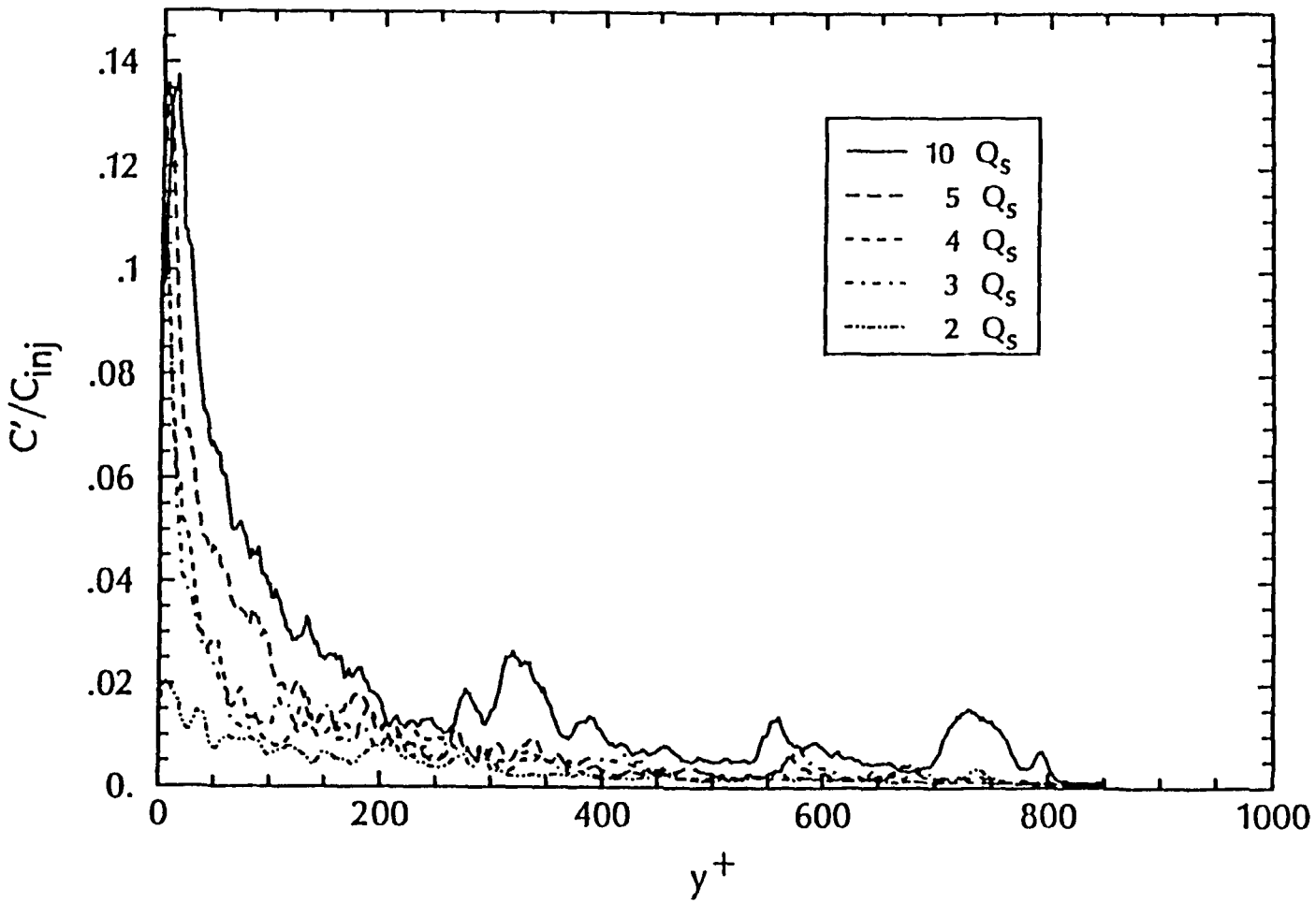

Figure 3.57. *Polymer injection standard deviation profiles in a LEBU modified TBL at* $\xi = 58.9$

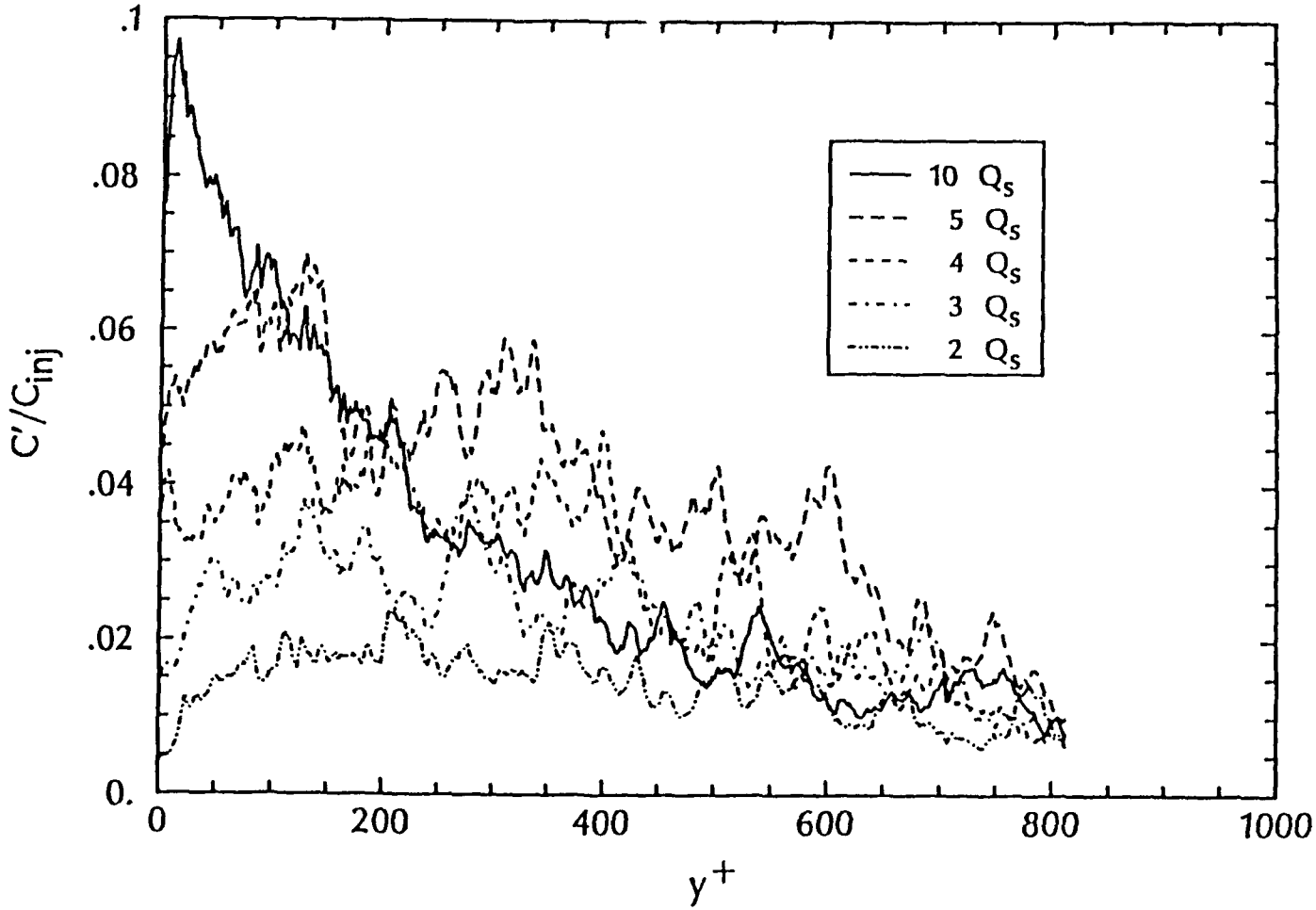

Figure 3.58. Polymer injection standard deviation profiles in a LEBU modified TBL at $\xi = 92.0$

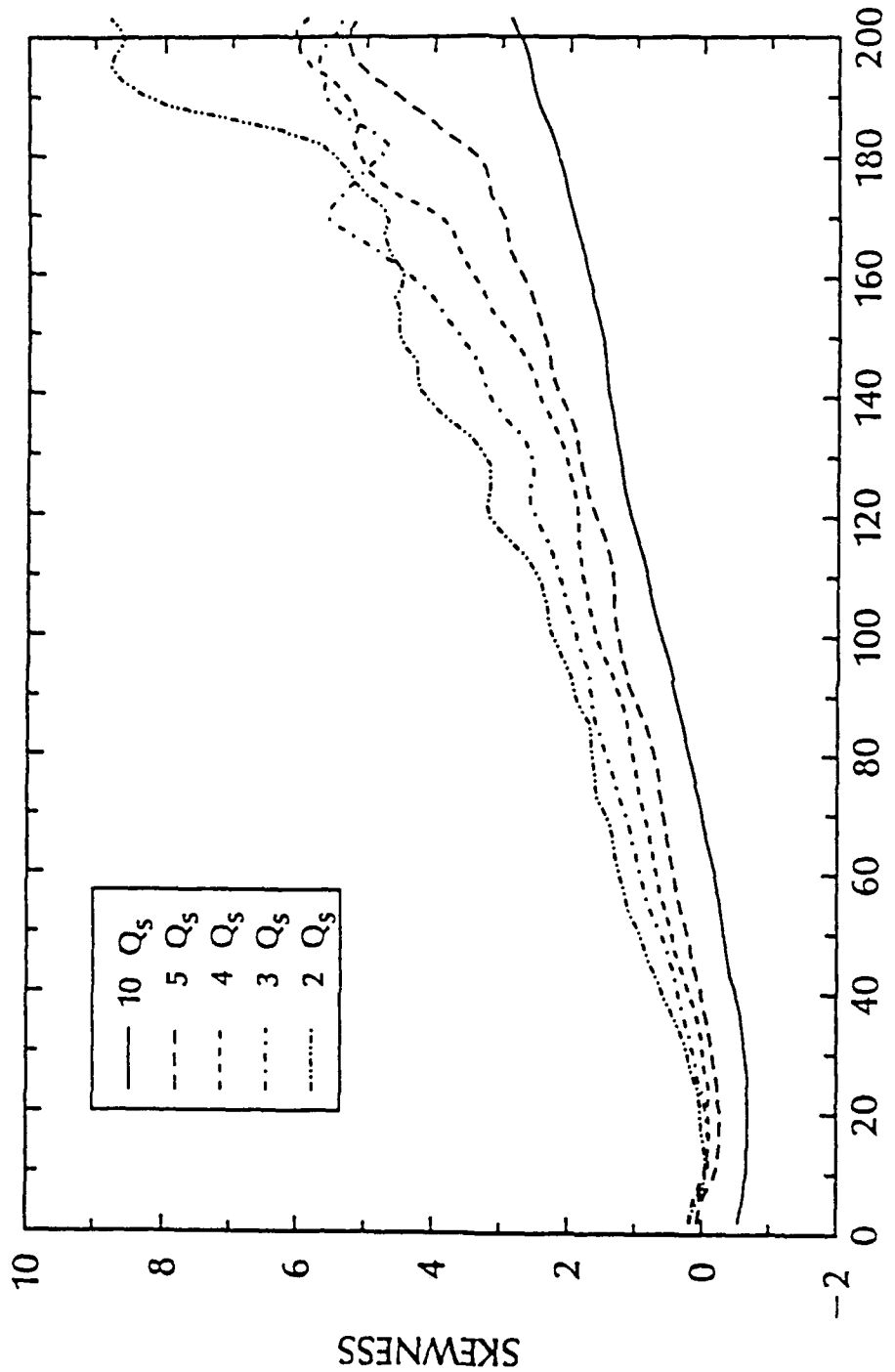

Figure 3.59. Polymer injection skewness profiles in a standard TBL [data taken from Brungart (1990)] at $\xi = 14.0$

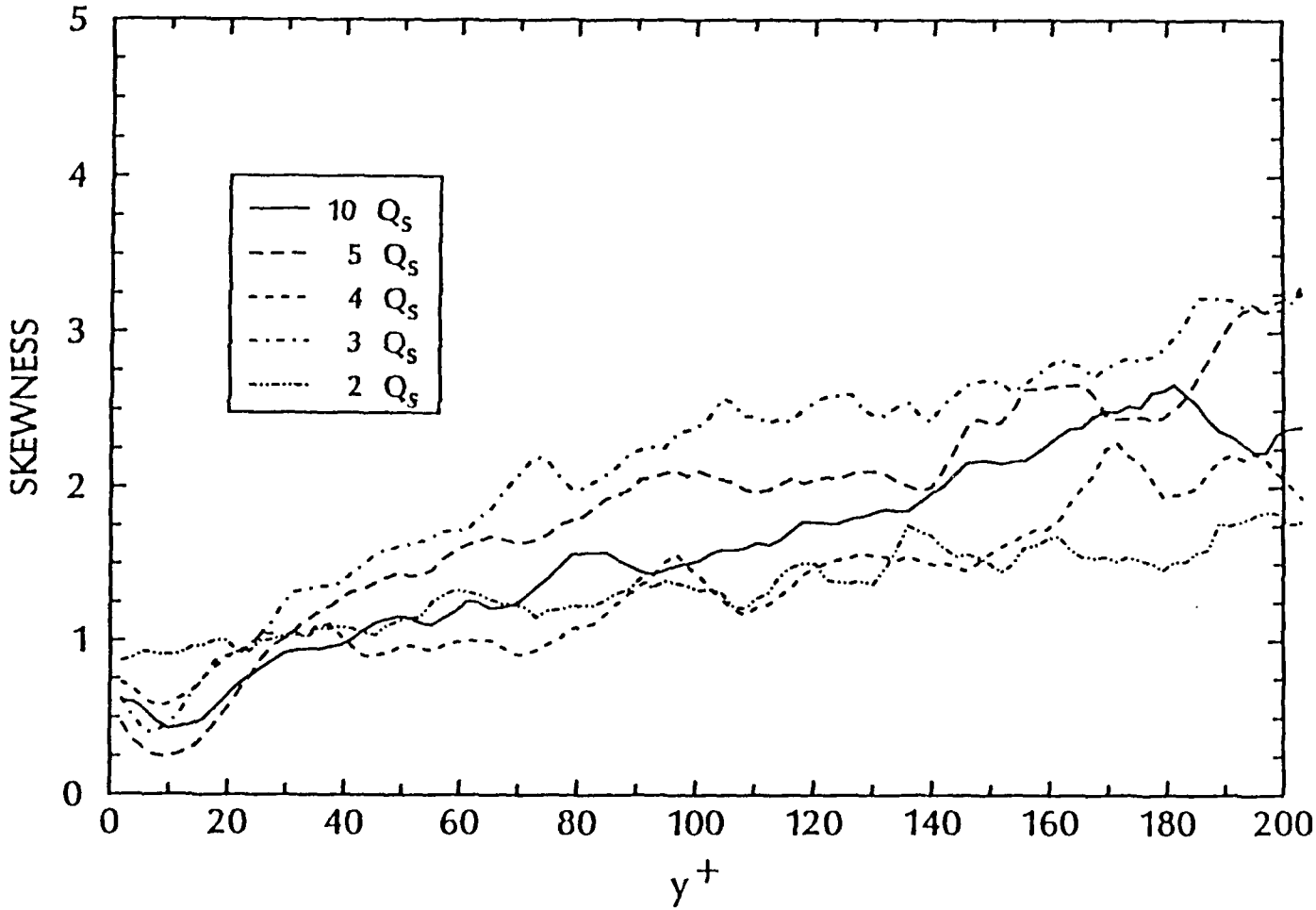

Figure 3.60. Polymer injection skewness profiles in a standard TBL [data taken from Brungart (1990)] at $\xi = 58.9$

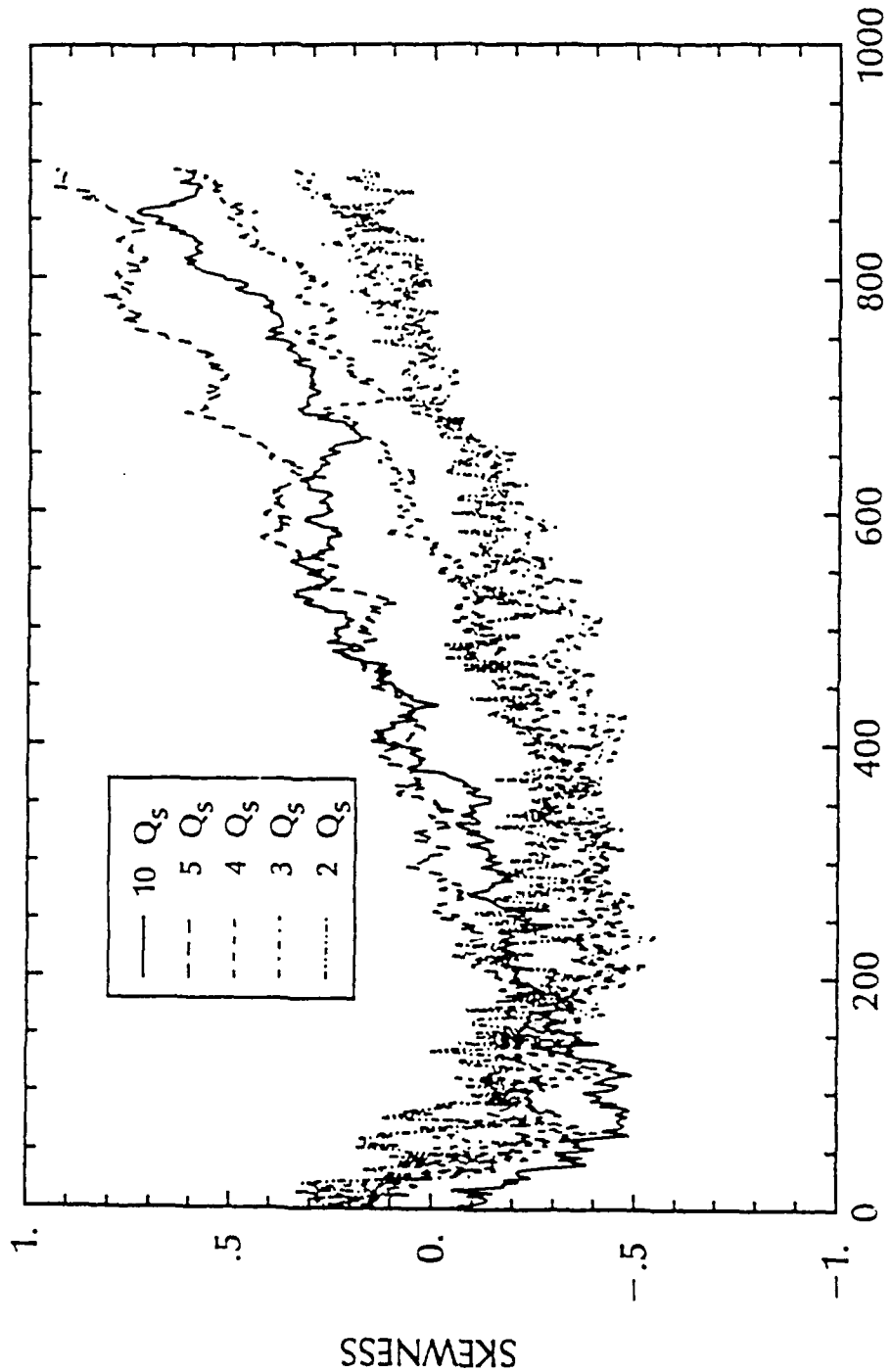

Figure 3.61. Polymer injection skewness profiles in a standard TBL [data taken from Brungart (1990)] at $\xi = 92.0$

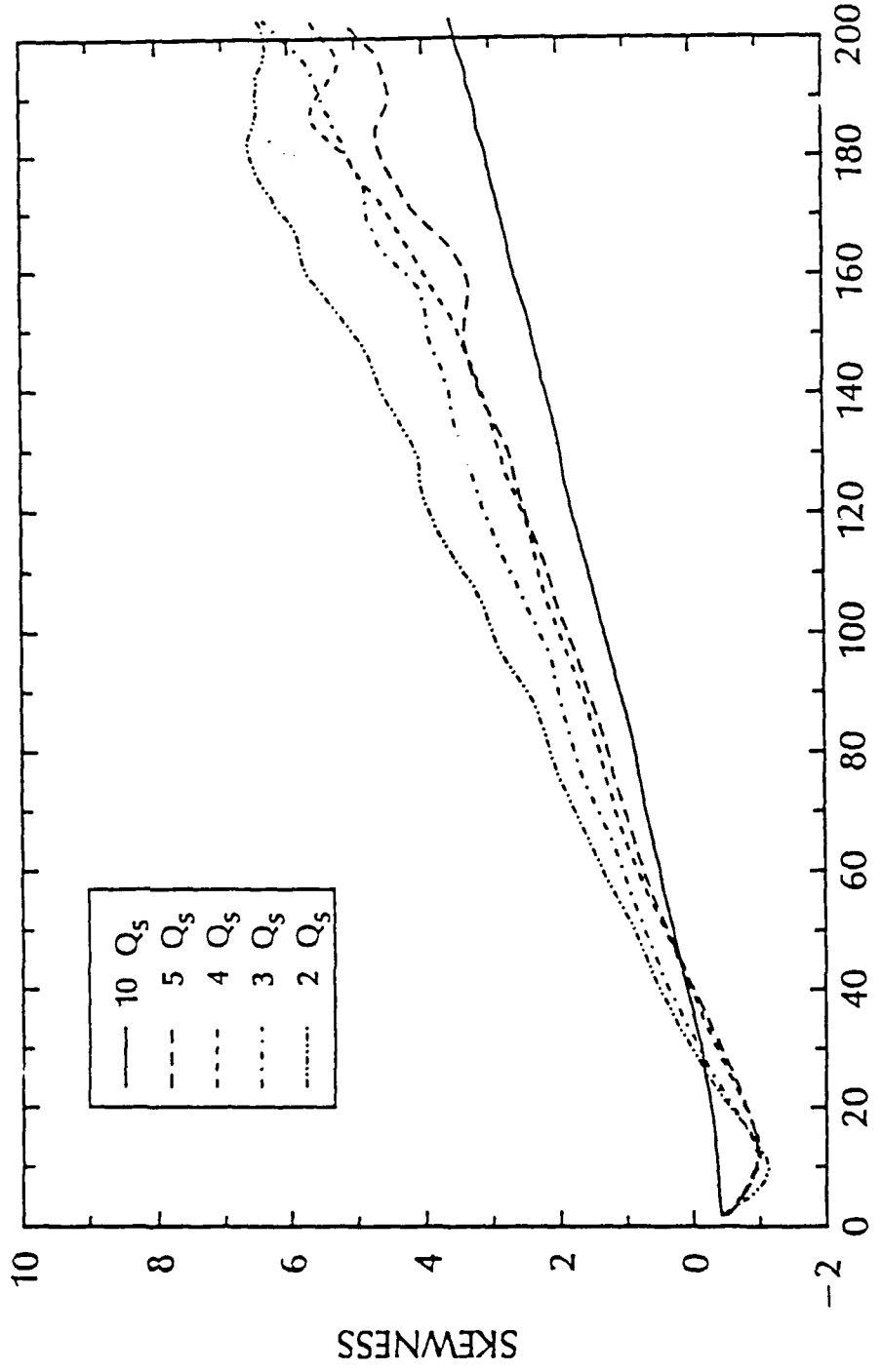

Figure 3.62. Polymer injection skewness profiles in a LEBU modified TBL at $\xi = 19.5$

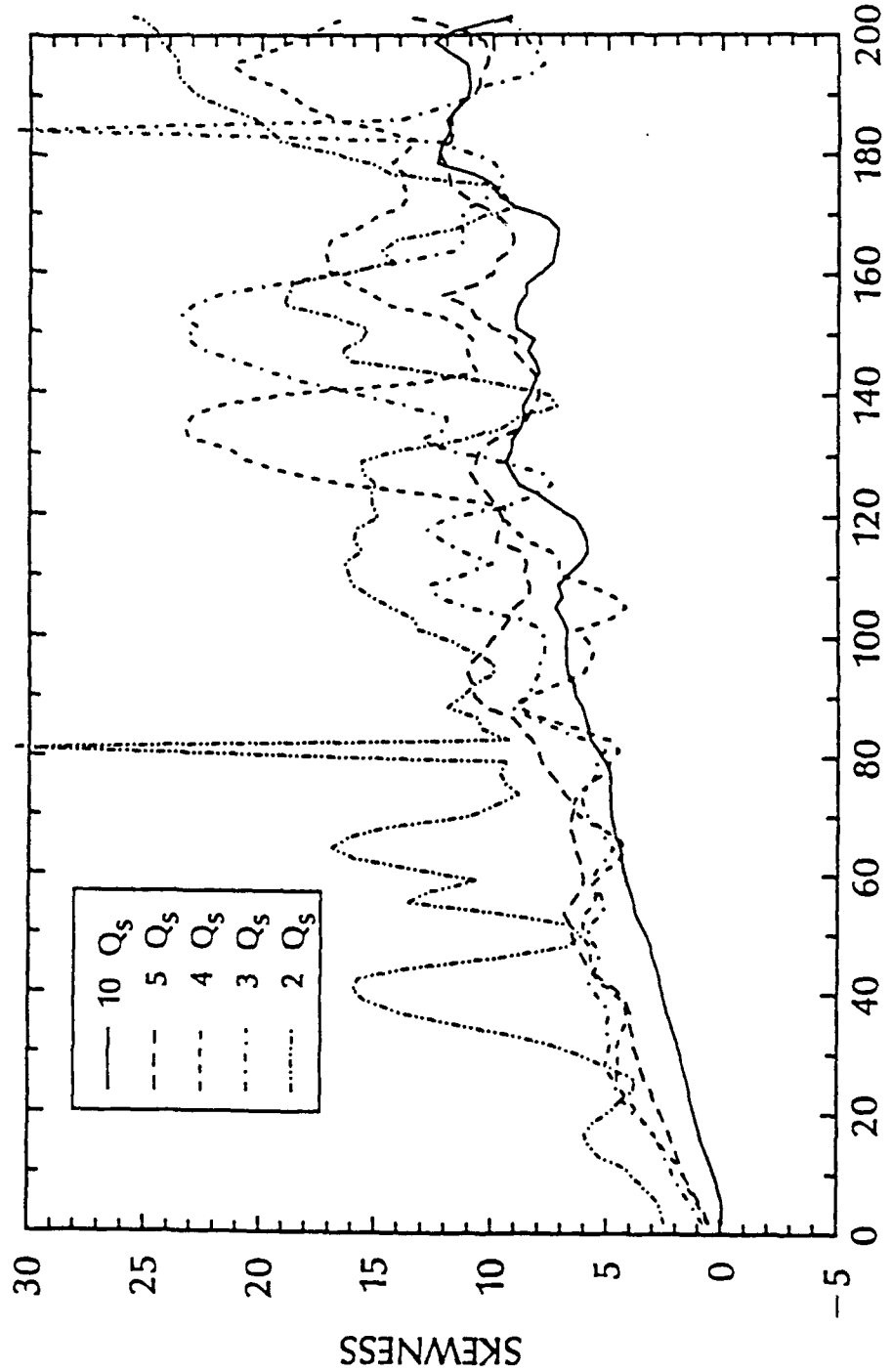

Figure 3.63. Polymer injectic ı skewness profiles in a LEBU modified TBL at $\xi = 58.9$

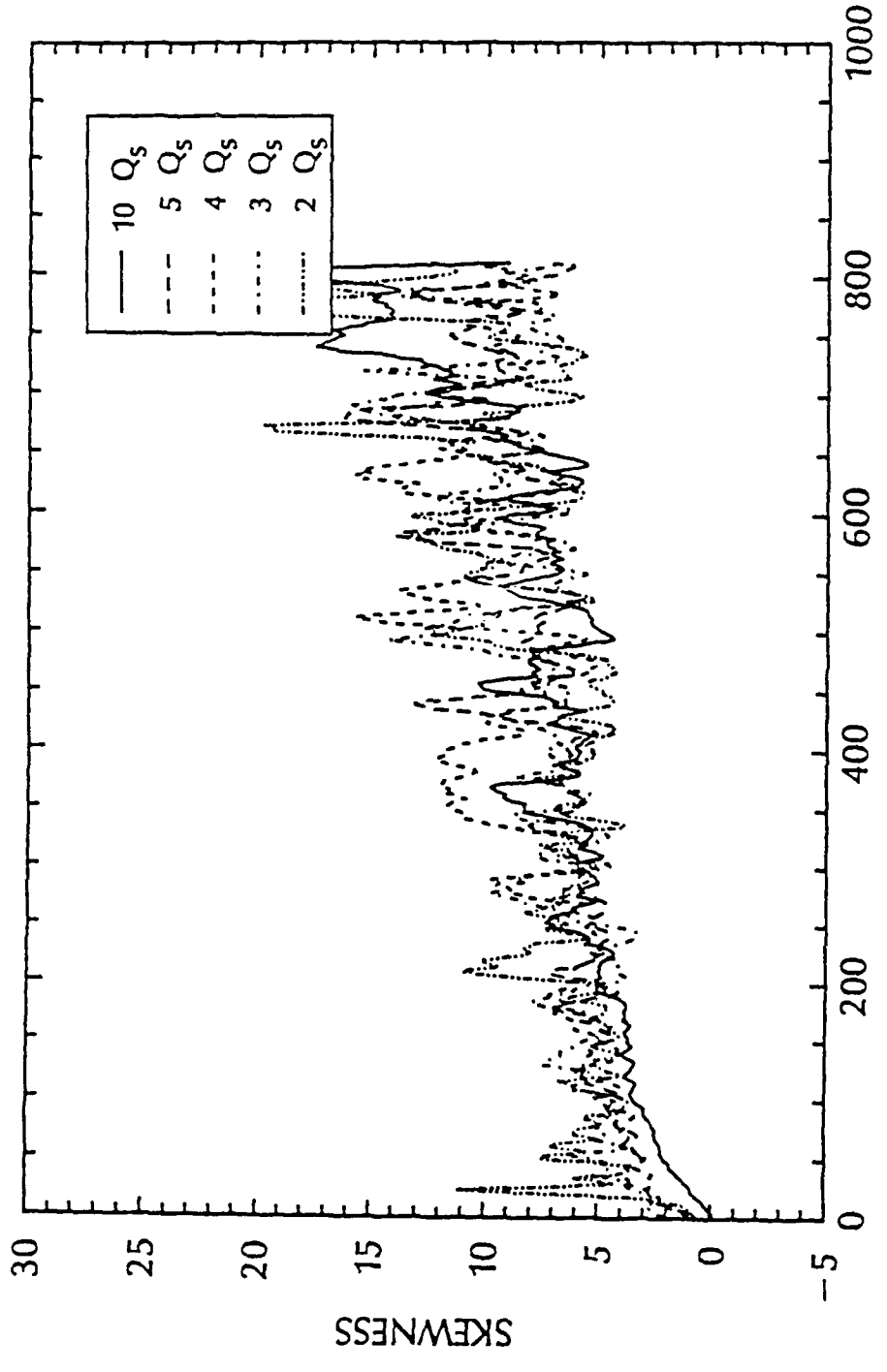

Figure 3.64. Polymer injection skewness profiles in a LEBU modified TBL at $\xi = 92.0$

for ξ = 19.5, 58.9, and 92.0, respectively. At the upstream most measurement location, both TBL data are very similar. Downstream, the LEBU modified TBL skewness profiles have larger magnitudes but show similar trends to standard TBL data. At ξ = 92.0, the LEBU modified TBL data show very similar trends to the upstream data, but like the standard deviation profiles, the standard TBL data look very similar to water. Also, consistent with water injection results in section 3.2.1 and Chatwin and Sullivan (1990), the skewness profiles go through zero at approximately the same location as the peak in the standard deviation profiles.

Figures 3.65–3.70 are kurtosis profiles and correspond to figures 3.59–3.64, respectively. Both the standard and LEBU modified TBL profiles are similar at the upstream most measurement location, but large differences in the magnitudes are seen in the LEBU modified TBL profiles at downstream locations. The large oscillations in the kurtosis profiles observed in figures 3.66, 3.69, and 3.70 can be attributed to the fact that kurtosis has been nondimensionalized with the standard deviation to the fourth power. Standard deviation values were found to decrease with increasing distance from the wall and the small numbers used for normalization is a source of statistical uncertainty. Also, the intermittent nature of the signal is a cause of this variability.

The polymer concentration skewness and kurtosis data presented are dependent on the injection rate in the LEBU modified TBL over all measurement locations, whereas Brungart (1990) found that dependence on injection rate only occurs at upstream measurement locations.

Chatwin and Sullivan (1990) claim that whether or not the contaminant is passive makes no difference on the character of the concentration profile statistics. Brungart *et al.* (1990) and Brungart's (1990) results support this claim in the standard TBL and similarity is seen in both injection types data sets. The

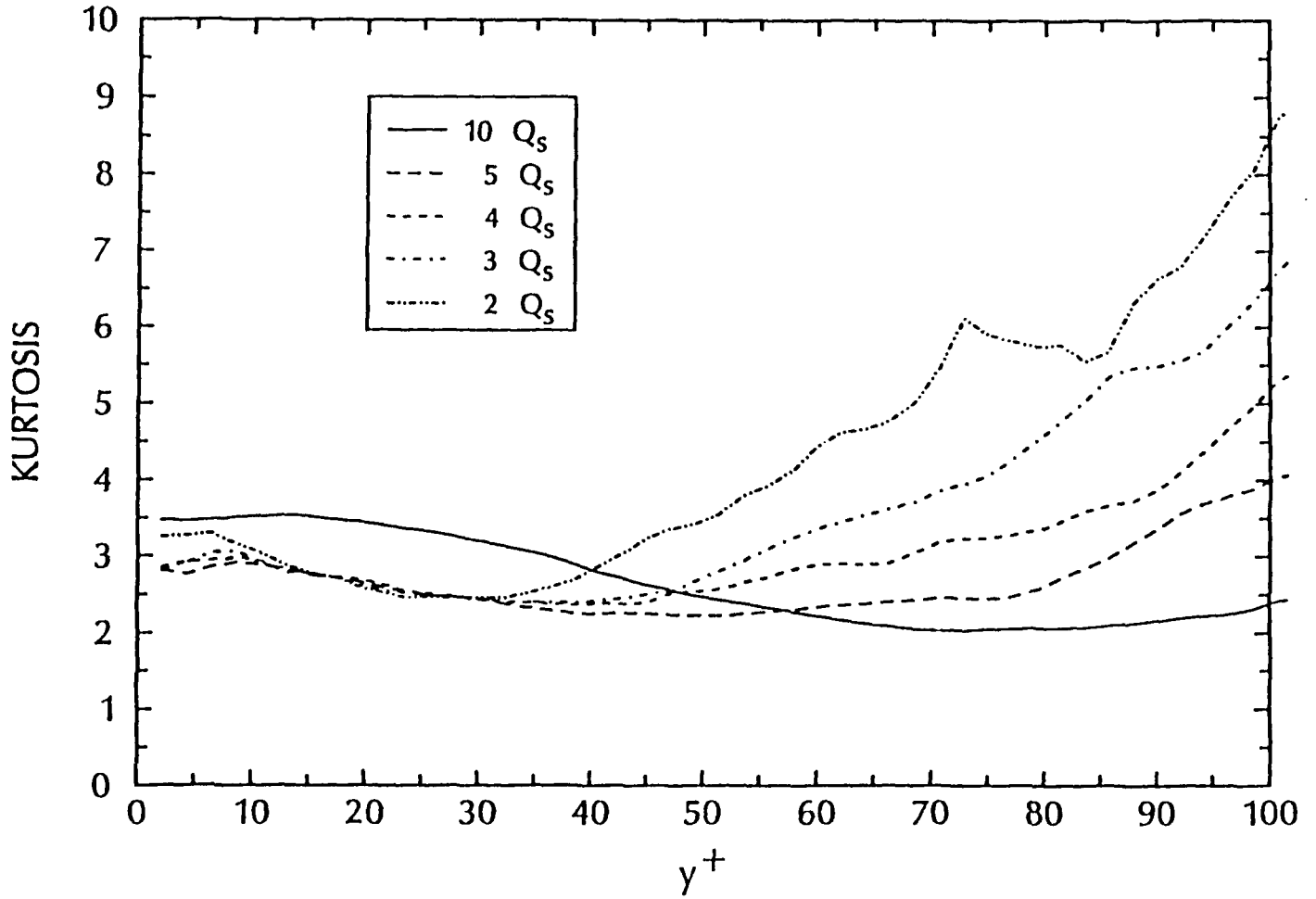

Figure 3.65. Polymer injection kurtosis profiles in a standard TBL [data taken from Brungart (1990)] at $\xi = 14.0$

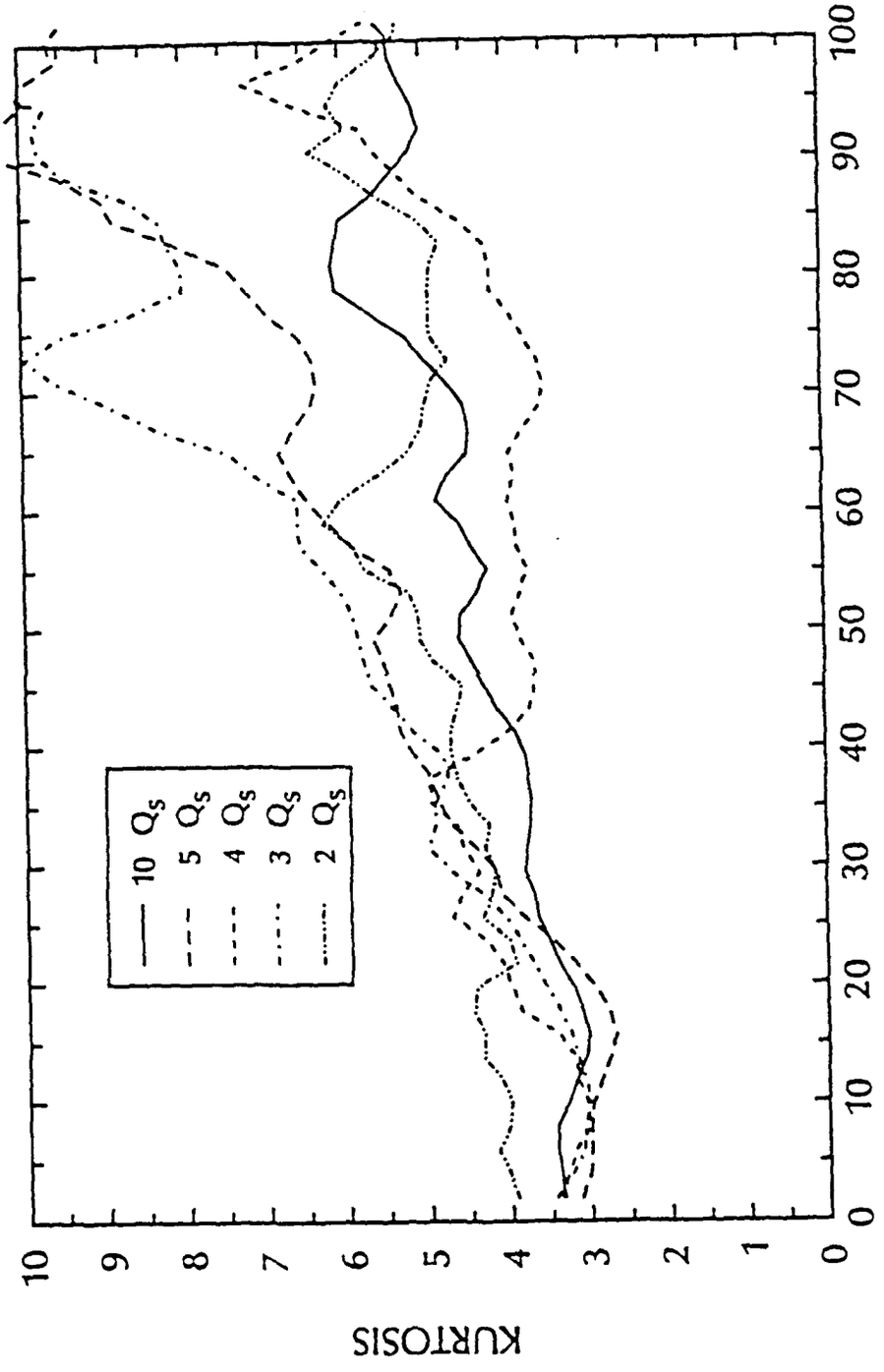

Figure 3.66. Polymer injection kurtosis profiles in a standard TBL [data taken from *Brungart (1990)*] at $\xi = 58.9$

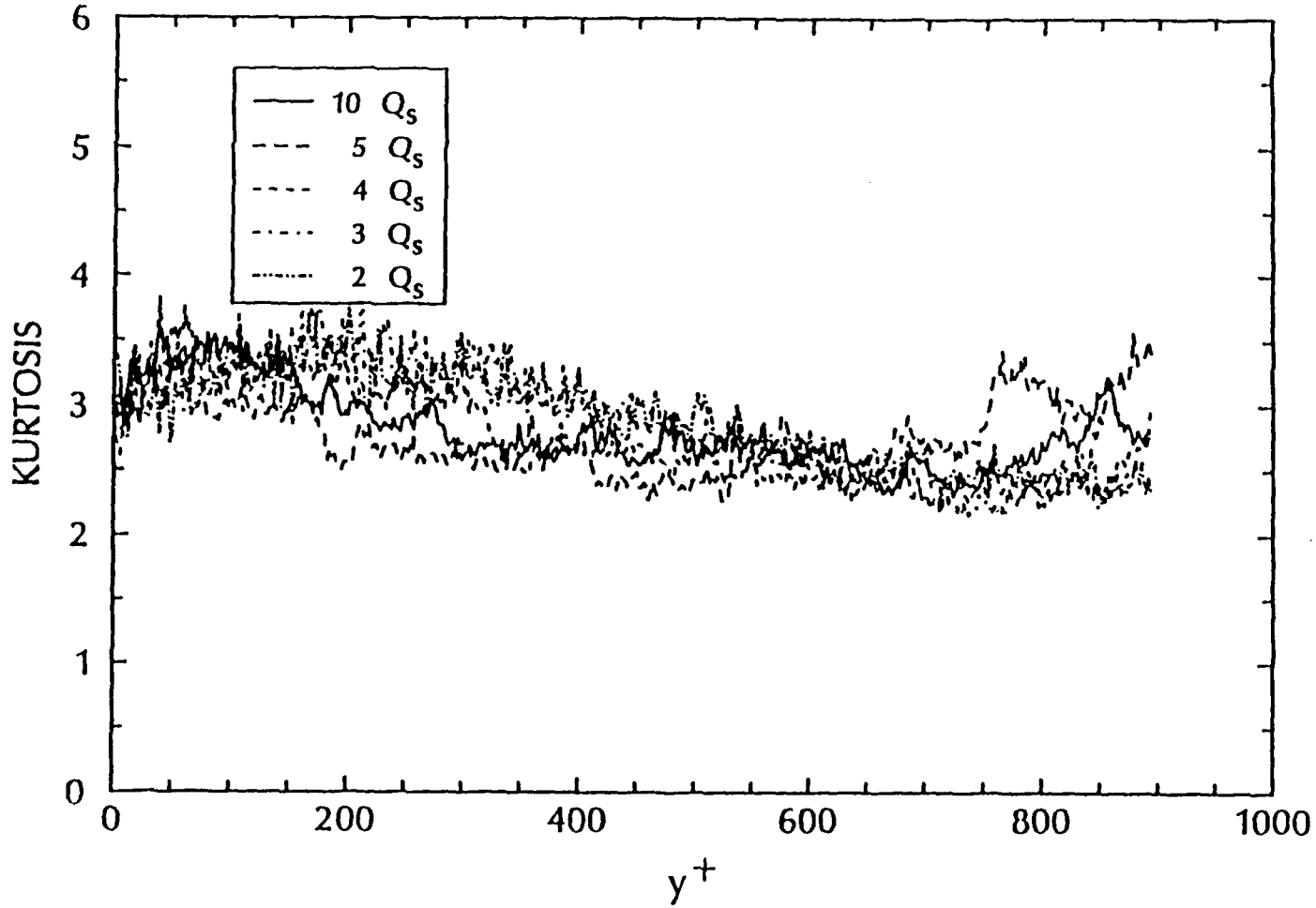

Figure 3.67. Polymer injection kurtosis profiles in a standard TBL [data taken from Brungart (1990)] at $\xi = 92.0$

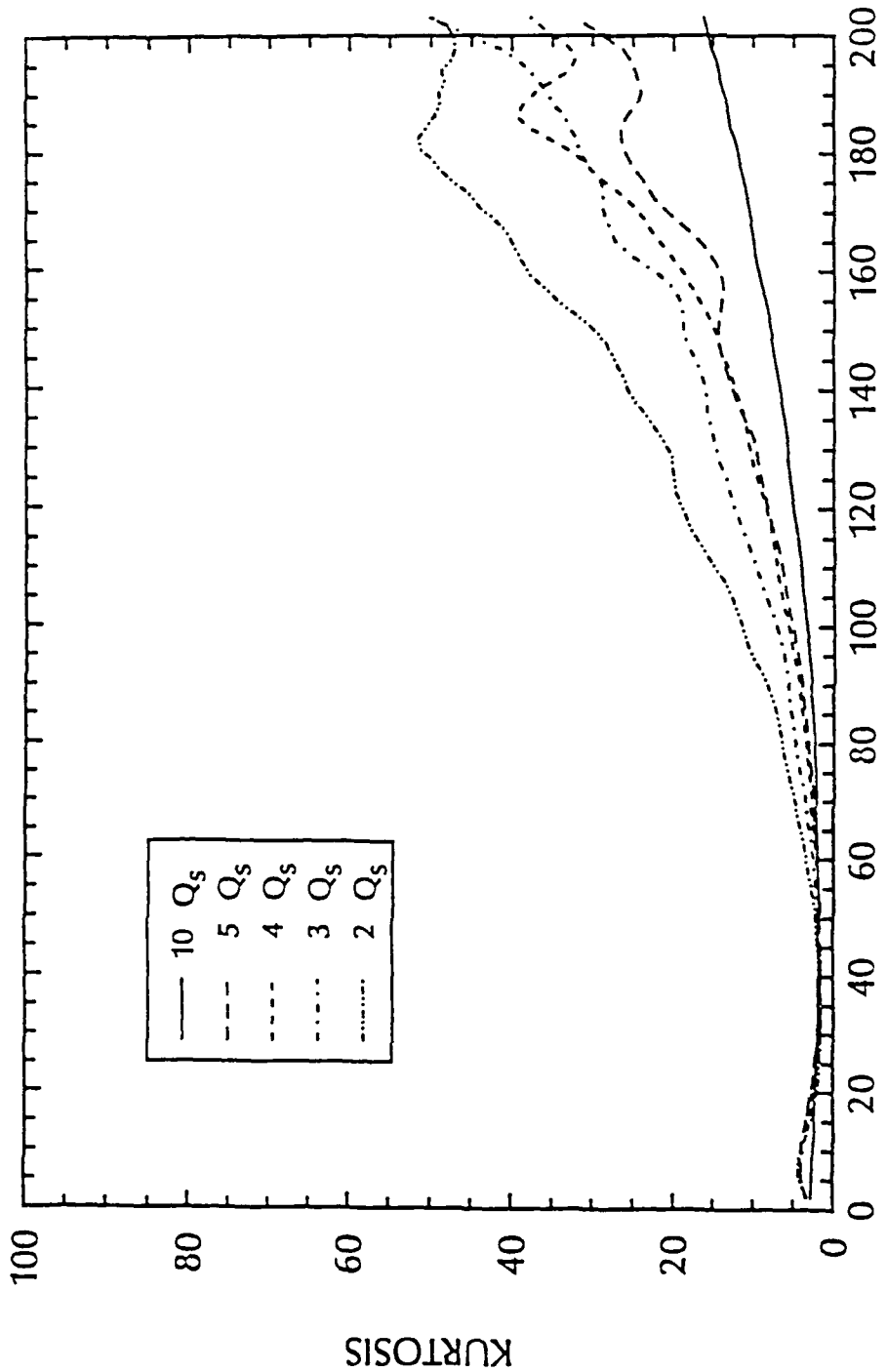

Figure 3.68. Polymer injection kurtosis profiles in a LEBU modified TBL at $\xi = 19.5$

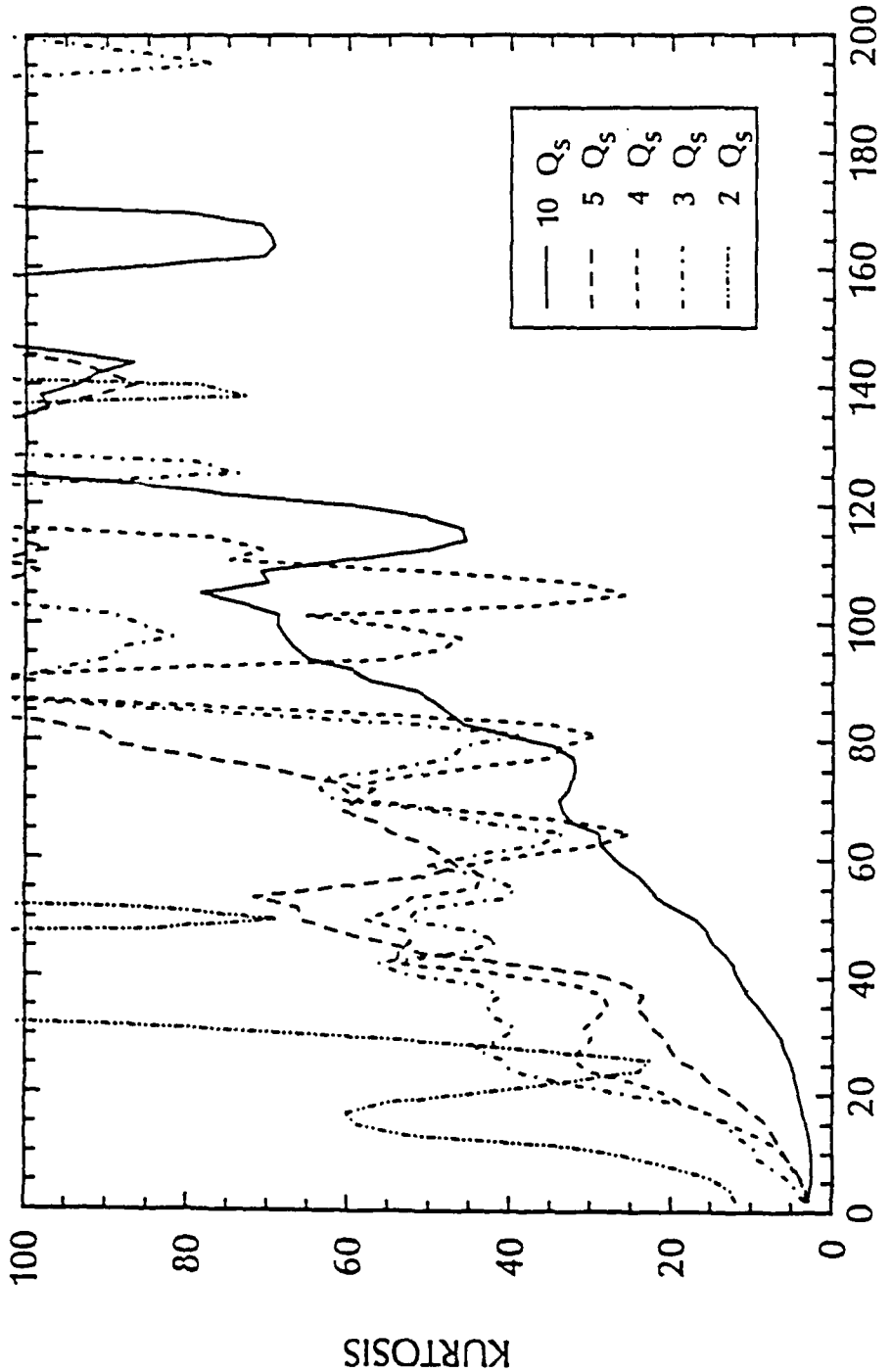

Figure 3.69. Polymer injection kurtosis profiles in a LEBU modified TBL at $\xi = 58.9$

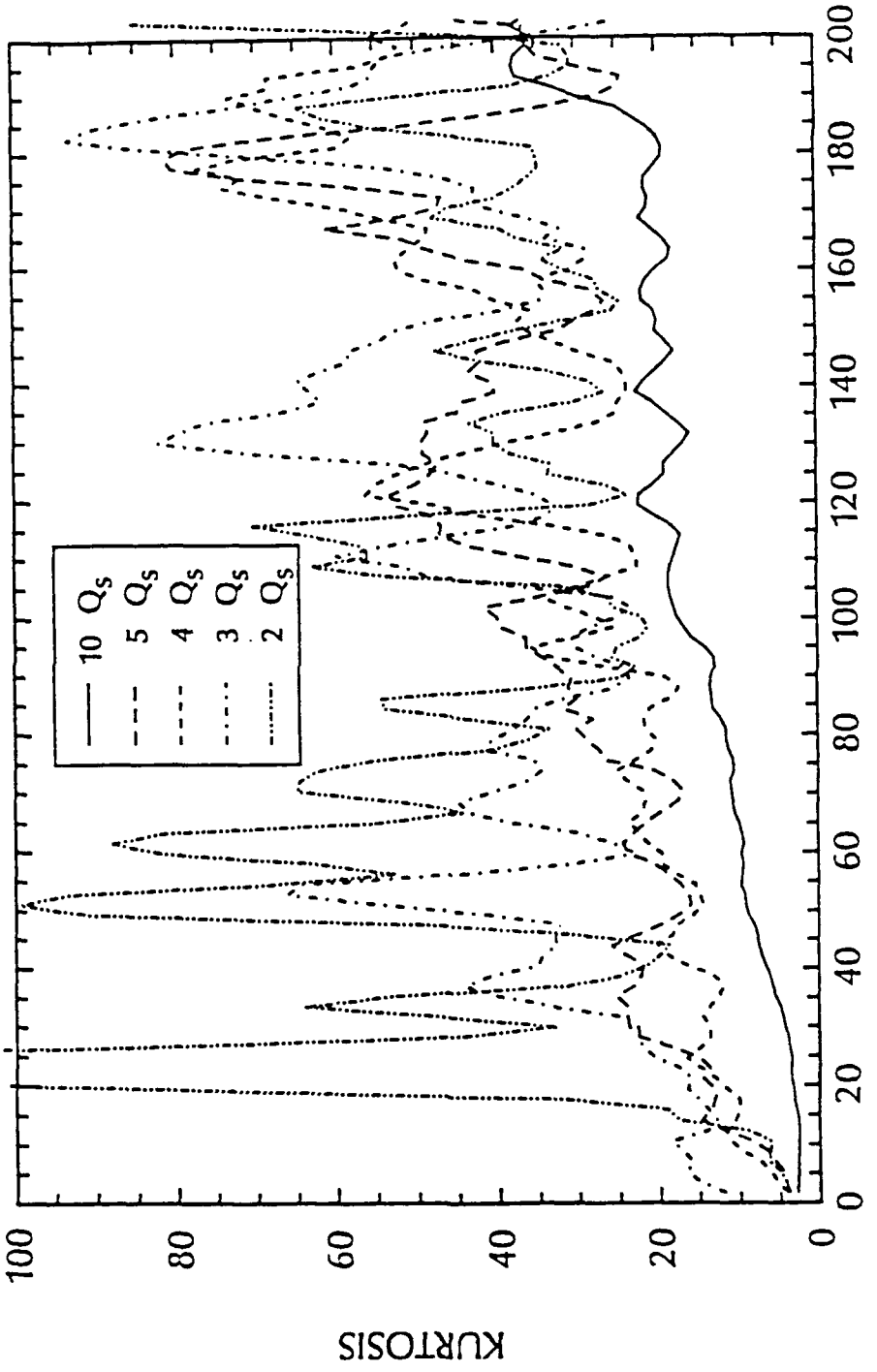

Figure 3.70. Polymer injection kurtosis profiles in a *LEDU modified* TBL at $\xi = 92.0$

LEBU modified TBL results with water and polymer injection are also similar with the results of Chatwin and Sullivan (1990) and it seems that although LEBU devices alter the diffusion of polymer, they do not effect the characteristics of the concentration profile statistics.

Chapter 4

CONCLUSIONS AND RECOMMENDATIONS FOR FUTURE STUDY

4.1 Conclusions

A tandem LEBU geometry was used successfully to modify a TBL flow with and without polymer injection. An integrated skin friction reduction of approximately 20% over the length of the test section was achieved in the LEBU modified TBL without injection. Large u' and v' reductions were found immediately downstream of the LEBU devices and slight effects were found at $\xi = 92$. These effects on the turbulence intensity extended further downstream than reported by Guezennec and Nagib (1990), Reidy and Mautner (1986), Chang and Blackwelder (1990), and Trigui and Guezennec (1990). Even larger reductions in u' and v' were found with polymer injection in the LEBU modified TBL flow with a displacement of the peak in the u' away from the wall. An integrated skin friction reduction over the length of the test section of approximately 53% for this case was found, as compared to approximately 31% for polymer injection into a standard TBL flow. The shape of the Reynolds stress profiles are similar to and have the same trends as the v' profiles. Also, the LEBU modified TBLs were found to have a less intermittent edge than the standard TBL.

The diffusion of a passive contaminant in a LEBU modified TBL flow was initially diminished, but returned to the standard TBL case by $\xi = 36.4$, which was faster than the mean velocity profiles relaxed. The initial diffusion zone of a passive contaminant, as defined by *Poreh and Cermak* (1964), was extended in the LEBU modified TBL.

The LEBUs had the greatest effect on polymer diffusion. Initially, the diffusion process was hindered to such an extent that by $\xi = 19.5$, the concentration at the wall has only begun to diminish. Higher concentrations of polymer were found over the entire downstream measurement region than found with polymer injection into a standard TBL flow. With no LEBUs present, only a maximum of 3% or less of the injected polymer concentration was found on the wall at $\xi = 92$, but approximately 39% of the 10 Q_s injected polymer concentration was still on the wall at the same location in the LEBU modified TBL flow. The bursting rates and strengths, which rapidly diffuse the polymer, were decreased in the LEBU modified TBL flow.

Finally, it was found that the LEBU devices did not affect the characteristics of the water and polymer concentration profile statistics, which supports the claims of Chatwin and Sullivan (1990).

4.2 Recommendations for Future Study

Although the researchers associated with this investigation feel that the optimum LEBU geometry was used given the constraints of the water tunnel, it was not clear if the position of the LEBUs relative to the injection slot was optimum. Further studies on this area are needed to maximize the effects of the LEBUs on diminishing polymer diffusion away from the wall.

All estimates on skin friction reduction in this investigation were performed based on boundary layer profile results. More reliable measurements on the local skin friction using drag balances would provide a more detailed account on the overall skin friction reduction in a LEBU modified TBL with polymer injection.

Finally, this investigation provided little information on the effects that polymer may have on the wake of the LEBU. Polymer ocean studies are needed to determine these effects.

REFERENCES

Anders, J. B. and Watson, R. D., Airfoil Large-Eddy Breakup Devices for Turbulent Drag Reduction, *AIAA-85-0520*, 1985, pp. 1–11.

Bandyopadhyay, P. R., REVIEW–Mean Flow in Turbulent Boundary Layers Disturbed to Alter Skin Friction, *Journal of Fluids Engineering*, vol. 108, 1985, pp. 127–140.

Bandyopadhyay, P. R., Drag Reducing Outer-Layer Devices in Rough Wall Turbulent Boundary Layers, *Experiments in Fluids 4*, 1986, pp. 247–256.

Berman, N. S., Drag Reduction by Polymers, *Annual Review of Fluid Mechanics*, 1978, pp. 47–64.

Bogard, D. G. and Tiederman, W.G., Burst Detection with Single-Point Velocity Measurements, *Journal of Fluid Mechanics*, vol. 162, 1986, pp. 389–413.

Brungart, T. A., A Laser-Induced Fluorescence Technique for Measurement of Slot-Injected Fluid Concentration Profiles in a Turbulent Boundary Layer, Master's Thesis, The Pennsylvania State University, 1990.

Brungart, T. A., Harbison, W. L., Petrie, H. L., and Merkle, C. L., A Fluorescence Technique for Measurement of Slot-Injected Fluid Concentration Profiles in a Turbulent Boundary Layer, To appear in Experiments in Fluids, 1990.

Bushnell, D. M., Turbulent Drag Reduction for External Flows, Aircraft Drag Prediction and Reduction, *AGARD R-723*, 1985, pp. 5–1 to 5–13.

Chang, S. and Blackwelder R. F., Modification of Large Eddies in Turbulent Boundary Layers, *Journal of Fluid Mechanics*, vol. 213, 1990, pp. 419–442.

Chatwin, P. C. and Sullivan, P. J., The Intermittency Factor of Scalars in Turbulence, *Physics of Fluids A*, vol. 1, April 1989, pp. 761–763.

Chatwin, P. C. and Sullivan, P. J., A Simple and Unifying Physical Interpretation of Scalar Fluctuation Measurements From Many Turbulent Shear Flows, *Journal of Fluid Mechanics*, vol. 212, 1990, pp. 533–556.

Coles, E. E., The Law of the Wake in the Turbulent Boundary Layer, *Journal of Fluid Mechanics*, vol. 1, 1956, pp. 191–226.

Corke, T. C., Digital Image Filtering in Visualized Boundary Layers, *AIAA Journal*, vol. 22, no. 8, Aug. 1984, pp. 1124–1131.

Corke, T. C., Guezennec, Y., and Nagib, H. M., Modification in Drag of Turbulent Boundary Layers Resulting from Manipulation of Large-Scale Structures, *Viscous Flow Drag Reduction, Progress in Astronautics and Aeronautics*, vol. 72, Nov. 1979, pp. 128–143.

Coughran, M. T. and Bogard, D. G., An Experimental Study of the Burst Structure in a LEBU Modified Boundary Layer, *Tenth Symposium on Turbulence*, Sept. 22–24, 1986, pp. 45-1 to 45-10.

Deutsch, S. and Zierke, W. C., NASA Contract Report, 179492, Aug. 1986.

Dowling, A. P., The Effect of Large-Eddy Breakup Devices on Oncoming Vorticity, *Journal of Fluid Mechanics*, vol. 160, 1985, pp. 447–463.

Fontaine, A. A., Petrie, H. L., and Brungart, T. A., Modification to a Turbulent Boundary Layer Due to Slot Injected Drag Reducing Polymer Solutions, *ASME Forum on Turbulent Flows*, FED vol. 94, Toronto, Ontario, Canada, 1990, pp. 43–50.

Fruman, D. H. and Marshall, P. T., Diffusion of a Tangential Drag-Reducing Polymer Injection of a Flat Plate at High Reynolds Numbers, *Journal of Ship Research*, vol. 20, no. 3, Sept. 1976, pp. 171–180.

Granville, P. S., Maximum Drag Reduction for a Flat Plate in Polymer Solution, *Journal of Hydronautics*, vol. 6, no. 1, 1972, pp. 58–59.

Guezennec, Y. G. and Nagib, H. M., Documentation of Mechanisms Leading to Net Drag Reduction in Manipulated Turbulent Boundary Layers, *AIAA-85-0519*, 1985, pp. 1–9.

Guezennec, Y. G. and Nagib, H. M., Mechanisms Leading to Net Drag Reduction in Manipulated Turbulent Boundary Layers, *AIAA Journal*, vol. 28, no. 2, Feb. 1990, pp. 245–252.

Hedley, T. B. and Keffer, J. F., Turbulent/Non-Turbulent Decisions in an Intermittent Flow, *Journal of Fluid Mechanics*, vol. 64, 1974, pp. 625–644.

Hefner, J. N., Dragging Down Fuel Costs, *Aerospace America*, Jan. 1988, pp. 14–27.

Hefner, J. N., Weinstein, L. M., and Bushnell, D. M., Large-Eddy Breakup Scheme for Turbulent Viscous Drag Reduction, *Viscous Flow Drag Reduction, Progress in Astronautics and Aeronautics*. vol. 72, Nov. 1979, pp. 110–127.

Hoyt, J. W., Turbulent Flow Interactions and Drag Reduction, *AIP Conference Proceedings*, no. 137, 1985, pp. 95–115.

Koochesfahani, M. M., Experiments on Turbulent Mixing and Chemical Reactions in a Liquid Mixing Layer, Ph. D. Thesis, California Institute of Technology, Pasadina, 1984.

Koochesfahani, M. M. and Dimotakis, P. E., Laser-Induced Fluorescence Measurements of Mixed Fluid Concentration in a Liquid Plane Shear Layer, *AIAA Journal*, vol. 23, no. 11, Nov. 1985, pp. 1700–1707.

Latto, B. and El Riedy, O. K. F., Diffusion of Polymer Additives in a Developing Turbulent Boundary Layer, *Journal of Hydronautics*, vol. 10, no. 4, Oct. 1976, pp. 135–139.

Lauchle, G. C., Billet, M. L., and Deutsch, S., High-Reynolds Number Liquid Flow Measurements, *Lecture Notes in Engineering 46*, 1989, pp. 95–157.

Lemay, J., Provencal, D., Gourdeau, R., Nguyen, V. D. and Dickinson, J., More Detailed Measurements Behind Turbulence Manipulators Including Tandem Devices Using Servo-Controlled Balances, *AIAA-85-0521*, 1985.

Luchik, T. S. and Tiederman, W. G., Turbulent Structure in Low-Concentration Drag-Reducing Channel Flows, *Journal of Fluid Mechanics*, vol. 190, 1988, pp. 241–263.

Lumley, J. L., Drag Reduction by Additives, *Annual Review of Fluid Mechanics*, vol. 1, 1969, pp. 367–383.

Lynn, T. B., Manipulation of the Structures of a Turbulent Boundary Layer, Ph.D. Thesis, Yale University, University Microfilms Order No. DA8729107, 1987.

McLaughlin, D. K., and Tiederman, W. G., Biasing Correction for Individual Realization of Laser Anemometer Measurements in Turbulent Flows, *The Physics of Fluids*, vol. 16, no. 12, Dec. 1973, pp. 2082–2088.

Morkovin, M. V., On Eddy Diffusivity, Quasisimilarity and Chemical Reactions in Turbulent Boundary Layers, *International Journal of Heat and Mass Transfer*, vol. 8, 1965, pp. 129–145.

Park, J. T., Flow Visualization of a Manipulated Turbulent Boundary Layer: Interaction of a Tandem Large-Eddy Breakup Device and Wall-Injection of a Drag-Reducing Polymer Solution, *Proceedings of the Symposium on Hydrodynamic Performance Enhancement for Marine Applications*, 1988, pp. 169–179.

Petrie, H. L., Samimy, M., and Addy, A. L., Laser Doppler Velocity Bias in Separated Turbulent Flows, *Experiments in Fluids 6*, 1988, pp. 80–88.

Plesniak, M. W., Optimized Manipulation of Turbulent Boundary Layers Aimed at Net Drag Reduction, Master's Thesis, Illinois Institute of Technology, 1984.

Plesniak, M. W. and Nagib, H. M., Net Drag Reduction in Turbulent Boundary Layers Resulting from Optimized Manipulation, *AIAA-85-0518*, 1985, pp. 1–11.

Poreh, M. and Cermak, J. E., Study of Diffusion from a Line Source in a Turbulent Boundary Layer, *International Journal of Heat and Mass Transfer*, vol. 7, 1964, pp. 1083–1095.

Poreh, M. and Hsu, K. S., Diffusion of Drag-Reducing Polymers in a Turbulent Boundary Layer, *Journal of Hydronautics*, vol. 6, No. 1, Jan. 1972, pp. 27–33.

Reidy, L. W. and Mautner, T. S., Turbulent Boundary Layer Modification in High-Speed Water Flow Using Large-Eddy Breakup Devices, *Technical Note 1445, Naval Oceans Systems Center*, March 1986, pp. 1–29.

Reischman M. M. and Tiederman, W. G., Laser-Doppler Anemometer Measurements in Drag-Reducing Channel Flows, *Journal of Fluid Mechanics*, vol. 70, 1975, pp. 369–392.

Sahlin, A., Alfredsson, P. H. and Johansson, A. V., Direct Drag Measurements for a Flat Plate with Passive Boundary Layer Manipulators, *Physics of Fluids*, March 1986, pp. 696–700.

Sahlin, A., Johansson, A. V., and Alfredsson, P. H., The Possibility of Drag Reduction by Outer-Layer Manipulators in Turbulent Boundary Layers, *Physics of Fluids*, vol. 31, No. 10, Oct. 1988, pp. 2814–2820.

Savill, A. M. and Mumford, J. C., Manipulation of Turbulent Boundary Layers by Outer-Layer Devices; Skin-Friction and Flow-Visualization Results, *Journal of Fluid Mechanics*, vol. 191, 1988, pp. 389–418.

Spalding, D. B., A Single Formula for the Law of the Wall, *Journal of Applied Mechanics*, vol. 28E, Sept. 1961, pp. 455-458.

Tennekes, H. and Lumley, J. L., A First Course in Turbulence, The Massachusetts Institute of Technology, 1972.

Tiederman, W. G., Luchik, T. S., and Bogard, D. G., Wall-Layer Structure and Drag Reduction, *Journal of Fluid Mechanics*, vol. 156, 1985, pp. 419–437.

Toms, B. A., Some Observations on the Flow of Linear Polymer Solutions Through Straight Tubes at Large Reynolds Numbers, *Proceedings, First International Congress on Rheology*, vol. 2, 1948, pp. 135–141.

Trigui, N. and Guezennec, Y. G., Turbulence modification by large eddy breakup devices in a passively heated turbulent boundary layer, *Fluids Engineering Division, Forum on Turbulent Flows*, Toronto, Ontario, Canada, 1990, pp. 17–22.

Virk, P. S., Mickley, H. S., and Smith, K. A., The Ultimate Asymptote and Mean Flow Structure in Toms' Phenomenon, *Journal of Applied Mechanics*, June 1970, pp. 488–493.

Walker, D. A., A Fluorescence Technique of Measurements of Concentration in Mixing Liquids, *Journal of Physics E: Science Instrumentation*, vol. 20, 1987, pp. 217–224.

Walker, D. T. and Tiederman, W. G., The Concentration Field in a Turbulent Channel Flow with Polymer Injection at the Wall, *Experiments in Fluids 8*, 1989, pp. 86–94.

Wells Jr., C. S. and Spangler, J. G., Injection of a Drag-Reducing Fluid into Turbulent Pipe Flow of a Newtonian Fluid, *The Physics of Fluids*, vol. 10, no. 9, Sept. 1967, pp. 1890–1894.

Westphal, R. V., Skin Friction and Reynolds Stress Measurements for a Turbulent Boundary Layer Following Manipulation Using Flat Plates, *AIAA-86-0283*, 1986, pp. 1–9.

White, F. M., Viscous Fluid Flow, McGraw Hill, Inc., 1974.

Wilkinson, S. P., Anders, J. B., Lazos, B. S. and Bushnell, D. M., REVIEW–Turbulent Drag Reduction Research at NASA Langley: Progress and Plans, *International Journal of Heat and Fluid Flow*, vol. 9, no. 3, Sept. 1988, pp. 266–277.

Willmarth, W. W., Wei, T., and Lee, C. O., Laser Anemometer Measurements of Reynolds Stress in a Turbulent Channel Flow with Drag Reducing Polymer Additives, *Physics of Fluids*, vol. 30, no. 4, April 1987, pp. 933– 935.

Wu, J. and Tulin, M. P., Drag Reduction by Ejecting Additive Solutions into Pure-Water Boundary Layer, *Journal of Basic Engineering*, Dec. 1972, pp. 749–756.

Yajnik, K. S. and Ancharya, M., Nonequilibrium Effects in a Turbulent Boundary Layer Due to th Destruction of Large Eddies, National Aeronautical Lab, Bangalore, NAL-BL-7, Aug. 1977.